TU Delft

Delft University of Technology

Exploring the use of AOx for organic synthesis and biofuel cells

Pedroso de Almeida, Tiago

DOI
10.4233/uuid:77bc6ed7-ad54-4d10-8765-eb089d174ccd

Publication date
2020

Document Version
Final published version

Citation (APA)
Pedroso de Almeida, T. (2020). *Exploring the use of AOx for organic synthesis and biofuel cells*. [Dissertation (TU Delft), Delft University of Technology]. https://doi.org/10.4233/uuid:77bc6ed7-ad54-4d10-8765-eb089d174ccd

Important note
To cite this publication, please use the final published version (if applicable).
Please check the document version above.

Exploring the use of AOx for organic synthesis and biofuel cells

TIAGO PEDROSO DE ALMEIDA

Exploring the use of AOx for organic synthesis and biofuel cells

Proefschrift

Ter verkrijging van de graad van doctor
aan de Technische Universiteit Delft,
op gezag van de Rector Magnificus Prof.dr.ir. T.H.J.J. van der Hagen,
voorzitter van het College voor Promoties.
In het openbaar te verdedigen op
maandag 24 februari 2020 om 12:30 uur

door

TIAGO PEDROSO DE ALMEIDA

Master of Science in Material Science, Universidade Federal de São Carlos, Brazilië
Geboren te São Paulo, Brazilië

Dit proefschrift is goedgekeurd door de promotoren:
Prof. dr. F. Hollmann
Prof. dr. A. Riul Jr.

Samenstelling promotiecommissie:
Rector Magnificus,   voorzitter
Prof. dr. F. Hollmann   Technische Universiteit Delft, promotor
Prof. dr. A. Riul Jr.   Universidade Estadual de Campinas, promotor

Onafhankelijke leden:
Prof.dr. O. Novaisde Oliveira Jr.   Universidade de São Paulo
Prof.dr. M. Alonso Cotta   UNICAMP
dr. C.E. Paul   Technische Universiteit Delft
Prof.dr. E.A. Pidko   Technische Universiteit Delft
Prof.dr. P. Osseweijer   Technische Universiteit Delft
Prof.dr. W.R. Hagen   Technische Universiteit Delft, reserve
lid

To my family

CONTENTS

Summary

Chapter 1 shows a general presentation of catalysts. Chapter 2 presents a cascade system for alcohol oxidase with the enzyme benzaldehyde lyase. The project was successful in producing in one container only a two-step compound; first, alcohol was converted into aldehyde by alcohol oxidase and, sequentially, the aldehyde converted into the compounds of interest. Background crystals are formed in the final product, turning the removal of the material of interest simpler and more effective.

In Chapter 3, alcohol oxidase was converted into aldehyde in a flow system, but now using the enzyme aryl alcohol oxidase. As oxidase requires oxygen as an electron acceptor, this is a limiting factor due to the low solubility of O_2 in the buffer solution. A flow system becomes more interesting as it can overcome this limitation by improving the oxygen mass transport in buffer solution due to the increased contact area between two fluids. Vigorous agitation is required to achieve similar results in a standard system, which normally compromises the enzymatic structure due to mechanical stress generated by aeration strength. The expected impairment of the structured tertiary enzyme was not observed for the aryl alcohol oxidase enzyme.

The findings in Chapter 3 about the mechanical resistance of aryl alcohol oxidase under vigorous motivated us to scale up the system from 50mL to 1L, presented in Chapter 4. It was possible to obtain high catalytic frequency values in this new configuration, but another challenge appeared: the low solubility of both substrate and product in an aqueous medium. This

challenge was overcome by the biphasic liquid system composed the organic phase in the upper portion and the buffer in the lower part of the solution. In this system, the aqueous phase was fed with the substrate by the organic phase at all times, and the product removed. The encouraging results showed that aryl alcohol oxidase is a strong candidate for industrial applications.

In Chapter 5, we have evaluated carbon compounds deposited on electrodes to produce locally hydrogen peroxide for peroxidase; the idea is getting the halogenation of a model compound by combining catalytic and electrochemical techniques. Here, a fine tune of the voltage or current on a gas diffusion electrode covered with carbon nanotubes enabled the hydrogen peroxide formation. Since the *Ci*VCPO (vanadium chloroperoxidase from *Curvularia inaequalis*) enzyme used in this project needs hydrogen peroxide, the system is interesting to make the enzymatic reaction always working at its maximum efficiency. Finally, Chapter 6 shows a synthesis of carbon-based materials to support the enzyme immobilization on electrodes, bringing a new possibility of using some of the enzymes studied here in biofuel cells and third-generation biosensors. The main idea is to work with enzymes without mediators using these carbon-based materials to sequester electrons from the enzymes to the electrodes. Higher currents were achieved with the newly synthesized carbon-based materials and glucose oxidase, paving the way to design devices having faster electrochemical responses.

Resumo

O capítulo 1 mostra uma apresentação geral sobre catalisadores. O capítulo 2 apresenta um sistema em cascata com a álcool oxidase com a enzima benzaldeídoliase. O projeto foi bem sucedido na obtenção do produto desejado, de duas etapas, usando apenas um frasco. Nesse processo, primeiro o álcool foi convertido em aldeído pela enzima álcool oxidase e, posteriormente, o aldeído foi convertido no composto de interesse. No produto final, temos a formação de cristais de fundo que tornaram simples e eficaz a remoção do material de interesse.

No capítulo 3, usamos novamente a álcool oxidase, mas para esse projeto foi usado uma outra variante, nesse caso a aril-álcool oxidase, para a conversão de álcool em aldeído usando um sistema de fluxo. Como as oxidases utilizam oxigênio como aceptor de elétrons, isso acaba sendo um fator limitante no sistema devido à baixa solubilidade do O_2 na solução tampão. Esse fato torna o sistema em fluxo interessante, pois pode ser usado para superar essa limitação, melhorando o sistema de transporte de massa de oxigênio na solução devido ao aumento da área de contato entre os dois fluidos. É necessária uma agitação vigorosa para obter resultados semelhantes em um sistema padrão, que normalmente compromete a estrutura enzimática devido ao estresse mecânico gerado pela força da aeração. O comprometimento esperado da estrutura terciária enzimática não foi observado para a enzima aril-álcool oxidase.

A partir das descobertas no capítulo 3 de que a enzima aril-álcool oxidase possui resistência mecânica à agitação vigorosa, fomos motivados a aumentar o sistema de 50mL para 1L, apresentado no capítulo 4. Nessa nova

configuração, foi possível obter altos valores de frequência catalítica, mas outro desafio surgiu: a baixa solubilidade de ambos, substrato e produto, em meio aquoso. Esse desafio foi superado pelo sistema líquido bifásico composto pela fase orgânica na porção superior e pelo tampão na parte inferior da solução. Neste sistema, a fase aquosa é alimentada com o substrato pela fase orgânica o tempo todo e, por sua vez, o produto formado é removido para a fase orgânica. Os resultados mostraram que a aril-álcool oxidase é uma forte candidata para aplicações industriais.

No capítulo 5 avaliamos compostos de carbono em eletrodos para produção local de peróxido de hidrogênio para peroxidases, a fim de obter a halogenação de um composto modelo pela combinação de técnicas catalíticas e eletroquímicas. Aqui, o eletrodo de difusão de gás usado foi recoberto com nanotubos de carbono oxidados, com a variação da tensão ou corrente nos eletrodos usados para o controle fino na formação de peróxido de hidrogênio. Como a enzima *Ci*VCPO (vanadium cloroperoxidase da *Curvularia inaequalis*) aplicada neste projeto necessita de peróxido de hidrogênio, o sistema é interessante, pois podemos acompanhar de maneira precisa a produção desse composto, fazendo com que a reação enzimática funcione sempre em seu nível máximo. Finalmente, o capítulo 6 mostra uma síntese de materiais à base de carbono para apoiar a imobilização enzimática em eletrodos, trazendo uma nova possibilidade de uso dessas enzimas em sensores de terceira geração e/ou biocélulas combustíveis. Os novos materiais sintetizados foram capazes de retirar ou doar elétrons diretamente do centro ativo da enzima glicose oxidase sem a necessidade de um mediador, abrindo caminho para projetos de dispositivos com respostas mais rápidas. Para ilustrar, no caso das biocélulas combustíveis esse tipo de

pesquisa pode implicar na futura redução da perda de energia consumida pelos mediadores.

Samenvatting

In hoofdstuk 1 geven we een overzicht van de katalysatoren die gebruikt zijn in deze thesis. In hoofdstuk 2 presenteren we een cascade met een alcohol oxidase en het enzym benzaldehyde lyase. In dit project wisten wij in één reactievat een twee-stappen reactie uit te voeren; eerst werd de alcohol omgezet tot de aldehyde door de alcohol oxidase waarna de aldehyde vervolgens werd omgezet tot de beoogde componenten. Het uiteindelijke product vormde kristallen wat de scheiding van componenten simpel en effectief maakten.

In hoofdstuk 3 gebruikten we opnieuw een alcohol oxidase variant, de aryl alcohol oxidase, voor de conversie van een alcohol naar een aldehyde met behulp van een flow system. Oxidases gebruiken zuurstof als elektron acceptor. Dit is een limiterende factor in het systeem door de lage oplosbaarheid van O_2 in waterige buffers. Dit maakt het flow systeem zo interessant, aangezien het deze limitatie, door middel van massa transport verbeteringen, op kan heffen. In het standaard systeem was hevige agitatie van de oplossing nodig om gelijke resultaten te behalen, wat normaal gezien zou resulteren in enzym denaturatie door de mechanische stress. Het verwachte effect op de tertiaire structuur van het enzym werd echter niet geobserveerd voor de aryl alcohol oxidase.

De bevindingen in hoofdstuk 3, dat het enzym aryl alcohol oxidase resistent was tegen mechanische stress door hevige agitatie, motiveerde ons om het systeem op te schalen van 50 mL tot 1 liter, zoals te zien in hoofdstuk 4. In deze opstelling was het mogelijk om hoge katalytische omzettingen te verkrijgen, maar een nieuwe uitdaging kwam in zicht: de

lage oplosbaarheid van het substraat en het product in waterige oplossingen. Deze uitdaging werd aangegaan door een twee-vloeistof fase oplossing te gebruiken. Hierin bestaat het reactiemengsel uit een organische fase boven op een waterige buffer. In dit systeem voedt de organische fase continu het substraat aan de waterige fase, terwijl het tevens het product continu opneemt. De resultaten gaven weer dat het enzym aryl alcohol oxidase een goede kandidaat is voor industriële applicaties.

In hoofdstuk 5 evalueren we het gebruik van koolstof componenten op elektroden om lokaal waterstofperoxide te kunnen produceren voor peroxygenases. Zo krijgen we een gehalogeneerd modelproduct, door combinatie van katalytische en elektrochemische technieken. Een gasdiffusie elektrode werd behandeld met geoxideerde nano-buisjes, waarna, door middel van controle over het voltage en de stroom over de elektrode, de waterstofperoxide formatie kon worden beheerst. Aangezien het enzym, *Ci*VCPO, gebruikt voor dit project, waterstofperoxide nodig heeft, is dit systeem zeer interessant. Het enzym kan zo namelijk ten alle tijden optimaal functioneren. Tot slot laat hoofdstuk 6 de synthese van een, op koolstof gebaseerd, materiaal zien, dat enzymen kan immobiliseren op elektroden. Dit brengt nieuwe mogelijkheden met zich mee om deze enzymen te gebruiken in derde-generatie sensoren en/of biobrandstof cellen. De nieuwe materialen maakten het mogelijk elektronen direct op te nemen en te geven aan het actieve centrum van een glucose oxidase, zonder gebruik van mediatoren. Dit maakt snellere respons van deze apparaten

| **Thesis introduction** | **1** |

Catalysis

A general definition of catalysis

Chemical reactions need an amount of energy to occur, and the so-called activation energy is required to elevate the starting material into an excited state in which it can react and form the product. The chemical reaction rate depends on the extent of the activation energy through the Arrhenius relationship (equation 1):

$$k = Ae^{\frac{-Ea}{RT}} \tag{1}$$

k is the constant rate, T is the temperature in Kelvin, A is the frequency of collisions in a specific orientation, Ea is the activation energy for the reaction, and R is the universal gas constant. The chemical reaction rate increases either by raising the reaction temperature or lowering the required activation energy (E_A) (Figure 1). The latter process is clearly preferred due to the need for more benign and less energy-demanding chemistry. Catalysis is defined as the process in which the activation energy of a given reaction decreases and, consequently, the reaction rate increases. Catalysts are chemical compounds bringing such effect[1], and after a century of catalysis research, we can find out a broad range of catalysts ranging from simple protons to highly defined transition metal complexes and heterogeneous catalysts such as zeolites. Today's chemistry cannot be imagined without catalysis.
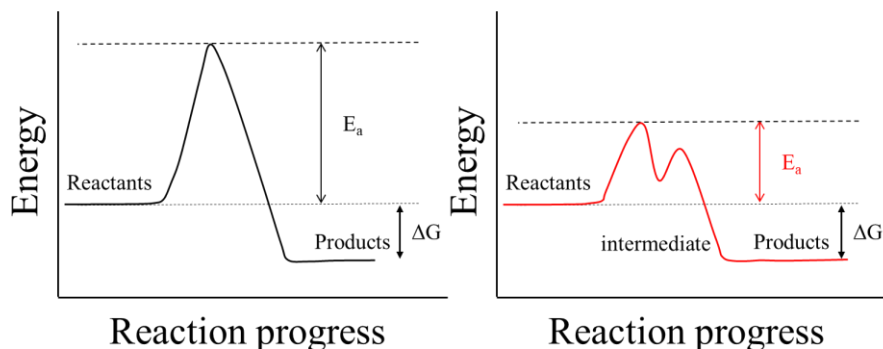
Figure 1. Energy profile of a non-catalyzed (left) and a catalyzed (right) reaction.

The catalysts mode of action is as diverse as the catalysts themselves, ranging from the stabilization of energetic transition states by H-bonds and ionic interactions to alternative reaction pathways avoiding high-energy transition states. To illustrate an alternative path, we can cite the catalyst formation mechanism of vinyl acetate from ethylene and acetic acid by using Pd as catalyst (table 1) [2]. Another example is the ammonia synthesis (table 2) using N_2, H_2 and Co_3Mo_3N-(111) as catalysts [3].
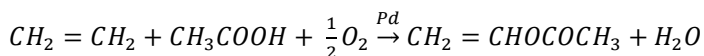
The global reaction of vinyl acetate formation is:

$$CH_2 = CH_2 + CH_3COOH + \frac{1}{2}O_2 \xrightarrow{Pd} CH_2 = CHOCOCH_3 + H_2O$$

Table 1 Main reaction vinyl acetate formation

$$
\begin{aligned}
C_2H_4 + 2Pd &\leftrightarrow CH_2CH - Pd + Pd - H \\
O_2 + 2Pd &\leftrightarrow 2Pd - O \\
CH_3COOH + Pd &\leftrightarrow Pd - CH_3COOH \\
Pd - CH_3COOH + PdO &\leftrightarrow Pd - OCOCH_3 + Pd - OH \\
Pd - OCOCH_3 + CH_2CH - Pd &\leftrightarrow Pd - CH_2CHOCOCH_3 + Pd \\
Pd - CH_2CHOCOCH_3 &\leftrightarrow Pd + CH_2CHOCOCH_3 \\
Pd - OH + PdH &\leftrightarrow Pd - H_2O + Pd \\
Pd - H_2O &\leftrightarrow Pd + H_2O
\end{aligned}
$$
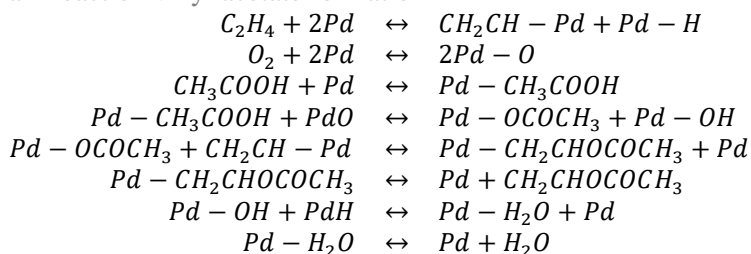
Table 2 Mechanism for ammonia synthesis on Co3Mo3N-(111) surfaces

$$* \xrightarrow{+N_{2(g)}} N_{2(ads)}$$

$$N_{2(ads)} \xrightarrow{+H_{2(g)}} N_2H_{2(ads)}$$

$$N_2H_{2(ads)} \xrightarrow{+H_{2(g)}} N_2H_{2(ads)} + H_{2(ads)}$$

$$N_2H_{2(ads)} + H_{2(ads)} \rightarrow N_2H_{3(ads)} + H_{(ads)}$$

$$N_2H_{3(ads)} + H_{(ads)} \xrightarrow{-NH_{3(g)}} N_{(ads)} + H_{(ads)}$$

$$N_{(ads)} + H_{(ads)} \rightarrow NH_{(ads)}$$

$$HN_{(ads)} \xrightarrow{+H_{2(g)}} NH_{(ads)} + H_{2(ads)}$$

$$NH_{(ads)} + H_{2(ads)} \rightarrow NH_{2(ads)} + H_{(ads)}$$

$$NH_{2(ads)} + H_{(ads)} \rightarrow NH_{3(ads)}$$

$$NH_{3(ads)} \xrightarrow{-NH_{3(g)}} *$$
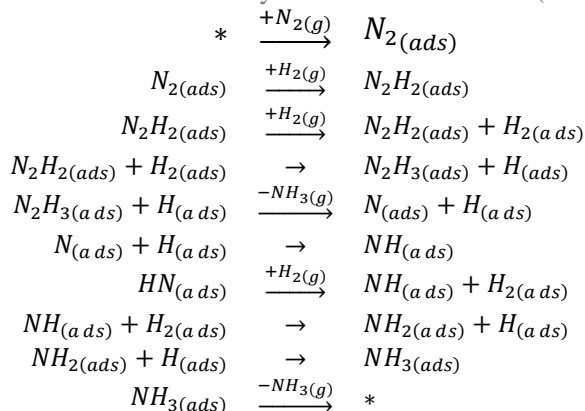
It is important to note that catalysis only accelerates chemical reactions, but they do not influence the reaction equilibrium as it is based on the relative energies of the starting materials and products.[1] Another essential feature of catalysts is that they are not, in principle, consumed during the reaction and can undergo the catalytic process/cycle indefinitely. Nevertheless, catalysts degrade over time due to undesired side reactions.

The catalyst inactivation can become a significant cost-driver process in industrial settings, and a convenient method to quantitatively assess the robustness of a catalyst is the so-called turnover number (TON). TON is the number of catalytic cycles, which is the ratio between product and catalyst. Another typical evaluation criterium is the so-called turnover frequency (TOF = TON divided by the reaction time), which is a direct measurement of the efficiency of a catalyst.[4]

Oxidation reactions

Oxidation is the process wherein electrons are removed from a starting material. Hence a reduced starting material is transformed by an oxidant (an electron acceptor) into the oxidized product. Frequently,

oxidation reactions come along with the introduction of oxygen atoms into the starting material. Typical examples of oxidation in our daily life are the combustion of alkanes into CO_2 liberating thermal energy to run engines or glucose oxidation in the human breathing process. Moreover, the chemical industry frequently uses controlled oxidation reactions, and probably the first oxidation process on a commercial scale was the sulfur dioxide oxidation to produce sulphuric acid.[5] The oxidation of alcohols to aldehydes or ketones, for example, is a wide-spread transformation in organic chemistry in both laboratory and industrial scale. When it comes to oxidants, textbooks often mention chromate (CrO_4^{2-}) or permanganate (MnO_4^-), which are questionable from an environmental point of view due to both the toxicity of the reagents and products, and the generation of large waste streams. Current research efforts focus on their substitution by O_2 or H_2O_2, more benign oxidants yielding ideally only water as a by-product. For instance, the stoichiometric oxidation of isopropyl alcohol to acetone by chromic acid is expressed by[6]:

$$2HCrO_4^- + 3CH_3CHOHCH_3 + 8H^+ \rightarrow 2Cr^{3+} + 3CH_3CHOHCH_3 + 8H_2O$$
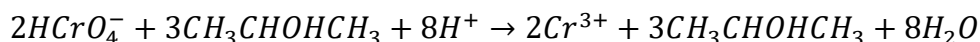
In the same way, there is the oxidation of 4-thiouridine to uridine 4-sulfonate by potassium permanganate:[7]

$$R-SH + 2\ KMnO_4 \rightarrow R-SO_3K + 2\ MnO_2 + KOH$$
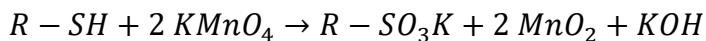
Currently, the main focus of chemical oxidation catalysis is on transition metals, which poses sustainability issues due to the use of rare metals. Furthermore, the catalytic performance of these catalysts, despite the frequently rather harsh reaction conditions that tend to be rather poor.

Oxidative enzymes

A promising alternative to conventional transition metal oxidation catalysts is oxidoreductases, i.e., enzymes catalyzing redox reactions. Enzymes are catalysts of life as they catalyze essential reactions in every living organism. They have been optimized over billions of years by Darwinian Evolution, becoming highly efficient and selective catalysts. Particularly, selectivity distinguishes enzyme catalysis from chemocatalysis. While enzymatic reactions usually yield only one product, chemical catalysts frequently produce several products that have to be separated afterward. Furthermore, their very high efficiency allows performing reactions at much lower temperatures when compared to chemical catalysis. Consequently, enzymes are promising materials to the current state-of-the-art in oxidation catalysis.

For alcohol oxidation, we have two subclasses within the oxidoreductase that stand out: the nicotinamide-dependent dehydrogenases and the flavin-dependent oxidases.

The first one is a sub-class for dehydrogenases, promoting the reversible oxidation reaction, which requires the use of an oxidant in a super-stoichiometric amount. Consequently, the reaction equilibrium shifts to the desired product. (see an example on the Scheme 1A)

A   B
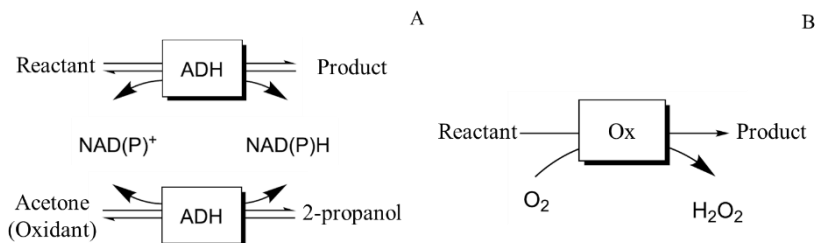
Scheme 1. Comparison of alcohol-dehydrogenase (ADH) -catalyzed oxidation with oxidase (Ox)-catalysed oxidation.

The second one is an irreversible oxidation reaction that uses ambient air as the oxidant (Scheme 1B), avoiding the disposal of harmful materials to the environment, making this method more advantageous than the previous one[8].

The aryl alcohol oxidase from *Pleurotus eryngii*

The enzyme aryl alcohol oxidase is an extracellular enzyme secreted by the fungi of the genus *Pleurotus*. It aims to produce H_2O_2 for lignin biodegradation. This enzyme is capable of converting primary aromatic alcohols into their respective aldehydes,[9] also presenting a catalytic activity for aliphatic alcohols.[10] It has enzymatic activity in a wide pH range (between 4.0 to 9.0), and a relatively high thermal resistance with a maximum activity between 45 - 50°C,[8,9] being a strong candidate for industrial applications.

Electrochemistry

An electrochemical reaction is a complex process in which a charge movement is required for the chemical reaction to occur. In a balanced amount, there is a migration of anions to the anode and cations going to the

cathode.[11] Electrochemical processes are of significant interest due to their diverse range of applications in areas such as energy conversion, pollution control, water treatment, organic and inorganic synthesis, and sensing.[12] Nowadays, the search for environmentally friendly sources leads to the resumption of electricity conversion/storage, with particular attention to the hydrogen production and fuel cells.[13]

Bioelectrochemical systems arise when electrochemistry is focused on biocompouds, then transport and charge accumulation on electrodes are linked to the specific response such as biocatalysts in the chemical conversion processes. Some advantages are excellent control and online monitoring of the electrochemical systems, as well as the high precision and selectivity provided by the enzymatic catalysis. In this kind of system, there is also the possibility of placing the electrode as a direct electron acceptor or donor, increasing the catalytic rate of the system. Bioelectrochemical systems are widely studied nowadays in biosensing,[14] as well as for the extraction of energy from chemical reactions in fuel cells.[15,16]

Scope of this thesis

This thesis presents an evolution of the knowledge on oxidases in cascade reaction with other enzymes (chapter 2), bringing basal information about the operation of enzymes and their responses when applied in organic synthesis. In chapter 3, a possible solution is presented for the limitations of O_2 solubility. Having observed their great enzymatic potential (chapter 4), it was verified of upscale the use of this kind of enzyme. With the knowledge of the limitations and possible solutions (chapter 5), we joined the enzymatic system with the electrochemistry to improve the response and production of the desired products. Finally, section 6 brings a hint of

carbon-based materials supporting enzymes to achieve maximum productivity without mediators.

Reference

1.   Richardson, J. T. *Principles of Catalyst Development*. (Springer US, 1989). doi:10.1007/978-1-4899-3725-4

2.   Atashi, H., Motahari, K., Tabrizi, F. F., Sarkari, M. & Fazlollahi, F. Effect of acetate promotor on the Pd-Au/SiO2-catalyzed synthesis of vinyl acetate from the reaction of ethylene with acetic acid. *J. Korean Chem. Soc.* **55**, 92–97 (2011).

3.   Zeinalipour-Yazdi, C. D., Hargreaves, J. S. J. & Catlow, C. R. A. Low-T Mechanisms of Ammonia Synthesis on Co3Mo3N. *J. Phys. Chem. C* **122**, 6078–6082 (2018).

4.   Lloyd, L. *Handbook of Industrial Catalysts*. (Springer US, 2011). doi:10.1007/978-0-387-49962-8

5.   V. Twigg, M. *Catalyst Handbook*. (Routledge, 2018). doi:10.1201/9781315138862

6.   Westheimer, F. H. & Novick, A. The kinetics of the oxidation of isopropyl alcohol by chromic. *J. Chem. Phys.* **11**, 506–512 (1943).

7.   Yano, M. & Hayatsu, H. Permanganate oxidation of 4-thiouracil derivatives. Isolation and properties of 1-substituted 2-pyrimidone 4-sulfonates. *BBA Sect. Nucleic Acids Protein Synth.* **199**, 303–315 (1970).

8.   Van Schie, M. M. C. H. *et al.* Biocatalytic synthesis of the Green Note trans-2-hexenal in a continuous-flow microreactor. *Beilstein J. Org. Chem.* **14**, 697–703 (2018).

9. Guillén, F., Martinez, A. & Martínez, M. Production of hydrogen peroxide by aryl-alcohol oxidase from the ligninolytic fungus *Pleurotus eryngii*. *Appl. Microbiol.* **32**, 465–469 (1990).

10. de Almeida, T. P. *et al.* Efficient Aerobic Oxidation of trans-2-Hexen-1-ol using the Aryl Alcohol Oxidase from Pleurotus eryngii. *Adv. Synth. Catal.* **361**, 2668–2672 (2019).

11. Pletcher, D. & Walsh, F. *Industrial electrochemistry*. (Blackie Academic & Professional, 1993).

12. Rajeshwar, K., Ibanez, J. G. & Swain, G. M. Electrochemistry and the environment. *J. Appl. Electrochem.* **24**, (1994).

13. Tarasevich, M. R., Sadkowski, A. & Yeager, E. Oxygen Electrochemistry. in *Comprehensive Treatise of Electrochemistry* 301–398 (Springer US, 1983). doi:10.1007/978-1-4613-3584-9_6

14. Yahiro, A. T., Lee, S. M. & Kimble, D. O. Bioelectrochemistry. I. Enzyme utilizing bio-fuel cell studies. *BBA - Spec. Sect. Biophys. Subj.* **88**, 375–383 (1964).

15. Nicolau, E., Méndez, J., Fonseca, J. J., Griebenow, K. & Cabrera, C. R. Bioelectrochemistry of non-covalent immobilized alcohol dehydrogenase on oxidized diamond nanoparticles. *Bioelectrochemistry* **85**, 1–6 (2012).

16. Ghindilis, A. L., Atanasov, P. & Wilkins, E. Enzyme-Catalyzed Direct Electron Transfer: Fundamentals and Analytical Applications. *Electroanalysis* **9**, 661–674 (1997).

Towards environmentally acceptable synthesis of chiral α-hydroxy ketones via oxidase-lyase cascades

2
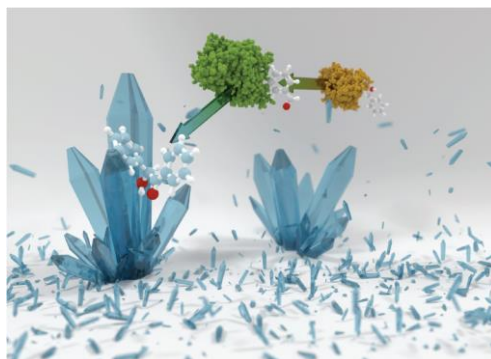
Introduction

Cascade reactions are an exciting part of organic chemistry,[1] being similar to the serial manufacture where catalysts work inline to reach the final product. It starts with a simple molecule, and each catalyst adds new complexity to the molecule by passing it through them, producing, in the end, a much more complex compound. This sort of reaction can be done, in many cases, in only one pot using only one solvent, avoiding particular challenges such as substrate instability, inhibition, and low solubility of the compound formed in the solution used, evading also several purification steps. Consequently, cascade reaction has some advantages such as shorter times, reduced labor management, costs and waste, in addition to bringing green chemistry label.[1]

Here, we present a successful cascade reaction used to produce chiral α-hydroxy ketones that are valuable building blocks in fine chemistry and pharmaceutical applications.[1–6] This compound can be conveniently produced from simple aldehydes with thiamine-dependent carboligases, catalyzing the biocatalytic version of the well-known benzoin condensation (albeit enantio-selectively and omitting the use of cyanides).[7–10] However, there are some practical issues related to the use of aldehydes as starting materials. First, aldehydes are reactive molecules prone to undesired side-reactions such as aerobic oxidation and hydroperoxide formation. More importantly, reactive aldehydes can form Schiff-bases with lysine residues of the biocatalysts, thereby blocking the access channel to the enzymes' active sites and modulating the polarity of the proteins (neutral imines instead of positively charged lysine residues) or both.[11] Furthermore,

aldehydes are relatively hydrophobic, having poor solubility in aqueous reaction media. Due to a significant higher solubility of alcohols compared to aldehydes (for example, benzyl alcohol at pH 7.0 and 25 °C is approximately 20 times more soluble than benzaldehyde), we have envisioned a buffered reaction system without cofactor addition exhibiting substrate concentrations > 350 mM in one liquid phase. Inhibitory effects of the intermediate aldehyde should be minimized due to the further conversion of the corresponding benzoin in the one-pot approach.

Inspired by the earlier work of Domínguez de María and coworkers,[12] we have evaluated a bi-enzymatic cascade comprising alcohol oxidase from *Pichia pastoris* (*Pp*AOX) and benzaldehyde yase from *Pseudomonas fluorescens* (*Pf*BAL) for the formation of chiral benzoins from the corresponding alcohols, illustrated in Scheme 1.
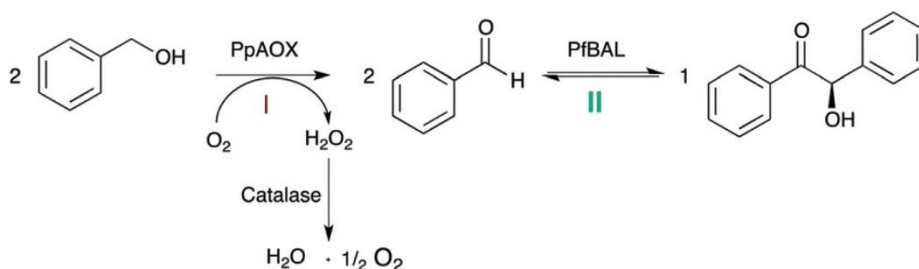
Scheme 1 The envisioned synthetic enzyme cascade consisting of alcohol oxidase (*Pp*AOX) from *Pichia* pastoris and benzaldehyde lyase (*Pf*BAL) from *Pseudomonas fluorescens* for the stereo-selective synthesis of (R)-benzoin. To circumvent the hazardous effect of H_2O_2 (formed in the alcohol oxidation step) catalase is added.

In the first set of experiments, *Pp*AOX and *Pf*BAL were combined under arbitrarily chosen conditions (based on the standard oxidase-lyase reaction conditions as reported by PerezSanchez et al.).[12] They were joined

in aqueous solution in the same pot, without the presence of co-solvent in 20 mM benzyl alcohol, yielding 56% of the desired enantiopure (R)-benzoin. The promising results obtained encouraged us to investigate the parameters further influencing the efficiency of the cascade reaction.

Results and discussion

*Pp*AOX has been reported preferentially to oxidize short-chain, aliphatic alcohols.[13,14] Indeed, *Pp*AOX activity towards benzyl alcohol was only ~ 1% compared to the observed rate in methanol (Figure 1).
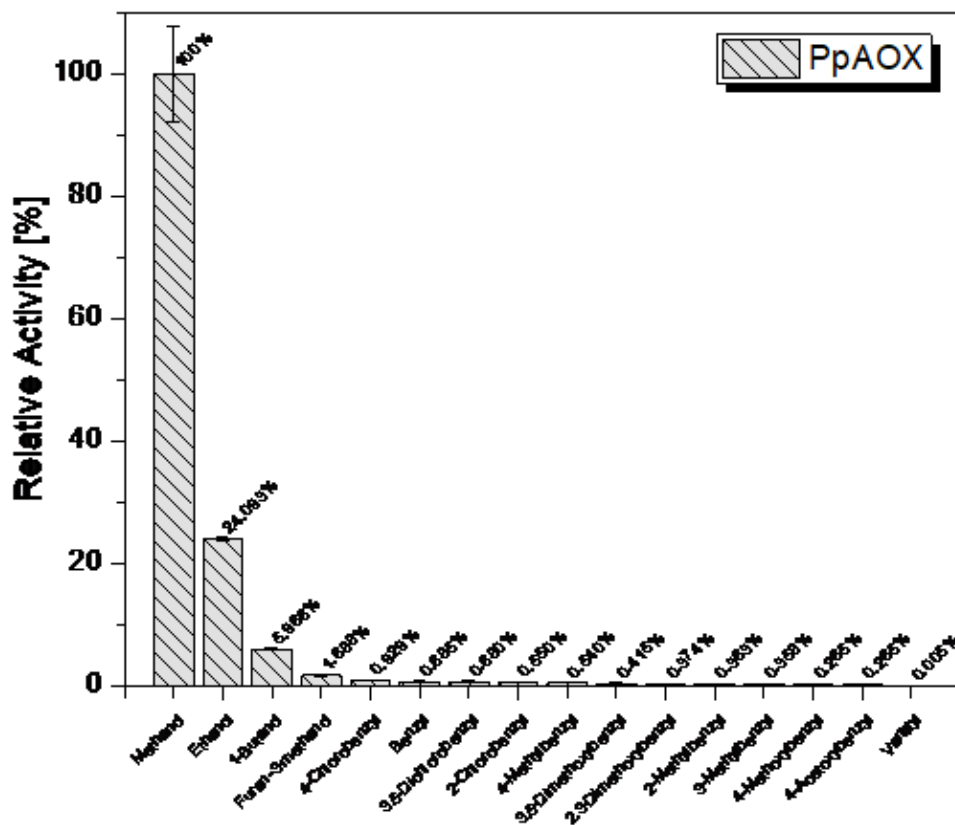
Figure 1 Substrate screening of *Pp*AOX against various aliphatic and aromatic alcohols. A) Residual activities. <u>Reaction conditions</u>: alcohol substrate (0.00033% [v/v]), *Pp*AOX (0.5 U, 1.5 mL), horseradish peroxidase (1.25 U, 1.5 mL), 1.86 mM ABTS, sodium phosphate buffer (100 mM, pH 7.5), 25°C. Activities were determined spectrophotometrically using the ABTS assay.

A comparatively high Km can be attributed (~ 140 mM) to some substrates against benzyl alcohol (Figure 2).
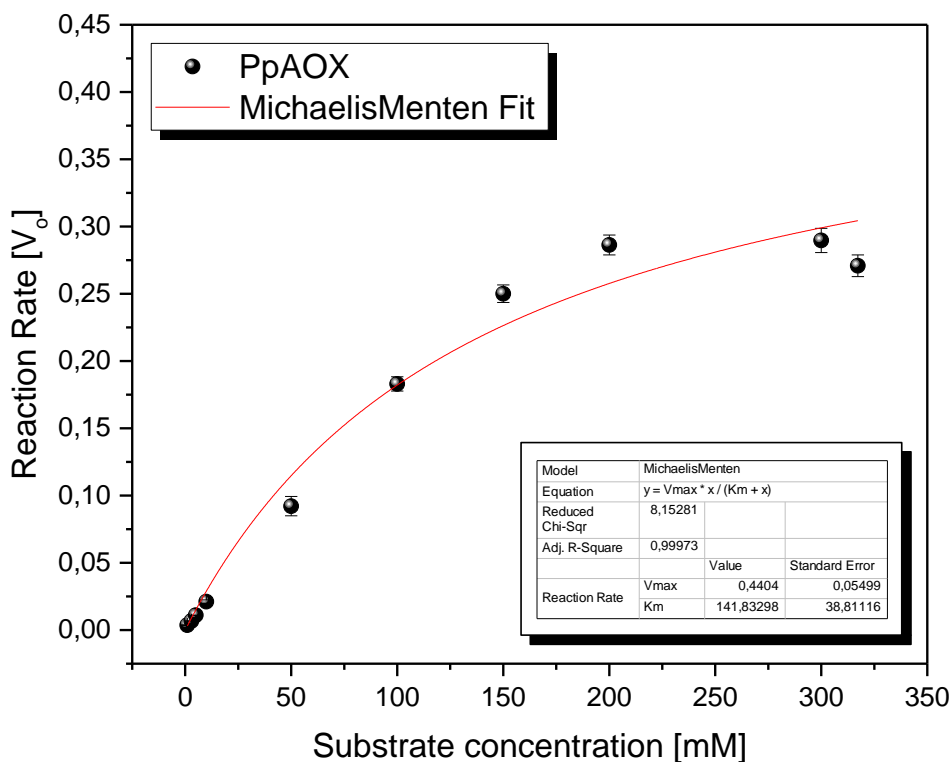
Figure 2 *Pp*AOX Michaelis-Menten kinetics for benzyl alcohol. <u>Reaction conditions</u>: *Pp*AOX (0.5 U, 1.5 mL), horseradish peroxidase (1.25 U, 1.5 mL), 1.86 mM ABTS, sodium phosphate buffer (100 mM), 25°C. Activities were determined spectrophotometrically using the ABTS assay, benzyl alcohol (0-325 mM), pH 7.5

Nevertheless, the intrinsic very high activity of *Pp*AOX converted the benzylic alcohols into the corresponding aldehydes. *Pp*AOX was mildly inhibited by aldehydes showing reduced activity above 50 mM in benzaldehyde (Figure 3).
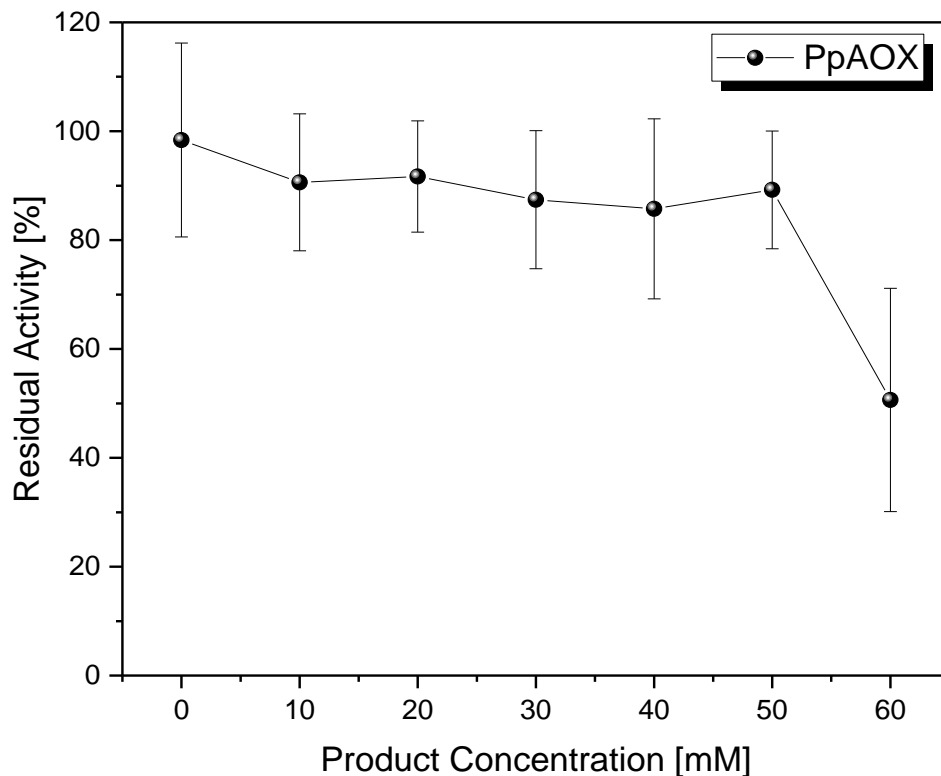
Figure 3 *Pp*AOX product inhibition against different benzaldehyde concentrations; <u>Reaction conditions</u>: *Pp*AOX (0.5 U, 1.5 mL), horseradish peroxidase (1.25 U, 1.5 mL), 1.86 mM ABTS, sodium phosphate buffer (100 mM), 25°C. Activities were determined spectrophotometrically using the ABTS assay. benzyl alcohol (0.00033% [v/v]), benzaldehyde (0-60 mM), pH 7.5.

Such inhibition, however, should not negatively influence the *Pp*AOX performance in the envisaged cascade, in which the concentration of the aldehyde should be low due to the direct ligation of the intermediate (see also Figure 3). H_2O_2 proved to be more detrimental to *Pp*AOX (Figure 4) as 10 min incubation with 10 mM leads to complete inactivation of the oxidase.
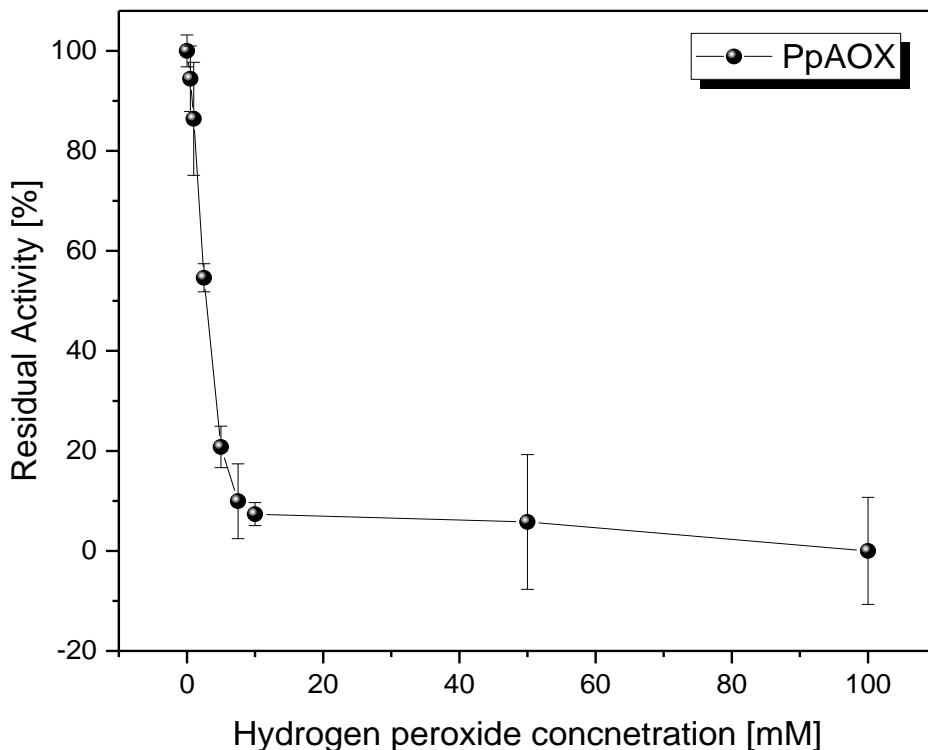
Figure 4 *Pp*AOX oxidative stability against different hydrogen peroxide concentrations *Reaction conditions*: *Pp*AOX (0.5 U, 1.5 mL), horseradish peroxidase (1.25 U, 1.5 mL), 1.86 mM ABTS, sodium phosphate buffer (100 mM), 25°C. Activities were determined spectrophotometrically using the ABTS assay. benzyl alcohol (0.00033% [v/v]), 0-100 mM hydrogen peroxide for 10 min pH 7.5.

Therefore, all subsequent experiments were performed in the presence of at least 1 g L^{-1} of bovine catalase. The optimal pH value for *Pp*AOX was around 7.5 (Figure 5), whereas *Pf*BAL best performs at pH 9.5.[8]
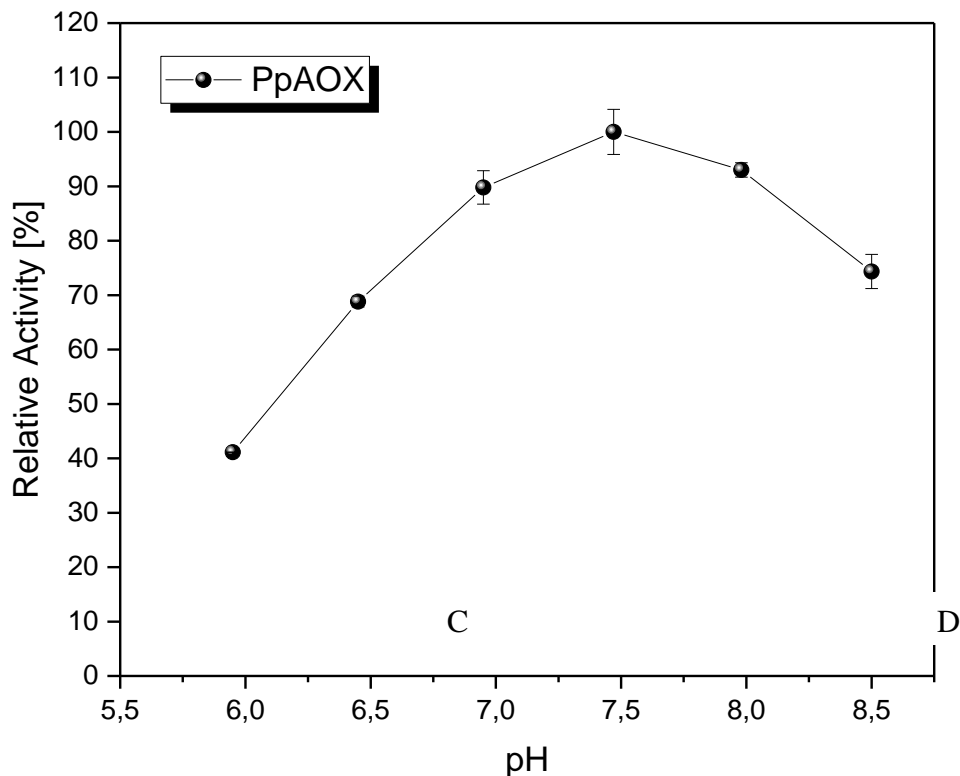
Figure 5 *Pp*AOX pH profile with benzyl alcohol as substrate. <u>Reaction conditions</u>: *Pp*AOX (0.5 U, 1.5 mL), horseradish peroxidase (1.25 U, 1.5 mL), 1.86 mM ABTS, sodium phosphate buffer (100 mM), 25°C. Activities were determined spectrophotometrically using the ABTS assay, benzyl alcohol (0.00033% [v/v]), pH 6.0 – 8.5.

Therefore, we have chosen a pH for both enzymes (pH 8.5) all subsequent experiments. The *Pp*AOX and *Pf*BAL ratio had a significant influence on the performance of the cascade reaction, with the optimal performance achieved at a molar ratio of approximately (1:2) (Figure 6).
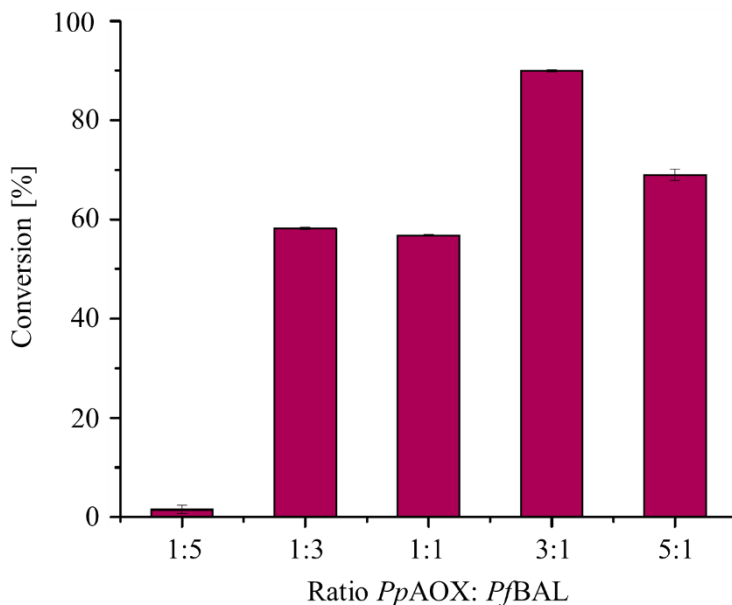
Figure 6 Conversion of benzyl alcohol to (R)-benzoin using different *Pp*AOX: *Pf*BAL ratios. <u>Reaction conditions</u>: alcohol substrate (20 mM), PpAOX (5-25 U), *Pf*BAL (5-25 U), MgCl2 (2.5 mM), ThDP (0.15 mM), Catalase from bovine liver (2.5 mg.mL^{-1}), phosphate buffer (50 mM, pH 8.5), 30°C.

Using the partially optimized reaction conditions, we performed a time-course experiment using 20 mM of benzyl alcohol (Figure 7). Within the first 10 h, more than 60% conversion was achieved, with significantly longer reaction time needed to achieve the full conversion (10 mM) of the desired benzoin. We attributed this to the comparatively high K_M values for both enzymes (K_M value for benzoin formation of *Pf*BAL is 10.0 ± 1.5 mM).[8]
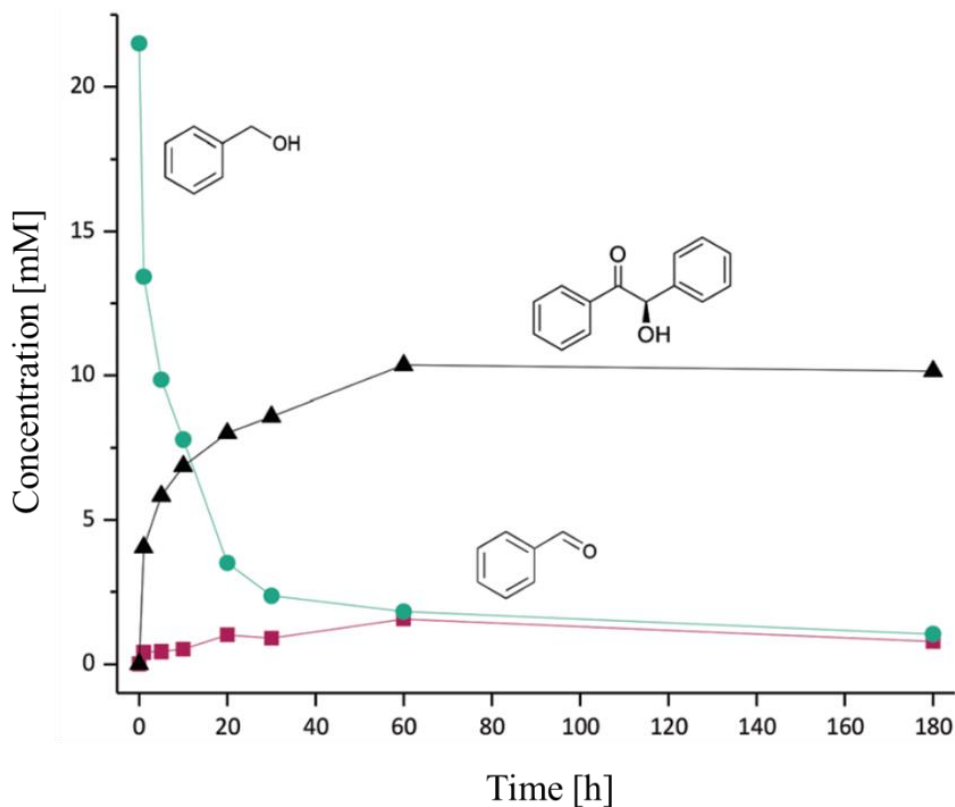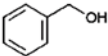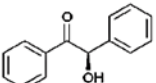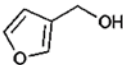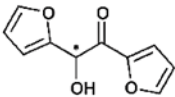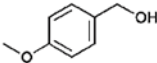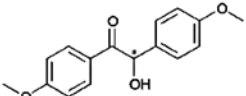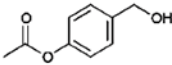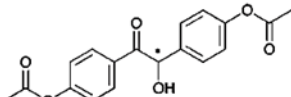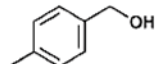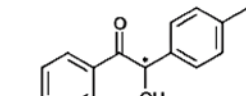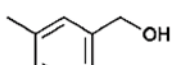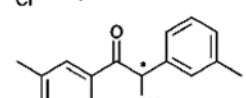
Figure 7 Kinetic profile obtained for the oxidase-lyase one-pot cascade reaction using benzyl alcohol as a substrate. The green line shows benzyl alcohol, the red line benzaldehyde and the black line (R)-benzoin. Reaction conditions: Alcohol substrate (20 mM), PpAOX (6.3 µM), crude cell extract containing PfBAL (39.13 µM), MgCl2 (2.5 mM), ThDP (0.15 mM), catalase from bovine liver (2.5 mg mL−1), pho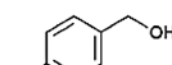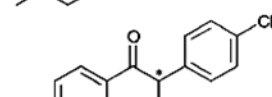sphate buffer (50 mM, pH 8.5), 30 °C. Due to the precipitation of the product, the product profile was determined by HPLC and 1H NMR.

Notably, the concentration of the intermediate aldehyde remained low during the whole reaction (0.4–1.5 mM). *Pf*BAL showed outstanding enantioselectivity of >99%, in agreement with the literature. [8,12,15,16] We subsequently investigated the further conversion of benzylic alcohol substrates (Table 1).

Table 1 Product yields and enantioselectivities obtained in the synthetic cascade reactions with *Pp*AOX and *Pf*BAL.

Substrate[a]	Product	Aldehyde [%]	Yield[b] [%]	ee[c] [%]
Soluble alcohol substrate				
		4	96	>99
		13	84	>99
		2	94	>99
		24	19	93
Slurry-to-slurry approach				
		8	81	99
		4	96	92
		6	15	94

Reaction conditions: phosphate buffer (50 mM, pH 8.5) containing MgSO$_4$ (2.5 mM), ThDP (0.15 mM) and catalase from bovine liver (2.5 mg mL-1). Crude cell extract containing *Pf*BAL (around 5 mg, 62.72 µM, 8 U), and *Pp*AOX (17.75 µL, 788.89 nM, 25 U), oxygen-supply, 800 rpm, 30 °C, 24 hours, [b] Determined from ^{1}H NMR spectra. [c] Enantioselectivities were determined by HPLC using enantiopure product standards or, if not available, literature data[17] was used. (soluble alcohols) the reaction mix contained the liquid alcohol substrate (350 mM), [a] Non-soluble alcohols formed a two-liquid phase system. (slurry-to-slurry) reaction mix

containing the solid alcohol substrate (350 mM). [a] Alcohols were directly used in their solid form due to their low solubility.

To circumvent kinetic limitations observed at low substrate concentrations and to show that high product concentrations can be achieved at high substrate loadings, we formally applied 350 mM of the starting alcohol. Liquid alcohols (Table 1 soluble alcohols and low solubility alcohols) were added directly to the aqueous solution of the biocatalysts, whereas in the case of solid alcohols (Table 1 shows slurry and without quality slurry) 5% (v/v) of 2-methyl tetrahydrofuran was added to facilitate the dissolution of the alcohols. Non- or p-substituted benzyl alcohols were converted to the enantiomerically pure benzoins in good to excellent yields. Other substitution patterns lead to significantly reduced conversions and optical purities of the final products. While the poor stereoselectivity cannot be ascribed to *Pf*BAL (always high optical purities were reported),[17,18] it is worth noting that in these cases, the concentration of the intermediate aldehyde was also low, indicating that the oxidation step was rate-limited on the whole. In addition, racemization was observed in some products under the current reaction conditions. In the case of vanillyl alcohol, for instance, the ee was only 43% after 72 hours of reaction, whereas after 18 hours the ee was > 99%. Optimized reaction setups (particularly adjusting the molar ratio of *Pp*AOX and *Pf*BAL) will enable higher conversion. It is worth mentioning here that in all cases, the final product precipitated from the reaction mixture and could be easily removed via filtration. The same selectivity pattern was also observed in the case of solid starting materials; particularly p-substituted benzyl alcohols excelled in terms of conversion and enantioselectivity. Our first attempts to perform these reactions under

'co-solvent free' conditions resulted in slow reactions. Most probably, this is due to slow dissolution kinetics of the starting material. Therefore, 5% (v/v) 2-methyl tetrahydrofuran was added to accelerate the process (Table 1 slurry). Interestingly, the presence of 2-Me-THF did not impair the facile downstream processing by simple filtration. Finally, we performed the semi-preparative scale conversion of benzyl alcohol with up to 500 mM substrate. Due to the limited solubility of benzyl alcohol and to avoid possible substrate inhibition on *Pp*AOX, benzyl alcohol was added to the reaction mixture in 10 portions at 50 mM (adding up to a nominal final concentration of 500 mM or 54 g L^{-1}). Almost instantaneously, the desired (R)-benzoin precipitated from the reaction mixture (Figure 8).
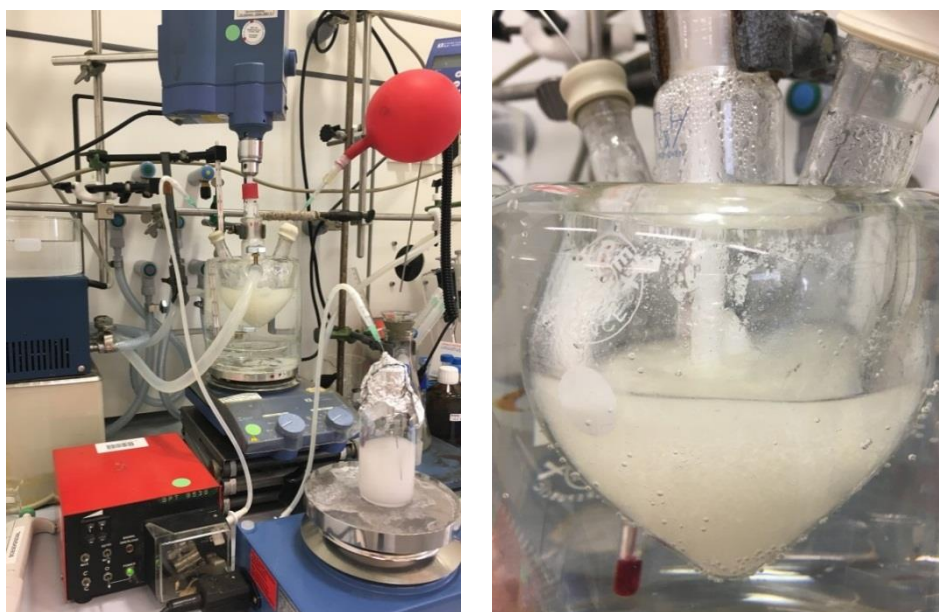

Figure 8 Picture of the reaction setup. Left: Whole reaction setup, including the pump for substrate feed from the substrate reservoir. Right: Close-up of the reaction solution after 3 hours of reaction. The product (*R*)-benzoin is visible as a white precipitate in the solution.

After filtration, the raw product contained 5.4 mM of the intermediate aldehyde, which was easily removed by evaporation in vacuum. Overall, enantiomerically pure (R)- benzoin was obtained in 83% isolated yield (4.6 g). Finally, we were interested in the environmental impact of the established cascade comprising *Pp*AOX and *Pf*BAL for the stereoselective synthesis of α-hydroxyketones. To assess the waste generation in the cascading oxidase-lyase reactions, we performed an E-factor analysis including downstream processing of the product (Table 2) and the catalyst preparation (Table 3).[19,20]

Table 2 Estimation of the generated waste in the cascading oxidaselyase reactions

Contribution	Enzymatic reaction with soluble product[a] [g] Perez-Sanchez *et al.*[12]	Cascade reaction with precipitating product[b] [g] This work
Reaction water	250	250
Wash water	2000	150
Buffer (phosphate)	3	3
Substrate	30	2
Catalase	0.09	0.6
*Pp*AOX[c]	0.09	0.2
*Pf*BAL[c]	0.25	0.1
MgCl$_2$	0.05	0.05
ThDP	0.01	0.01
2-Me-THF	—	0.06
Brine	50	—
EtOAc	1500	—
Sum	3835	406

[a] Calculations were performed for 1-butanol and benzaldehyde as substrates assuming the same conversion (91%) and substrate addition (6 mM) on a large scale based on the work of Perez-Sanchez et al. (2013).[12] [b] Calculations were

performed for the amount of crude product obtained (4.6 g). [c] Only the catalyst itself was included in the calculation, not the cell mass, which is not the catalyst.

Additionally, the waste generation in a similar cascade reaction reported by Perez-Sanchez et al. was calculated for comparison.[12] Table 2 illustrates solvents constituting the main contributors to the E-factor. Firstly, water as the reaction medium contributes by 25 kg kg^{-1}, and water as the solvent for the preparation of the biocatalysts also gives roughly 14 kg kg^{-1} to the final product (Table 3).

Table 3 Estimation of the generated waste in the production process of 1 g *Pp*AOX and *Pf*BAL, respectively.

Contribution	PpAOX[3,4] Waste [g]	PfBAL Waste [g]
Water in media	103	34
BMMY media	5[a]	
Cultivation media (yeast extract, peptone, glycerol, salts)		2.8[b]
Antibiotic	$\cong 0$	$\cong 0$
Inducer	1.0	$\cong 0$
Lysozyme/DNase/RNase	-	$\cong 0$
Sum	109	36.8

[a] Data for a secreted expression of PpAOX.
[b] Data for an intracellular expression of PfBAL, which makes a cell disruption necessary.

Secondly, ethyl acetate and 2-methyl tetrahydrofuran used as co-solvents in the reaction and for product removal, or both (work by Perez-Sanchez et al.) [12], also significantly contributed to the overall waste formed. Nevertheless, by exploiting the poor solubility of the products, problematical solvents such as ethyl acetate for extraction were avoided

simply by filtration. Furthermore, preliminary results indicated that the filtrate (containing the biocatalysts and traces of the reagents) could be re-used, thereby reducing the overall waste-contribution of the fermentation step.

Conclusions

Enzymatic cascade reactions have gained enormous interest in recent years as an alternative synthesis strategy, which overall bears a great potential to make organic syntheses environmentally more benign. The mere use of enzymes, however, does not automatically render the reaction 'green' or 'environmentally benign', and a critical evaluation of the environmental impact of a given reaction is important to identify bottlenecks and to adapt the whole reaction setup en route to a greener process. Here, we have demonstrated that reaction design exploiting the reagents' properties can significantly simplify product isolation and, thereby, reduce or even omit organic solvents. Particularly, solid products not necessarily need to be solubilized throughout the process.

On the contrary, product precipitation can shift the reaction equilibria and simplify product isolation. By emphasizing problems like waste generation, the search for simplified downstream processing and the need for integrated reactors in our work may trigger others to think along those premises to be able to develop more examples on how biocatalysis should move on the establishment of greener alternatives. Especially, the applicability of these systems for larger-scale reactions may also render this system attractive for greener syntheses in the future.

Materials and methods

Unless stated otherwise, all chemicals were purchased from Sigma-Aldrich (Steinheim, Germany), New England Biolabs (Ipswich, MA, USA), Merck (Darmstadt, Germany) or Alfa Aesar (Karlsruhe, Germany) in the highest quality available and used without further purification. Alcohol oxidase from *Pichia pastoris* (*Pp*AOX) was purchased from Sigma-Aldrich as a buffered aqueous solution (1 KU). Lyophilized benzaldehyde lyase ($\geq$ 1.6 U.mg^{-1}) was initially obtained from evoxx (evo-1.4.106.S, Monheim, Germany).

Bacterial strain and plasmid

Escherichia coli BL21 (DE3) were purchased from New England Biolabs (Beverly, MA, USA). The plasmid pET28a containing the gene encoding the benzaldehyde lyase from *Pseudomonas fluorescens* (NCBI_Nucleotide accession-number: P51853) bearing an additional N-terminal His$_6$-tag was kindly provided by Dr. Doerte Rother (Forschungszentrum Juelich, Juelich, Germany). The plasmid was transformed into the appropriate *E. coli* strain by the heat shock method.[1]

Cultivation conditions

Expression of *Pf*BAL was carried out by inoculation of 400 mL TB (terrific broth) medium supplied with the appropriate antibiotic (kanamycin) with an overnight culture to give an OD$_{600}$ of 0.05. E. coli BL21 (DE3) cells were used as an expression host. Cells were grown at 37°C in baffled shake flasks. *Pf*BAL expression was induced at an OD$_{600}$ of 0.6-0.8 with 1.0 mM IPTG. Cultivation was continued at 20°C for 24 hours. Cells were harvested

(centrifugation at 1344 g at 4°C for 15 min) and washed twice in Potassium phosphate buffer (pH 8.5, 50 mM). The bacterial cell (10.25 g) pellet was resuspended in the same buffer to give a wet cell weight (WCW) of $100g.L^{-1}$ and disrupted three times for 10 min by ultrasonication or directly frozen and freeze-dried afterward. *Pf*BAL was directly used as a crude cell extract and was not further purified.

Determination of PfBAL activity

One unit of ligase activity is defined as the amount of *Pf*BAL, which catalyzes the formation of 1 µmol of benzoin per minute under standard conditions (30 ˚C, pH 8.5).

Initial rates of *Pf*BAL-catalyzed benzoin formation were determined using HPLC (see details below in chapter Analytics). Samples containing 10-60 mM benzaldehyde in 50 mM potassium phosphate buffer, pH 8.5, 2.5 mM $MgSO_4$, 0.1 mM ThDP were incubated with 50 µL BAL at 30 ˚C in glass vessels. At appropriate time intervals, samples were taken to measure the amount of benzoin.

Determination of PpAOX activity

One unit is defined as the amount of *Pp*AOX which oxidizes 1.0 µmol of benzyl alcohol to benzaldehyde per min at pH 7.5 at 25 °C (Scheme 2)
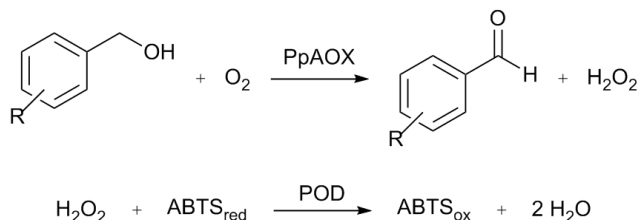
Scheme 2 Spectrophotometric assay to determine the activity of *Pp*AOX. *Pp*AOX: alcohol oxidase from *Pichia pastoris*, ABTS™: 2,2′-azino-bis-(3-ethylbenzothiazoline-6-sulfonic acid), POD: peroxidase from horseradish.

The following solutions were prepared directly before the measurements: Phosphate buffer (100 mM, pH 7.5 at 25 °C), ABTS solution (2 mM) in phosphate buffer which was bubbled with pure O_2 gas for ~5 minutes before use, alcohol solutions [1.0% (v/v)] in distilled water with 5% (v/v) of Dimethyl Sulfoxide (DMSO) or 2-Methyltetrahydrofuran (2-Me-THF) if necessary, peroxidase solution (250 units.ml^{-1} solution of peroxidase in phosphate buffer) and an alcohol oxidase solution (7.35 unit.ml^{-1} of alcohol oxidase in phosphate buffer).

In a 1.0 or 1.505 ml reaction mix, the final concentrations were 1.86 mM ABTS, 0.00033% (v/v) benzyl alcohol, 1.25 (1.505 mL) or 0.83 (1 mL) units POD, and 0.4935 (1.505 mL) or 0.3379 (1 mL) units alcohol oxidase.

First, the following reagents were pipetted into suitable cuvettes: 93 µL or 1.4 mL ABTS and 3.3 or 5 µL POD solution. The solutions were mixed with the pipette. The absorption at 405 nm was monitored until it was constant. After equilibration, 33.22 or 50 µL of the respective alcohol solution was added, mixed, and absorption at 405 nm was recorded again until it was constant. After the addition of 33.22 or 50 µL *Pp*AOX solution, the increase in A_{405} was recorded for (we change to 3 min) minutes. The

ΔA_{405}/minute was obtained using the maximum linear rate for both the sample and the blank.

The enzyme activities were calculated using the following formula:

$$\text{Units.ml}^{-1} \text{ enzyme} = \frac{(\Delta A_{405}/\text{minute sample} - \Delta A_{405}/\text{minute Blank}) (1.0) (df)}{(36.8) (0.03322)}$$

where:

1.0 = Total volume (in millilitres) of assay

df = Dilution Factor

36.8 = Millimolar extinction coefficient of ABTS at 405 nm

0.3322 = Volume (in milliliters) of enzyme used

By using the same activity assay, the *Pp*AOX was further investigated in terms of pH profile, temperature stability and temperature optimum, oxidative stability, product inhibition, and substrate scope:

Km

Reaction conditions: benzyl alcohol (0-325 mM), *Pp*AOX (0.5 U, 1.5 mL), horseradish peroxidase (1.25 U, 1.5 mL), 1.86 mM ABTS, sodium phosphate buffer (100 mM, pH 7.5), 25°C. Activities were determined spectrophotometrically using the ABTS assay

Temperature Optimum

To determine the temperature optimum, the phosphate buffer (100 mM, pH 7.5) and all reaction solutions were pre-incubated to the respective temperature (15-50˚C, in steps of 5˚C) until they reached the desired temperature (≈ 10 min). Afterward, the ABTS assay was performed as described above.

Temperature Stability

To determine the thermostability, the *Pp*AOX (0.35 mg.mL^{-1}) was incubated in phosphate buffer (100 mM, pH 7.5) at various temperatures ranging from 20-60 °C for 10 min. Afterward, the samples were immediately placed on ice, and the activity was measured at room temperature using the ABTS.

Inactivation of AOX

Inactivation of the enzyme was determined by incubation of *Pp*AOX (0.35 mg.mL^{-1}) in phosphate buffer (100 mM, pH 7.5) at 30˚C. After defined time intervals, samples were taken and immediately placed on ice. Residual activity was measured at room temperature using the ABTS assay.

Oxidative stability

*Pp*AOX (0.35 mg.mL^{-1}) was used to determine oxidative stability by incubating the enzyme in phosphate buffer (100 mM, pH 7.5) containing various concentrations of hydrogen peroxide (0-100mM) at 30˚C for 3 h. After the incubation time, 10 µL of a catalase solution (1 mg.mL^{-1} in buffer) was added to the samples and incubated further on ice. The residual activity of the *Pp*AOX was measured using the ABTS assay.
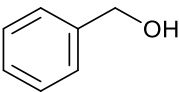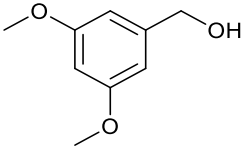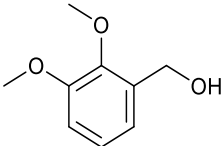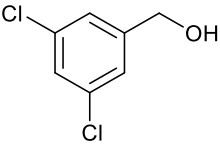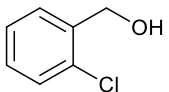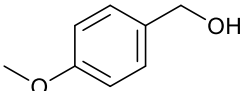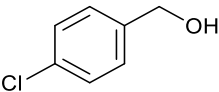
Product Inhibition
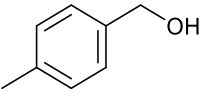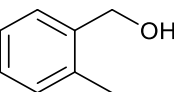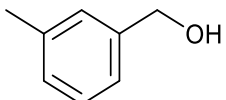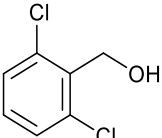
Product Inhibition of the enzyme was determined by incubation of *Pp*AOX (0.35 mg.mL^{-1}) in phosphate buffer (100 mM, pH 7.5) at 30˚C with different benzaldehyde concentrations (0-60 mM). After 3h, samples were taken and immediately placed on ice. Residual activity was measured at room temperature using the ABTS assay.

Substrate scope

The substrate scope of *Pp*AOX was determined using the ABTS assay according to the description above. All investigated substrates and their final assay concentrations were given in Table 4.

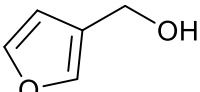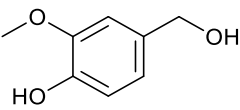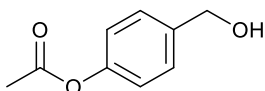Table 4 Various alcohol substrates which were investigated to determine the *Pp*AOX activity.

	Substrate	Structure	Final Assay Concentration [mM] (Co-Solvent)
1	Benzyl alcohol		1
2	3,5-Dimethoxybenzyl alcohol		1 (DMSO)
3	2,3-Dimethoxybenzyl alcohol		1
4	3,5-Dichlorobenzyl alcohol		1 (2-Me-THF)
5	2-Chlorobenzyl alcohol		1 (2-Me-THF)
6	4-Methoxybenzyl alcohol		1
7	4-Chlorobenzylalcohol		1 (DMSO)

8	4-Methylbenzyl alcohol		1 (DMSO)
9	2-Methylbenzyl alcohol		1 (DMSO)
1 0	3-Methylbenzyl alcohol		1
1 1	Furan-3-methanol		1
1 2	Vanillyl alcohol		1 (DMSO)
1 3	4-Acetoxybenzyl alcohol		1
1 4	2,6-Dichlorobenzyl alcohol		Not soluble

A general protocol for the biocatalytic oxidation-lyase reactions on an analytical scale

Benzyl alcohol (2.16 mg, 20 mM) was dissolved in a mixture of phosphate buffer (50 mM, pH 8.5) containing $MgSO_4$ (2.5 mM), *Th*DP (0.15 mM) and catalase from bovine liver (2.5 mg.mL^{-1}). After addition of *Pf*BAL (3.12 mg, 39.13 μM, 5 U) and *Pp*AOX (17.75 μL, 788.89 nM, 25 U) to a total reaction volume of 1 mL, the reaction vial was covered with a gas-filled oxygen balloon, and the mixture was shaken at 800 rpm in an Eppendorf shaker at 30°C for 24 h. The reaction mixture was extracted with

dichloromethane (3 x 1 mL), and the organic layer washed with water (3 x 1 mL) and brine (1 x 1 mL) and dried over Na_2SO_4 vacuum. The solvent was evaporated in vacuum. The reactions were followed by ^{1}H NMR, and the enantiomeric excesses were determined by chiral-phase HPLC (AD-H column, UV detection at 210 and 254 nm).

Slurry-to-slurry reactions

The liquid alcohol substrates (350 mM, Table 4) were dissolved in a mixture of phosphate buffer (50 mM, pH 8.5) containing $MgSO_4$ (2.5 mM), ThDP (0.15 mM) and catalase from bovine liver (2.5 mg/mL). In contrast, the solid alcohol substrates were directly used in their solid form (350 mM) in a slurry-to-slurry mixture with phosphate buffer (50 mM, pH 8.5) containing $MgSO_4$ (2.5 mM), ThDP (0.15 mM) and catalase from bovine liver (2.5 mg/mL). To the reactions, *Pf*BAL (5 mg, 62.72 μM, 8 U) and *Pp*AOX (17.75 μL, 788.89 nM, 25 U) to a total reaction volume of 1 mL were added, and the reaction vials were covered with a gas-filled oxygen balloon at 800 rpm in an Eppendorf shaker at 30°C for 24 h. The reactions were followed by ^{1}H NMR, and the enantiomeric excesses were determined by chiral-phase HPLC (AD-H column, UV detection at 210 and 254 nm).

After 72 hours (Figure 9), the reaction mixtures were centrifuged for 10 min at 1344 *g*. The supernatant was removed from the solid pellet but kept for HPLC analysis. The solid pellet was resuspended in 1 mL distilled water and centrifuged again for 10 min at 1344 *g*. The supernatant was again removed, and the solid pellet washed with distilled water. This process was repeated 5 times to wash the enzyme and all other reaction components away. The solid pellets were analyzed by ^{1}H NMR, and the enantiomeric

excesses were determined by chiral-phase HPLC (AD-H column, UV detection at 210 and 254 nm).

Figure 9 Picture of a representative slurry-to-slurry reaction after 72 hours.

Preparative scale synthesis of (R)-Benzoin

Preparation of the feeding solution: Benzyl alcohol (10.36 mL) was dissolved in 84.64 mL phosphate buffer (50 mM, pH 8.5) and 5 mL (5% (v/v)) 2-methyl tetrahydrofuran (2-Me-THF) to give a total volume of 100 mL. In the original reaction vessel a mixture of 87.5 mL phosphate buffer (50 mM, pH 8.5), ThDP (0.15 mM), $MgCl_2$ (2.5 mM), catalase from bovine liver (2.5 mg/mL), *Pf*BAL (350 μL crude cell extract, 1 mM, 130.5 U) and *Pp*AOX (300 μL, 13.33 μM, 392 U) to a volume of 100 mL were mixed. The reaction mixture was stirred using a KPG® stirrer (IKA Labortechnik) equipped with a Teflon stirrer, and the temperature was kept at 30°C using a jacketed beaker connected to a thermo-stated water bath (Colora Messtechnik GmbH). The reaction vessel was tightly closed with septa. One outlet of the reaction vessel was connected to a gas-filled oxygen balloon,

whereas the other was connected via the pump (BPT 8538, Watson-Marlow Limited, UK) to the feeding solution.

Due to the limited solubility of benzyl alcohol, the feeding solution (1 M benzyl alcohol in 5% (v/v) 2-Me-THF) was continuously stirred to enable the formation of an even emulsion. The total reaction volume was 200 mL. Therefore, the feeding solution was added in defined time intervals to the main reaction to avoid insolubility problems of the benzyl alcohol. The complete feed was finished after 6 hours and 20 minutes. The reaction was further continued for 96 hours at 30°C.

The reaction mixture was filtered applying vacuum. The filtration residue was washed three times with ultrapure water (3 x 200 mL) and dissolved in 50 mL dichloromethane. The aqueous reaction solution was additionally extracted three times with dichloromethane (3 x 200 mL), and the organic layer was washed with brine. The two organic phases were combined and dried over the appropriate amount sodium sulfate and the solvent was evaporated under vacuum. The white crystalline product was yielded in 71 % (NMR yield) and 2.5 g (48 % isolated yield).

An appropriate amount of product was dissolved in 600 μL $CDCl_3$ or DMSO, and the ^1H NMR spectra were recorded on a Bruker 400 MHz NMR unit.

HPLC

Enantiomeric excesses were determined by HPLC using the following described conditions. Retention times for all alcohol substrates, aldehyde intermediates, and condensation products were summarized in Table 5.
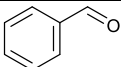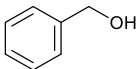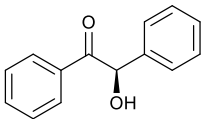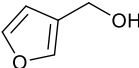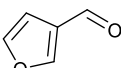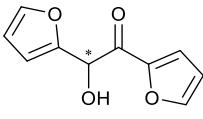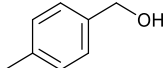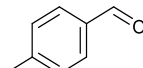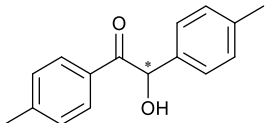
HPLC conditions:

Column: Daicel AD-H Chiralpak 4.6 x 250 mm 5μ
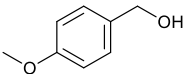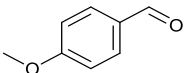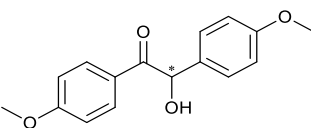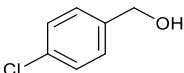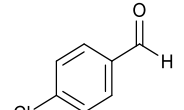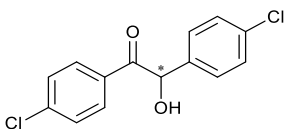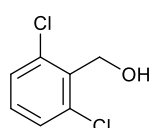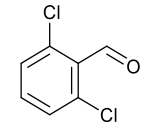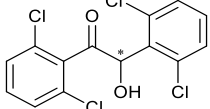
Eluent: 93% heptane, 7% isopropanol (v/v)
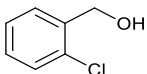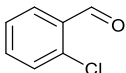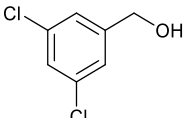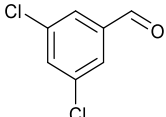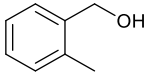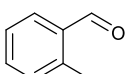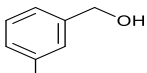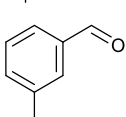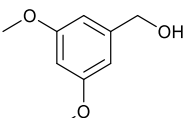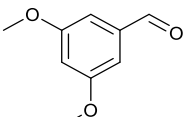
Flowrate: 1.0 mL.min^{-1}
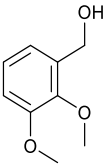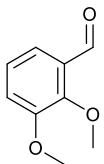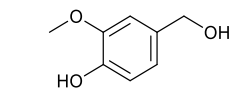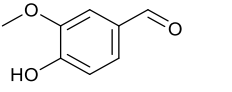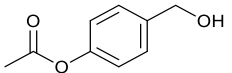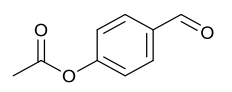
Detection wavelengths: 210 and 254 nm

Table 5 Retention times of the reaction components.

Entry	Method	Name Substrate	Compounds	Retention time [min]
1	7% isopropanol, flow 1 mL/min, 30 min, 254 nm	Benzyl alcohol		4.6
				7.5
				17.5
2	7% isopropanol, flow 1 mL/min, 30 min, 254 nm	Furan-3-methanol		4.1
				-
				E1: 17.6 E2: 21.7
3	7% isopropanol, flow 1 mL/min, 30 min, 254 nm	4-Methyl benzyl alcohol		7.5
				4.7
				E1: 19.6

E2: 21.2

	Conditions	Substrate	Product	Value
			(4-methoxyphenyl)methanol	6.4
4	7% isopropanol, flow 1 mL/min, 30 min, 254 nm	4-Methoxy benzyl alcohol	4-methoxybenzaldehyde	4.1
			1,2-bis(4-methoxyphenyl)-2-hydroxyethanone	E1: 15.4 E2: 22.5
			(4-chlorophenyl)methanol	7.5
5	7% isopropanol, flow 1 mL/min, 30 min, 254 nm	4-Chloro benzyl alcohol	4-chlorobenzaldehyde	4.7
			1,2-bis(4-chlorophenyl)-2-hydroxyethanone	E1: 19.6 E2: 20.9
			(2,6-dichlorophenyl)methanol	4.1
6	7% isopropanol, flow 1 mL/min, 30 min, 254 nm	2,6-Dichloro benzyl alcohol	2,6-dichlorobenzaldehyde	7.4
			1,2-bis(2,6-dichlorophenyl)-2-hydroxyethanone	E1: 11.8 E2: 12.8

7	7% isopropanol, flow 1 mL/min, 30 min, 254 nm	2-Chloro benzyl alcohol		7.3
				4.2
8	7% isopropanol, flow 1 mL/min, 30 min, 254 nm	3,5-Dichloro benzyl alcohol		6.3
				4.5
9	7% isopropanol, flow 1 mL/min, 30 min, 254 nm	2-Methyl benzyl alcohol		6.8
				-
10	7% isopropanol, flow 1 mL/min, 30 min, 254 nm			6.8
				4.4
11	7% isopropanol, flow 1 mL/min, 30 min, 254 nm	3,5-Dimethoxy benzyl alcohol		12.9
				5.9

12	7% isopropanol, flow 1 mL/min, 30 min, 254 nm	2,3-Dimethoxy benzyl alcohol	10.4
			5.5
13	7% isopropanol, flow 1 mL/min, 30 min, 254 nm	Vanillyl alcohol	22.1
			11.1
14	7% isopropanol, flow 1 mL/min, 30 min, 254 nm	4-Acetoxy benzyl alcohol	12.3
			7.4 P1: 23.7 P2: 26.9

Representative HPLC chromatograms (Figure 10 to Figure 22)
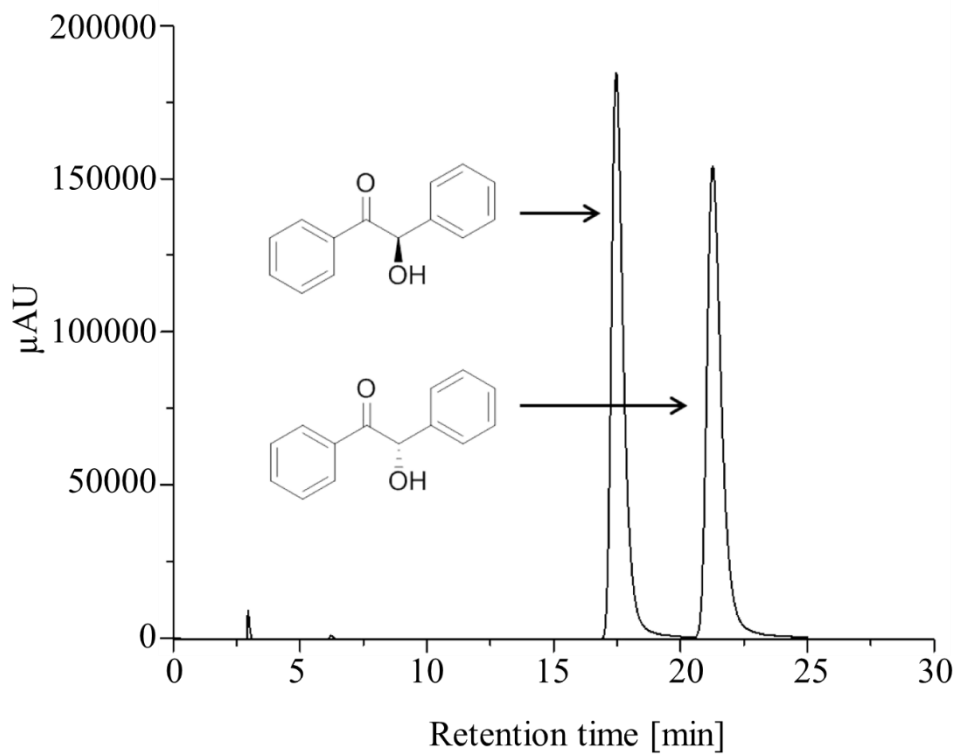
Figure 10 The separation and determination of the (R)-and (S)-enantiomers of benzoin.
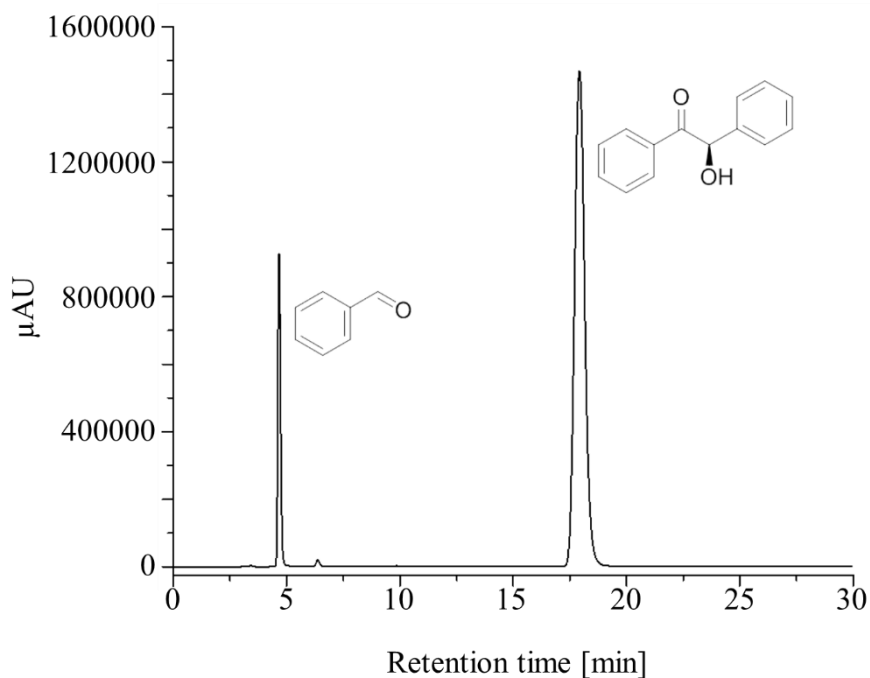
Figure 11 Representative HPLC-chromatogram for the cascade reaction starting from 500 mM benzyl alcohol showing the enantioselective formation of (R)-benzoin after 72 hours. Benzaldehyde (RT = 4.6 min) remained at 6 mM.
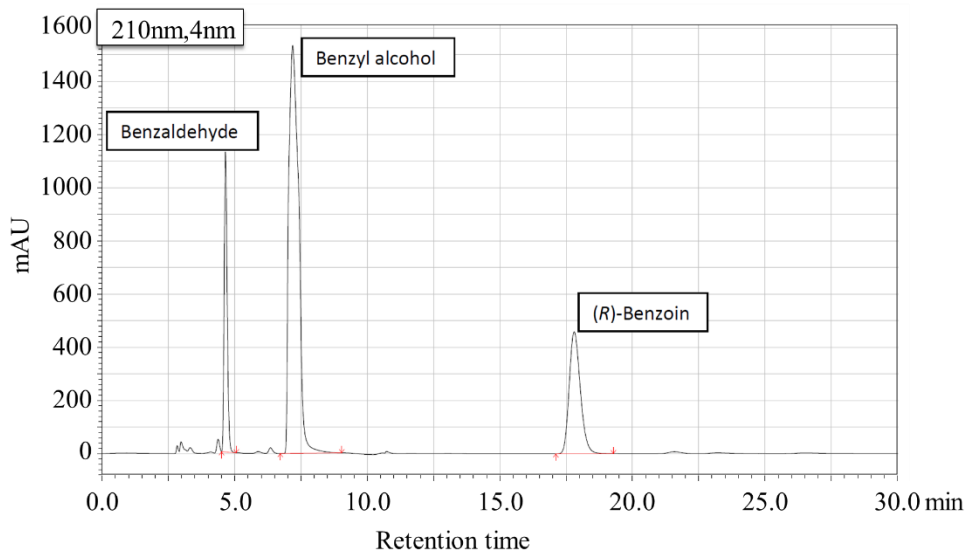
Figure 12 Representative HPLC-chromatogram for the biotransformation starting from benzyl alcohol showing all reaction components.
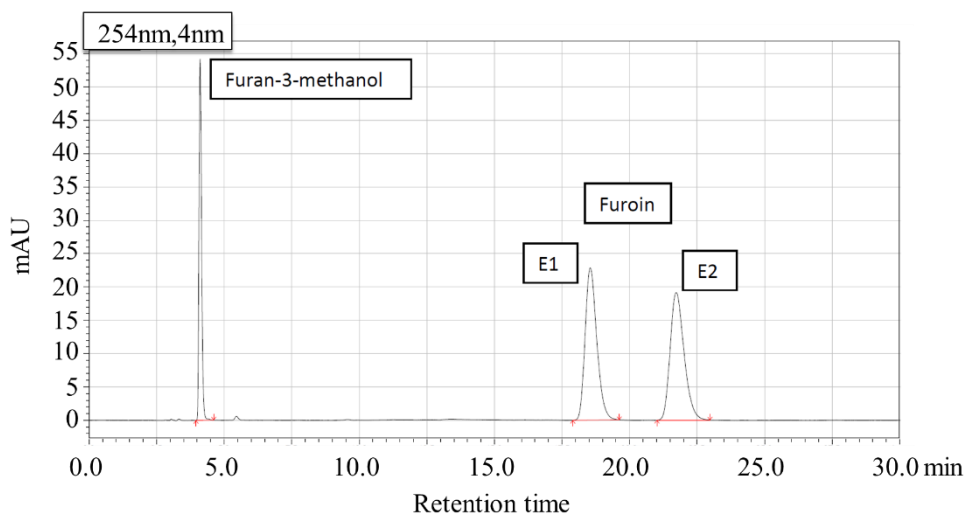
Figure 13 Representative HPLC-chromatogram is showing furan-3-methanol and the two enantiomers of the product furoin (E1 and E2).
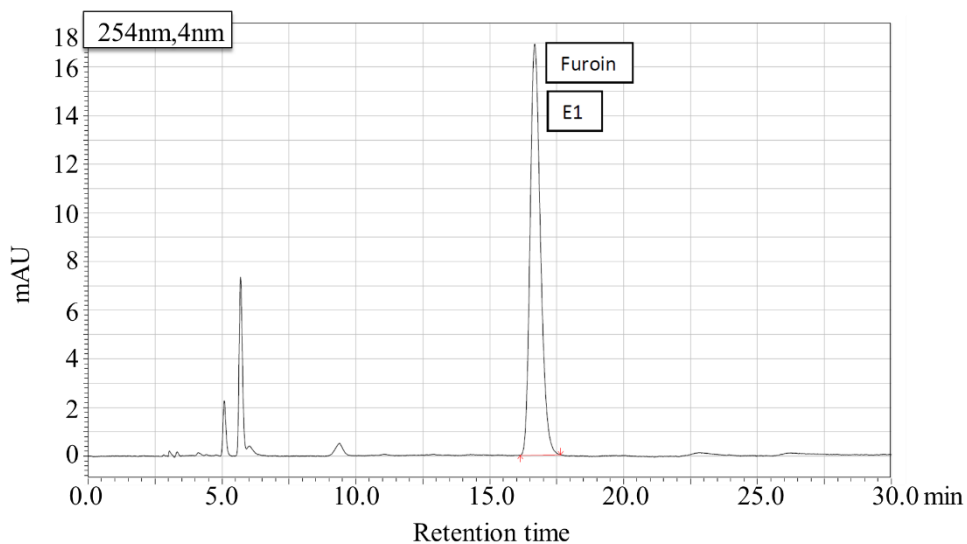
Figure 14 Representative HPLC-chromatogram for the cascade reaction starting from 20 mM furan-3-methanol showing the enantioselective formation of furoin after 30 hours. Furan-3-methanol: 4.1 min. (R)- or (S)-furoin: E1: 17.0 min, E2: 21.7 min.
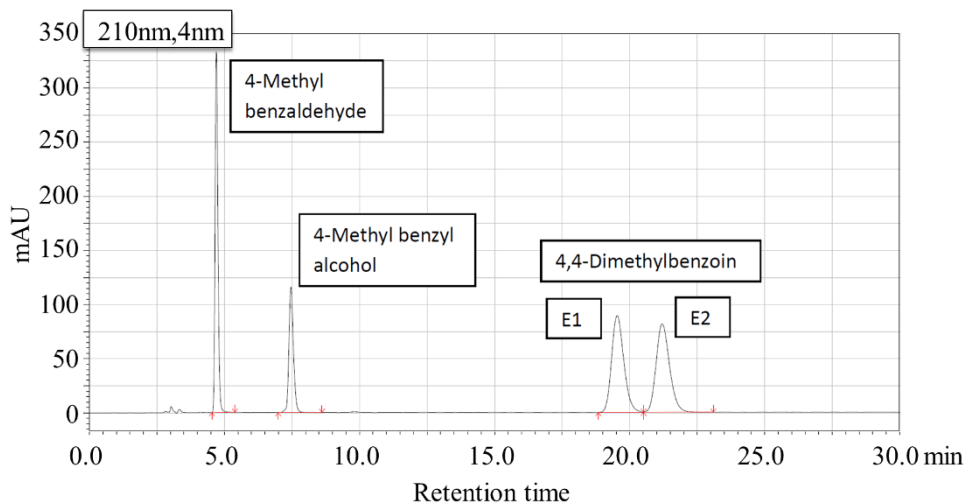
Figure 15 Representative HPLC-chromatogram showing 4-methyl benzyl alcohol and the two enantiomers of the product 4,4-dimethylbenzoin (E1 and E2).
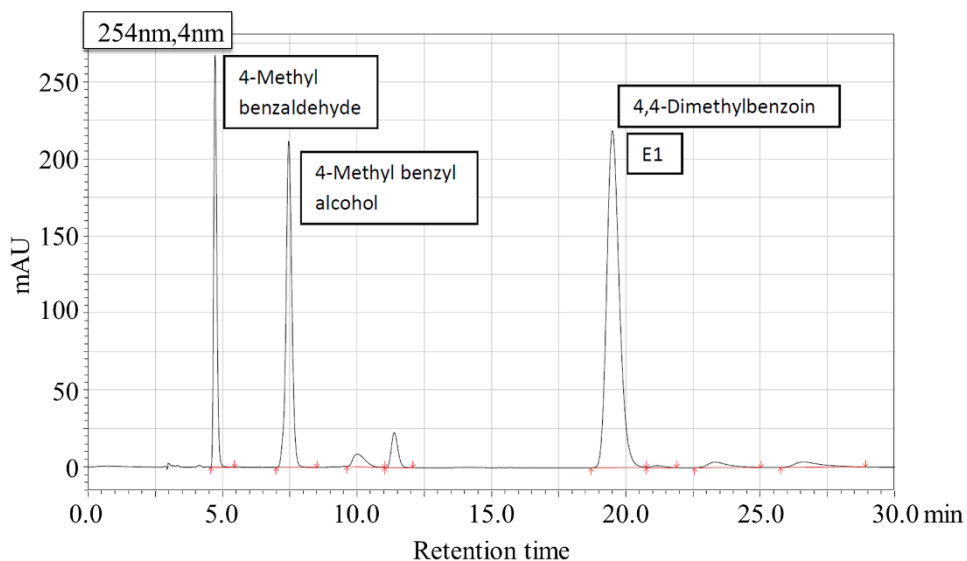
Figure 16 Representative HPLC-chromatogram for the cascade reaction starting from 20 mM 4-methyl benzyl alcohol showing the enantioselective formation of 4,4-dimethylbenzoin after 72 hours. 4-Methyl benzyl alcohol: 7.5min; 4-Methyl benzaldehyde: 4.7min; (R)- or (S)-4,4-dimethylbenzoin:E1:19.6min, E2:21.2.
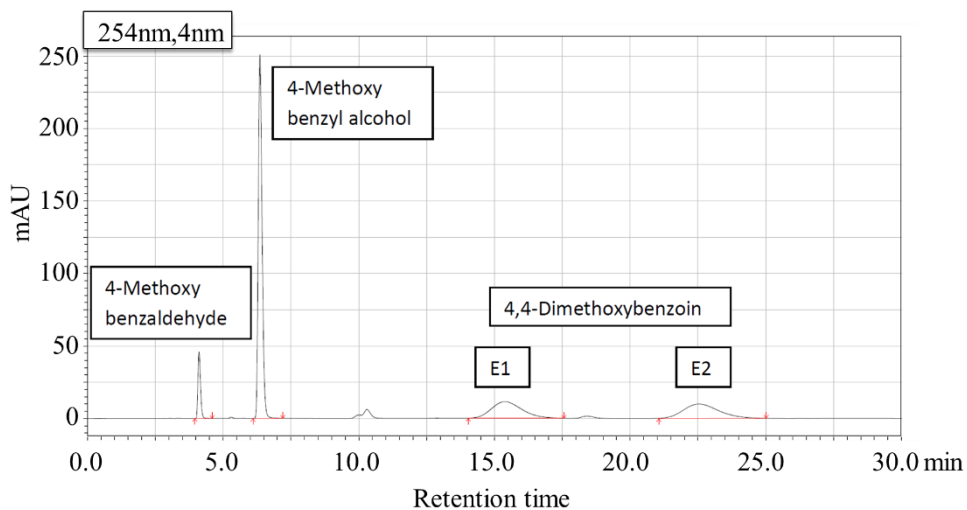
Figure 17 Representative HPLC-chromatogram is showing 4-methoxy benzyl alcohol and the two enantiomers of the product 4,4-dimethoxbenzoin (E1 and E2).
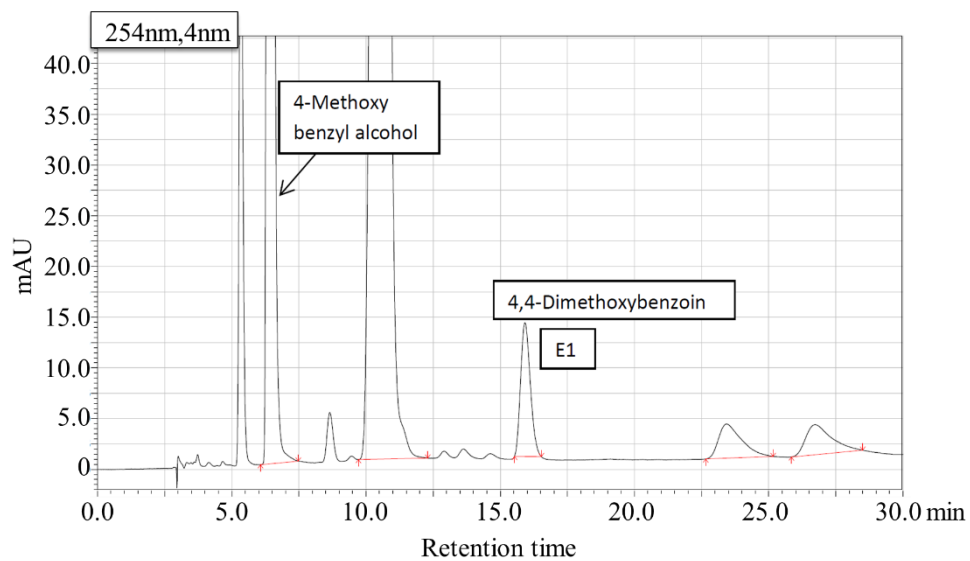
Figure 18 Representative HPLC-chromatogram for the cascade reaction starting from 20 mM 4-methoxy benzyl alcohol showing the enantioselective formation of 4,4-dimethoxy benzoin after 72 hours. 4-Methoxy benzyl alcohol: 6.4 min; 4-Methoxy benzaldehyde: 4.1 min; (*R*)- or (*S*)-4,4-Di Methoxybenzoin: E1: 15.4 min, E2: 22.6 min.
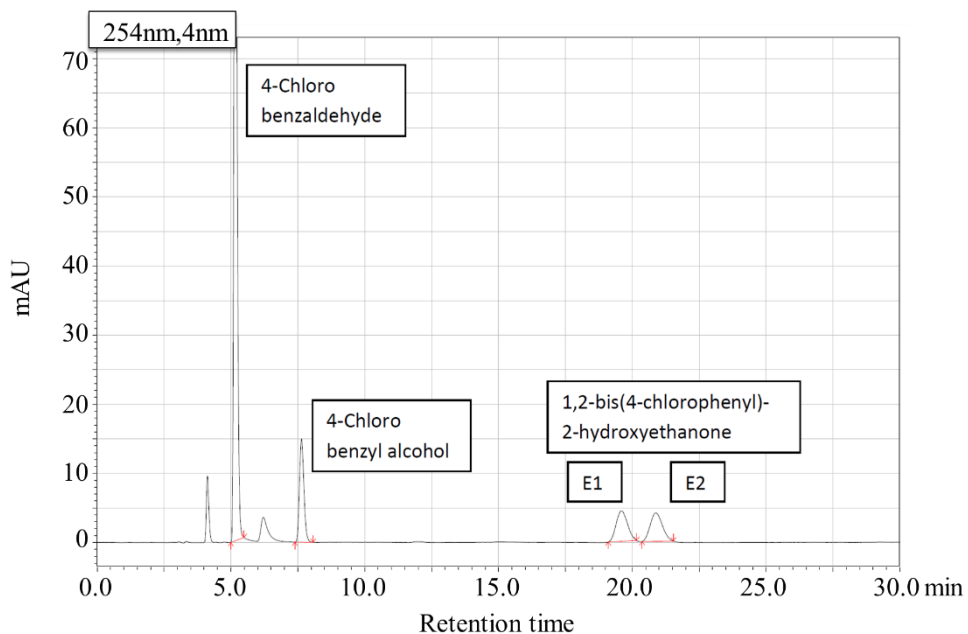
Figure 19 Representative HPLC-chromatogram is showing 4-chloro benzyl alcohol and the two enantiomers of the product 1,2-bis(4-chlorophenyl)-2-hydroxyethanone (E1 and E2).
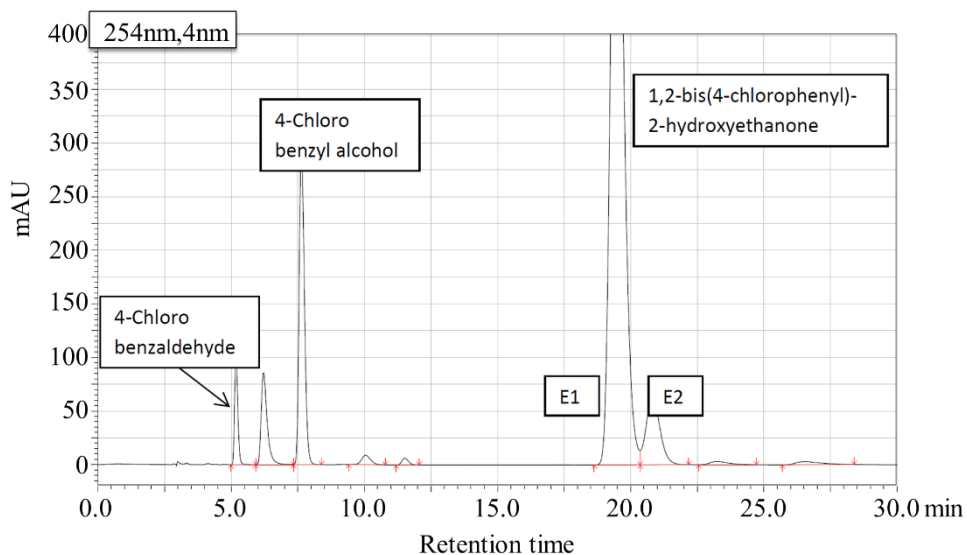
Figure 20 Representative HPLC-chromatogram for the cascade reaction starting from 20 mM 4-chloro benzyl alcohol showing the enantioselective formation of 1,2-bis(4-chlorophenyl)-2-hydroxyethanone after 72 hours. 4-Chloro benzyl alcohol: 7.5 min; 4-Chloro benzaldehyde: 4.7 min; (*R*)- or (*S*)- 1,2-bis(4-chlorophenyl)-2-hydroxyethanone: E1: 19.6 min, E2: 20.9 min.
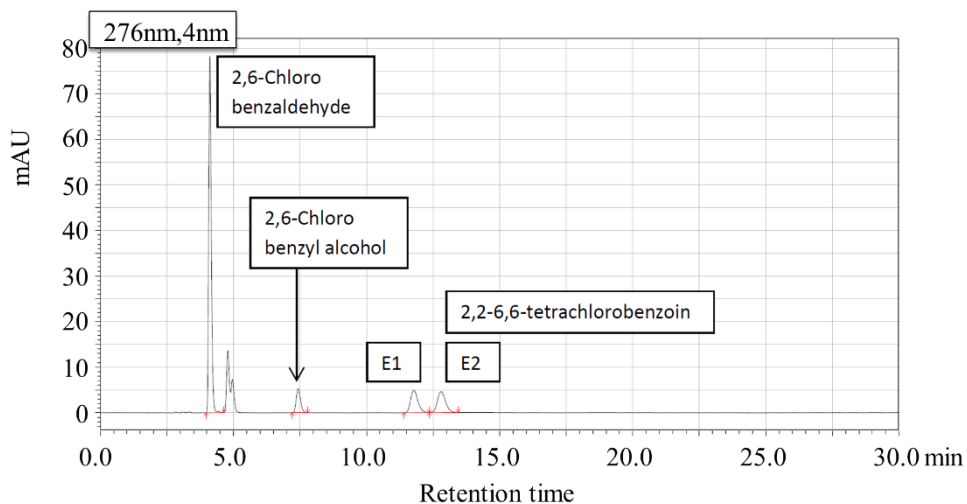
Figure 21 Representative HPLC-chromatogram is showing 2,6-chloro benzyl alcohol and the two enantiomers of the product 2,2-6,6-tetrachlorobenzoin (E1 and E2).
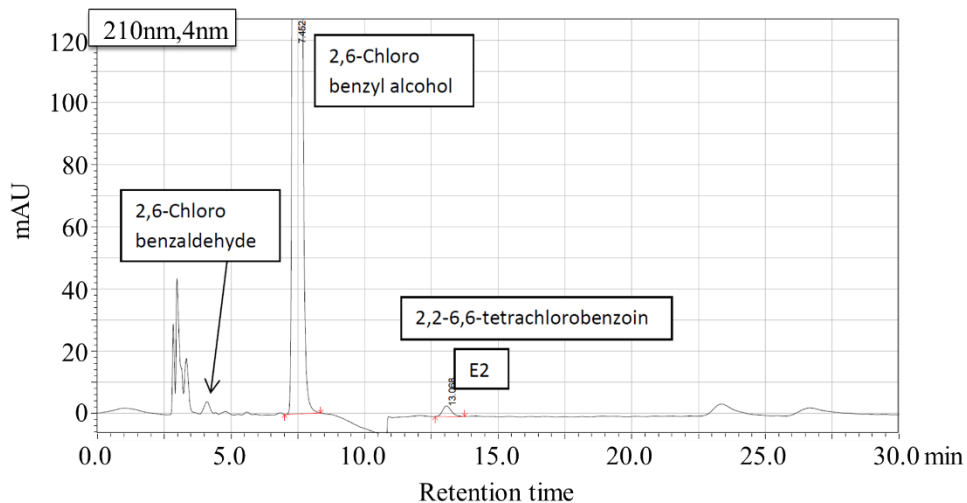
Figure 22 Representative HPLC-chromatogram for the cascade reaction starting from 20 mM 2,6-chloro benzyl alcohol showing the enantioselective formation of 2,2-6,6-tetrachlorobenzoin after 72 hours. 2,6-Chloro benzyl alcohol: 7.4 min; 2,6-Chloro benzaldehyde: 4.6

^{1}H-NMR spectroscopy

All measurements were recorded on a Bruker NMR unit (Bruker, Karlsruhe, Germany) at 400 (^{1}H) MHz. The ^{1}H NMR spectra were recorded either in CDCl$_3$ or deuterated DMSO. The impurities observed in the spectra were identified according to Gottlieb et al. [21]

Representative NMR spectra (Figure 23 to Figure 27)
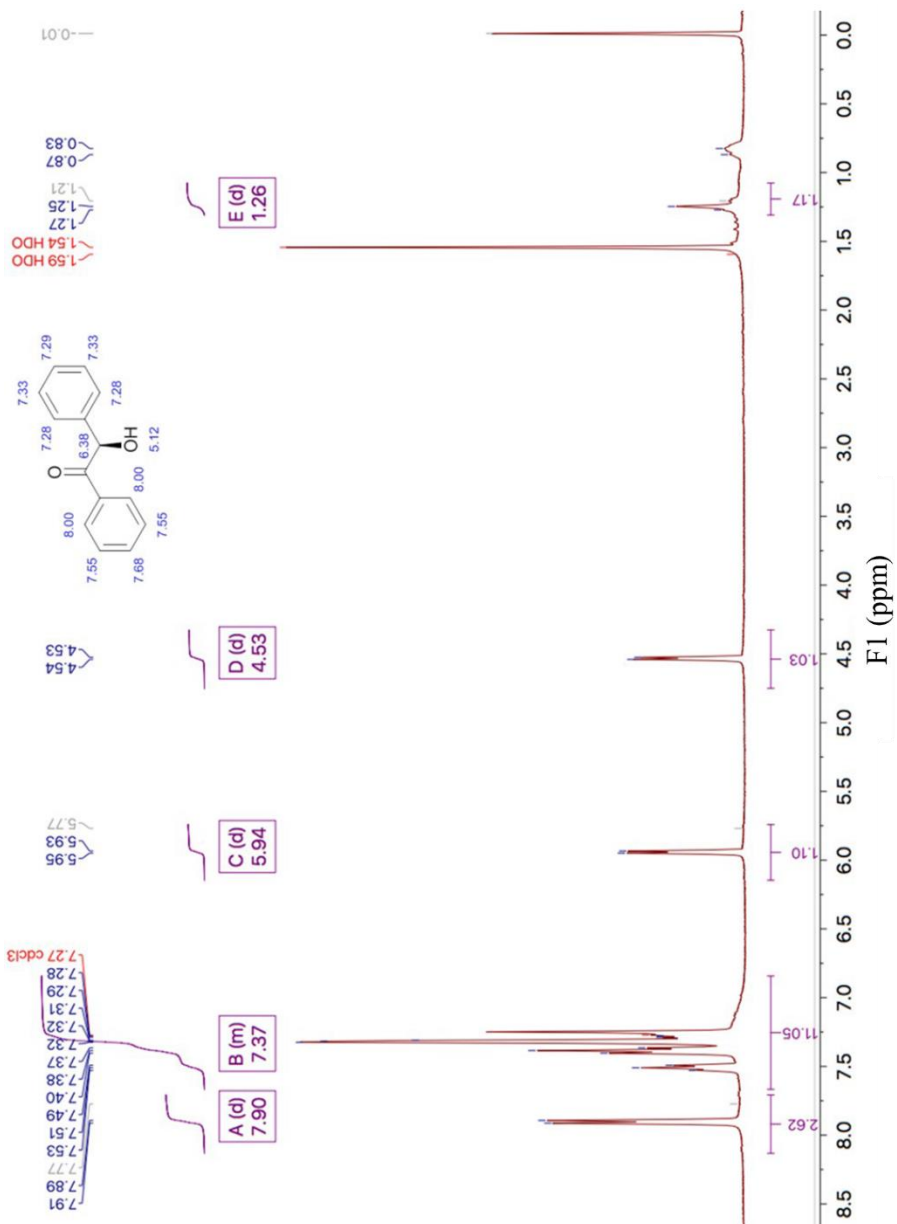
Figure 23 ^{1}H NMR in CDCl$_3$ from the crude (*R*)-benzoin product filtered from the preparative scale synthesis after 96 hours.
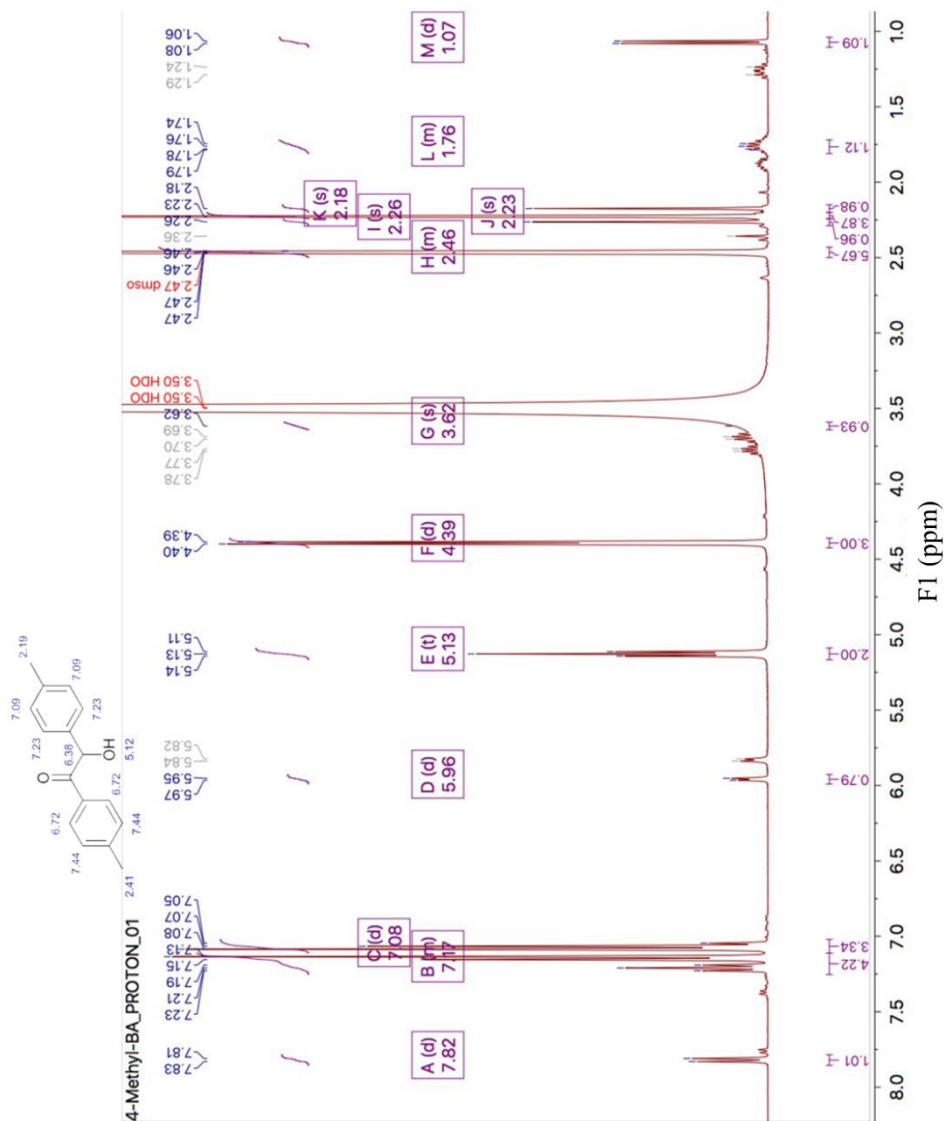
Figure 24 ¹H NMR in DMSO from the crude 4,4-dimethylbenzoin product filtered from biotransformation after 96 hours

Figure 25 ^{1}H NMR in DMSO from the crude 4,4-dimethoxybenzoin product filtered from biotransformation after 96 hours
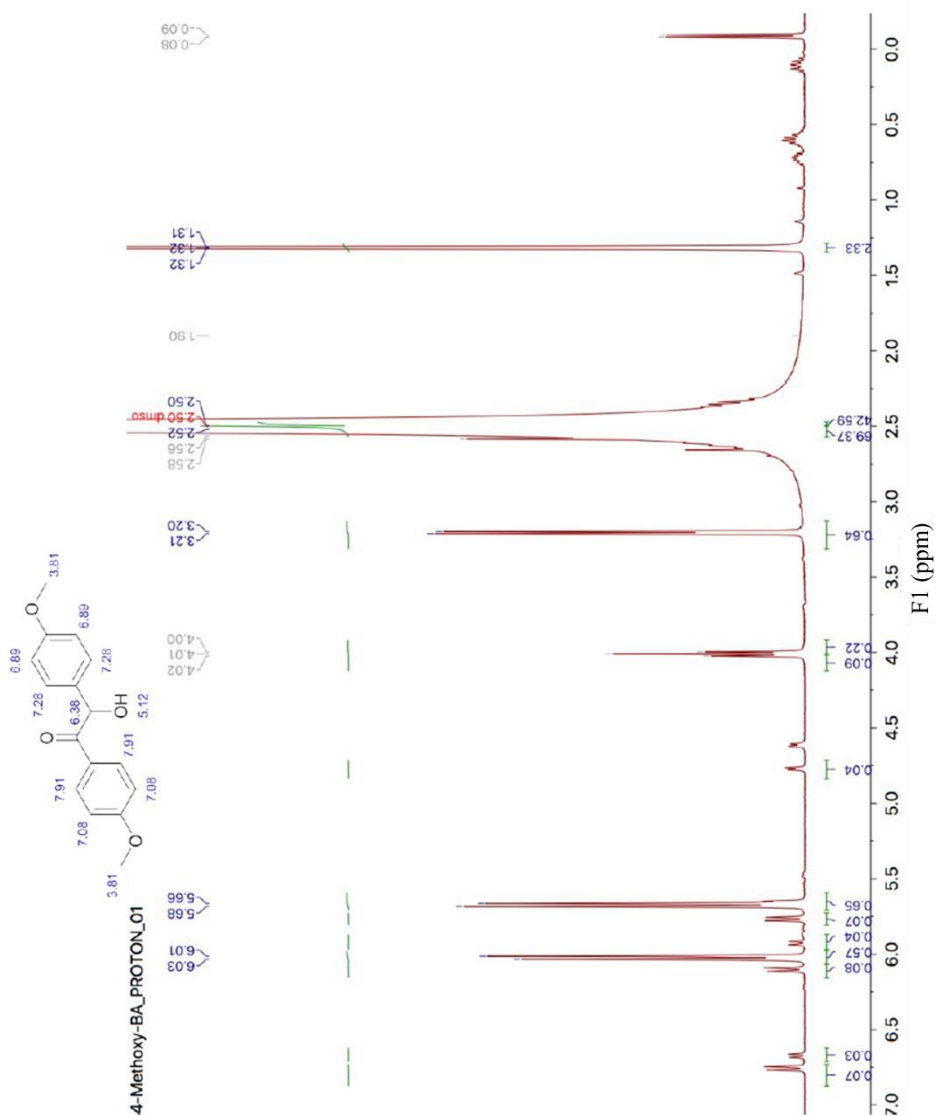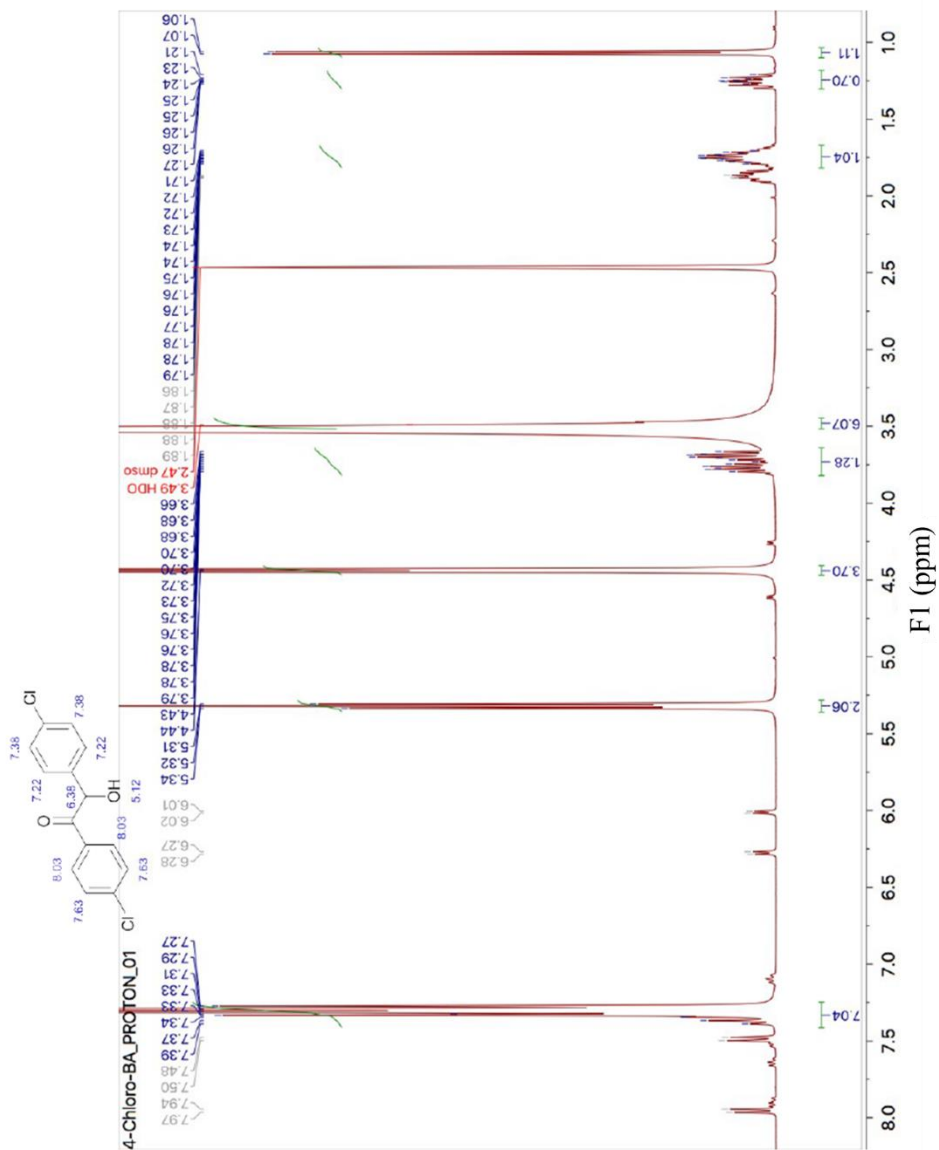
Figure 26 ^{1}H NMR in DMSO from the crude 1,2-bis(4-chlorophenyl)-2-hydroxyethanone product filtered from biotransformation after 96 hours.
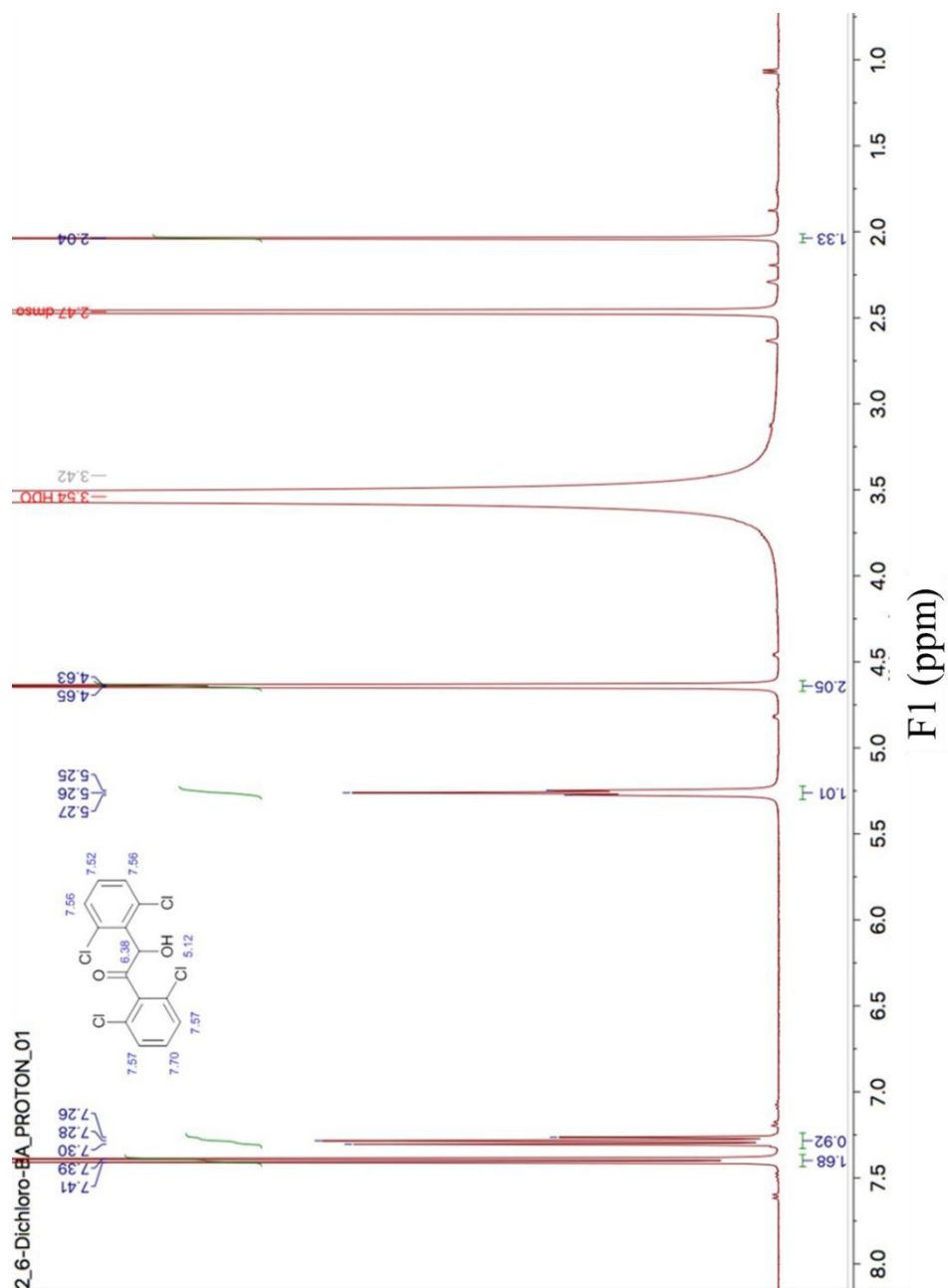
Figure 27 ^{1}H NMR in CDCl$_3$ from the crude (R)-benzoin product filtered from the preparative scale synthesis after 96 hours.

Supporting results (Figure 28 to Figure 30)
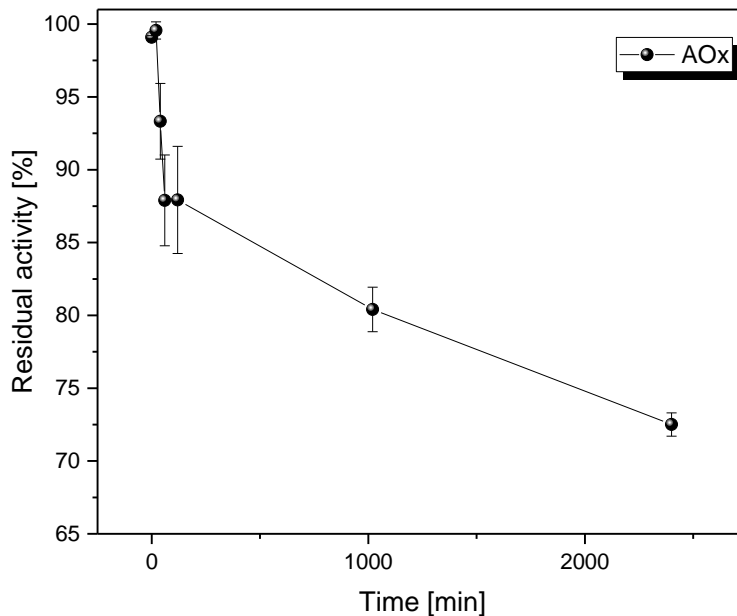
Figure 28 Inactivation of *Pp*AOX during incubation at 30˚C. The activity was measured using the ABTS assay after defined time intervals against benzyl alcohol. Reaction conditions: benzyl alcohol (0.00033% [v/v]), *Pp*AOX (0.5 U, 1.5 mL), horseradish peroxidase (1.25 U, 1.5 mL), 1.86 mM ABTS, sodium phosphate buffer (100 mM, pH 7.5), 30°C for 0-2700 min. Activities were determined spectrophotometrically using the ABTS assay.
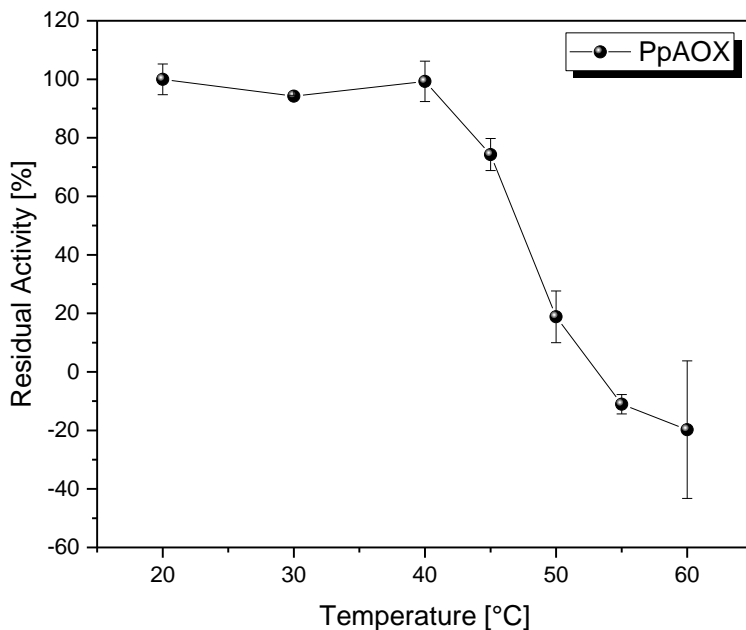
Figure 29 Temperature stability of *Pp*AOX during incubation at various temperatures. The activity was measured using the ABTS assay after incubation of the enzyme for 10 min against benzyl alcohol. Reaction conditions: benzyl alcohol (0.00033% [v/v]), *Pp*AOX (0.5 U, 1.5 mL), horseradish peroxidase (1.25 U, 1.5 mL), 1.86 mM ABTS, sodium phosphate buffer (100 mM, pH 7.5), 20-60°C for 10 min. Activities were determined spectrophotometrically using the ABTS assay.
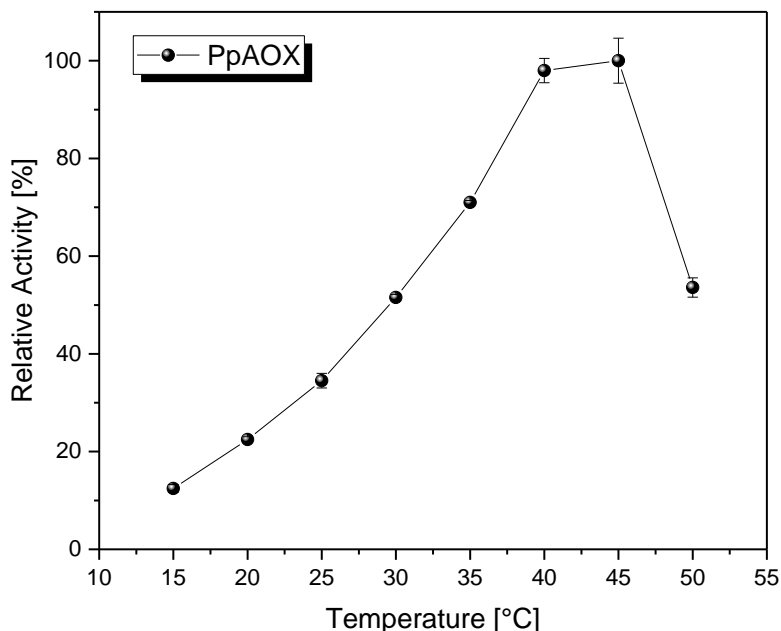
Figure 30 Temperature optimum of *Pp*AOX during incubation at various temperatures. The activity was measured at the respective temperature using the ABTS assay after against benzyl alcohol. Reaction conditions: benzyl alcohol (0.00033% [v/v]), *Pp*AOX (0.5 U, 1.5 mL), horseradish peroxidase (1.25 U, 1.5 mL), 1.86 mM ABTS, sodium phosphate buffer (100 mM, pH 7.5), 15-50°C for 10 min.

Acknowledgments

Contribution to this paper

Almeida T.P. contributed with the Alcohol oxidase analyses before the cascade reaction with *Pf*BAL.

References

1.   Hoyos, P., Sinisterra, J. V., Molinari, F., Alcántara, A. R. & De María, P. D. Biocatalytic strategies for the asymmetric synthesis of α-hydroxy ketones. *Acc. Chem. Res.* **43**, 288–299 (2010).

2.   Streuff, J. An update on catalytic strategies for the synthesis of α- hydroxyketones. *Synlett* **24**, 276–280 (2013).

3.   Wallace, O. B., Smith, D. W., Deshpande, M. S., Polson, C. & Felsenstein, K. M. Inhibitors of Aβ production: Solid-phase synthesis and SAR of α-hydroxycarbonyl derivatives. *Bioorganic Med. Chem. Lett.* **13**, 1203–1206 (2003).

4.   Fang, Q. K. *et al.* Rapid access to enantiopure bupropion and its major metabolite by stereospecific nucleophilic substitution on an α-ketotriflate. *Tetrahedron Asymmetry* **11**, 3659–3663 (2000).

5.   Tanaka, T., Kawase, M. & Tani, S. α-Hydroxyketones as inhibitors of urease. *Bioorganic Med. Chem.* **12**, 501–505 (2004).

6.   Palomo, C., Oiarbide, M. & García, J. M. α-Hydroxy ketones as useful templates in asymmetric reactions. *Chemical Society Reviews* **41**, 4150–4164 (2012).

7.   Giovannini, P. P., Bortolini, O. & Massi, A. Thiamine-Diphosphate-Dependent Enzymes as Catalytic Tools for the Asymmetric Benzoin-Type Reaction. *European Journal of Organic Chemistry*, 4441–4459 (2016).

8.   Janzen, E. *et al.* Characterization of benzaldehyde lyase from Pseudomonas fluorescens: A versatile enzyme for asymmetric C-C bond formation. *Bioorg. Chem.* **34**, 345–361 (2006).

9.   Hailes, H. C. *et al.* Engineering stereoselectivity of ThDP-dependent enzymes. *FEBS J.* **280**, 6374–94 (2013).

10.   Westphal, R. *et al.* A tailor-made chimeric thiamine diphosphate dependent enzyme for the direct asymmetric synthesis of (S)-benzoins. *Angew. Chem. Int. Ed. Engl.* **53**, 9376–9 (2014).

11.   Franken, B., Eggert, T., Jaeger, K. E. & Pohl, M. Mechanism of acetaldehyde-induced deactivation of microbial lipases. *BMC Biochem.* **12**, 10 (2011).

12.   Pérez-Sánchez, M., Müller, C. R. & DomínguezdeMaría, P. Multistep oxidase-lyase reactions: Synthesis of optically active 2-hydroxyketones by using biobased aliphatic alcohols. *ChemCatChem* **5**, 2512–2516 (2013).

13.   Dienys, G., Jarmalavičius, S., Budriene, S., Čitavičius, D. & Sereikaite, J. Alcohol oxidase from the yeast Pichia pastoris - A potential catalyst for organic synthesis. in *Journal of Molecular Catalysis B: Enzymatic* **21**, 47–49 (2003).

14.   Pickl, M., Fuchs, M., Glueck, S. M. & Faber, K. The substrate tolerance of alcohol oxidases. *Applied Microbiology and Biotechnology* **99**, 6617–6642 (2015).

15.   De María, P. D. *et al.* Preparative enantioselective synthesis of benzoins and (R)-2-hydroxy-1- phenylpropanone using benzaldehyde lyase. *J. Mol. Catal. B Enzym.* **38**, 43–47 (2006).

16.   De María, P. D. *et al.* Asymmetric synthesis of aliphatic 2-hydroxy ketones by enzymatic carboligation of aldehydes. *European J. Org. Chem.* 2940–2944 (2007). doi:10.1002/ejoc.200600876

17. Demir, A. S. *et al.* Enantioselective Synthesis of α-Hydroxy Ketones via Benzaldehyde Lyase-Catalyzed C-C Bond Formation Reaction. *Adv. Synth. Catal.* **344**, 96–103 (2002).

18. Hischer, T. *et al.* Stereoselective synthesis of novel benzoins catalysed by benzaldehyde lyase in a gel-stabilised two-phase system. *Tetrahedron* **61**, 7378–7383 (2005).

19. Sheldon, R. A. E factors, green chemistry and catalysis: An odyssey. *Chemical Communications,* 3352–3365 (2008). doi:10.1039/b803584a

20. Ni, Y., Holtmann, D. & Hollmann, F. How green is biocatalysis? to calculate is to know. *ChemCatChem* **6**, 930–943 (2014).

21. Gottlieb, H. E., Kotlyar, V. & Nudelman, A. NMR Chemical Shifts of Common Laboratory Solvents as Trace Impurities. *J. Org. Chem.* **62**, 7512–7515 (1997).

Biocatalytic synthesis of the Green Note *trans*-2-hexen-1-al in a continuous-flow microreactor

3

Introduction

The food and fragrance industry has a great interest in aldehydes compounds due to their participation in aromas and flavors. The routes to obtaining aldehydes are already well established; however, many of them using compounds that are toxic or not environmentally friendly. In this approach, we focused on two biocatalytic approaches available (Scheme 1 A) for the clean conversion of primary alcohols to aldehydes.[1–4] On the first one, the alcohol dehydrogenases catalyzes the reversible oxidation of alcohols in a Meerwein–Ponndorf–Verley-type reaction (Scheme 1 B). Due to the poor thermodynamic driving forces of this reaction, it is necessary to significant molar surpluses of the stoichiometric oxidant (such as acetone). This not only negatively influences the environmental impact of reaction [5] but also complicates downstream processing. Furthermore, the nicotinamide cofactor (even if used in catalytic amounts only) causes additional costs.
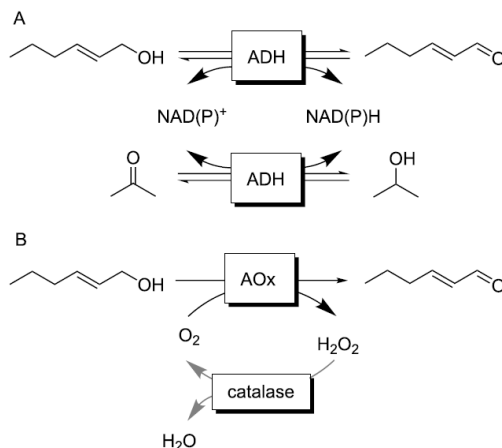
Scheme 1 Enzymatic reaction schemes for the selective oxidation of *trans*-2-hexen-1-ol. A: Alcohol dehydrogenase (ADH)-catalysed oxidation producing stoichiometric amounts of NAD(P)H, which needs to be recycled in situ; the overall reaction is reversible requiring surpluses of the co-substrate (e.g., acetone) to shift the overall equilibrium to the side of *trans*-2-hexen-1-al. B: Envisioned aerobic oxidation using alcohol oxidases (AOx). H_2O_2 is formed as a byproduct and dismutated by catalase into H_2O and O_2.

So we focus on the second approach based on a reaction catalyzed by oxidases (Scheme1 B), which is a class of enzymes that use O_2 as the terminal electron acceptor for the oxidation reaction, yielding H_2O_2 as sole side-product, which can be disproportionated by using catalase (Scheme 1 B). Furthermore, O_2 reduction adds sufficient thermodynamic driving forces to make the reaction essentially irreversible. The benefits of using O_2, however, come with the disadvantage of poor solubility in aqueous media (ca. 0.25 mM at room temperature). Consequently, in the course of an oxidation reaction, dissolved O_2 is rapidly consumed into the reaction medium, and the O_2 diffusion becomes rate-limited to a large extent. The O_2 diffusion rate into the medium directly correlates with the interfacial area between the aqueous medium and the gas phase. Large interfacial surface areas can be achieved via heterogeneous in-take, by

bubbling, stirring, etc. However, soluble enzymes are often rather unstable under these conditions, possibly owing to the mechanical stress that leads to the irreversible inactivation of the biocatalyst.[6,7] Methods of bubble-free aeration have been described in the literature to alleviate the inactivation issue described above.[8–11] The micro-continuous-flow micro-reactor technology has emerged as a safe and scalable way to approach oxidation reactions.[12,13] Due to its small dimensions, hazardous reactions can be easily controlled, owing to the large surface-to-volume ratio, minimizing hot-spot formation and allowing the control over mixing and heating phenomena.[14,15]

Furthermore, a well defined gas-liquid regime can be easily maintained.[16,17] High mass-transfer coefficients are generally the consequence of small vortices induced by the segmented flow regime. The flow pattern guarantees enhanced contact between the two phases and provides a uniform gas concentration in the liquid segment. Therefore, it is not very surprising that the high interest in flow chemistry by the biocatalysis community. Several biocatalytic processes report flow reactors,[18] mostly advocating easier process intensification in combination with enzyme immobilization.[19–22]. Several groups have emphasized the higher oxygen transfer rates in flow reactions compared to batch reactions. Here, reactor designs ranging from simple flow reactors, tube-in-tube reactors,[23] agitated tube reactors,[24,25] and continuous agitated cell reactors[26] have been reported. Encouraged by these contributions, we asked ourselves whether or not a slug-flow approach may combine mechanically less demanding conditions with high O_2-transfer rates. That would enable efficient and robust oxidase-catalyzed oxidation reactions using as model *trans*-2-hexen-1-ol to *trans*-2-hexen-1-al target components of the green

notes of fruits and vegetables surcharge as apples, strawberries, cherries, and more.

Results and discussions

Selection and characterization of the biocatalyst

Here we focus on the recombinant aryl alcohol oxidase from *Pleurotus eryngii* (*Pe*AAOx) as biocatalyst.[27–30] The promising activity on allylic alcohols makes *Pe*AAOx a promising starting point, especially the availability of recombinant enzyme enabling future at-scale production and protein engineering. Commercially available alcohol oxidases from *Pichia pastoris* and *Candida boidinii* showed no significant activity for the substrate under the same conditions. As *trans*-2-hexen-1-ol had not been reported as a substrate for *Pe*AAOx, we evaluated its catalytic properties, particularly the substrate concentration-dependency of the enzymatic oxidation. Initial rate measurements (performed in 1 mL cuvettes) revealed a Michaelis–Menten dependency of the enzyme activity (Figure 1). Apparent KM and k_{cat} values of approximately 1 mM and 22 s^{-1} were estimated, respectively.
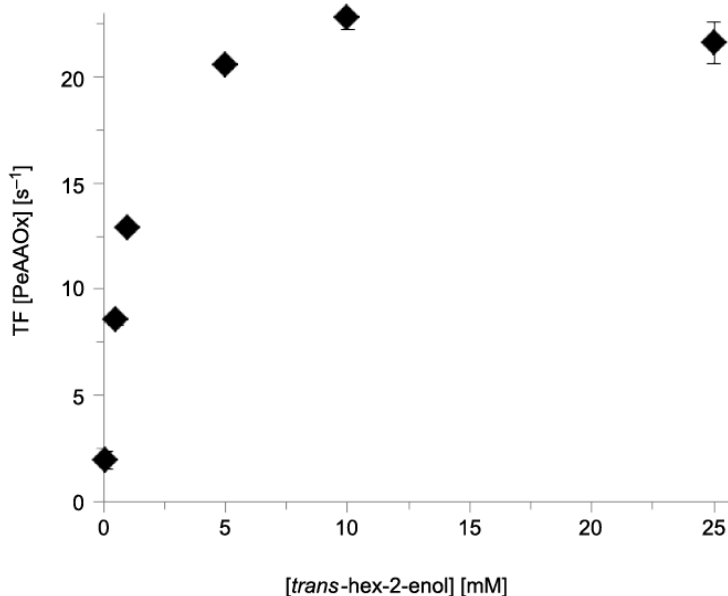
Figure 1 Michaelis–Menten kinetics of the *Pe*AAOx-catalysed oxidation of *trans*-2-hexen-1-ol. Conditions: 50 mM KPi buffer (pH 7, 30 °C), [*trans*-2-hexen-1-ol] = 3 mM, [*Pe*AAOx] = 0.044 µM, [horseradish peroxidase] = 500 U mL^{-1}, [ABTS] = 2 mM.

These values are in the same order of magnitude as those previously reported for benzyl alcohol substrates.[28] The slightly decreasing enzyme activity at elevated substrate concentrations may be indicative of slight substrate inhibition. We observed a pronounced product inhibition by performing these initial rate measurements in the presence of varying product concentrations (Figure 2).
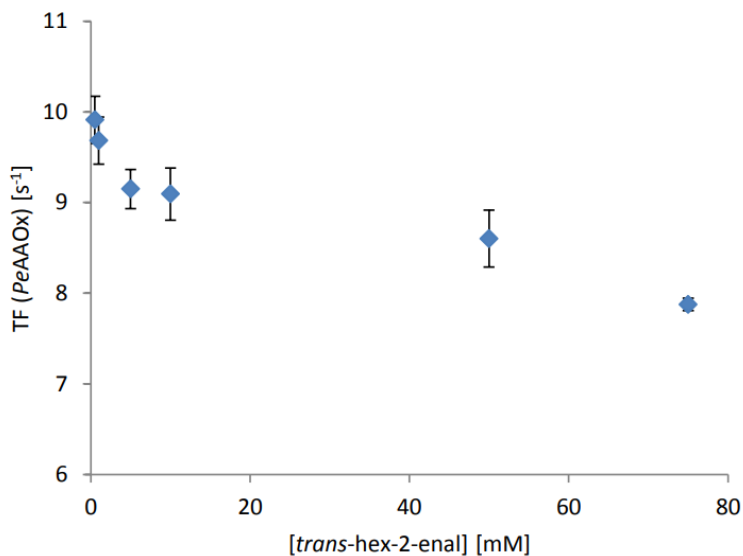
Figure 2 The residual activity of *Pe*AAOx in the presence of the product *trans*-2-hexen-1-al. Conditions: 50 mM KPi buffer (pH 7, 20 °C), [*trans*-2-hexen-1-ol] = 3 mM, [*Pe*AAOx] = 0.044 µM, [horseradish peroxidase] = 500 U ml^{-1} , [ABTS] = 2 mM.

Continuous-flow reactor enzymatic oxidation

We also performed the *Pe*AAOx-catalysed oxidation of *trans*-2-hexen-1-ol in a slug-flow reactor setup (Scheme 2 and Figure 10, Figure 11, Figure 12Figure).
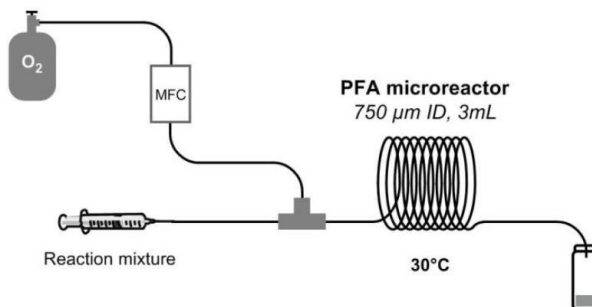
Scheme 2 - View of the reaction setup. The oxygen gas flow was controlled by a mass flow controller (MFC), and a syringe pump controlled the reaction mixture flow. The sample was collected on ice or directly in ethyl acetate at the end of the reactor.

In the first set of experiments, we systematically varied the residence time of the reaction mixture in the flow reactor (and thereby the reaction time, Figure 3).
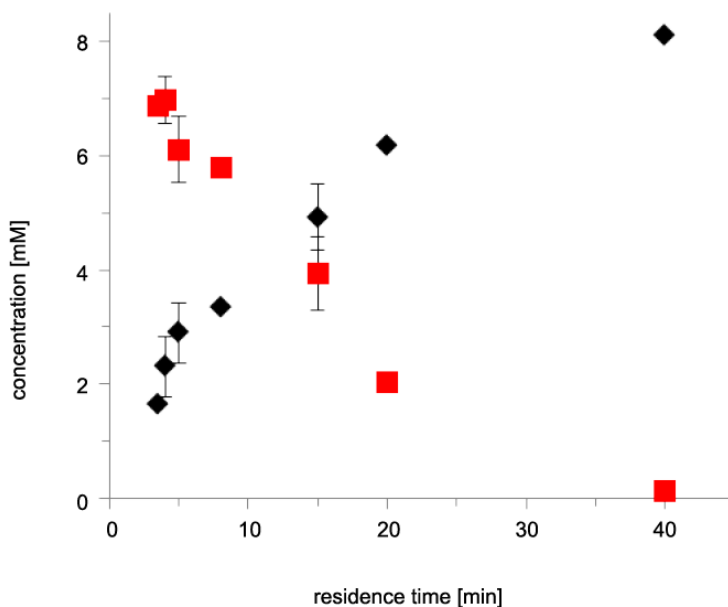
Figure 3 The influence of the residence time on the conversion of *trans*-2-hexen-1-ol (red squares) to *trans*-2-hexen-1-al (black diamonds) in a flow reactor. Conditions: 3 mL flow reactor, 50 mM KPi buffer (pH 7, 30 °C), [*trans*-2-hexen-1-ol] = 10 mM, [*Pe*AAOx] = 0.25 μM, [catalase] = 600 U mL^{-1}.

A full conversion of the starting material into the desired *trans*-2-hexen-1-al was observed at residence (reaction) times of approximately 40 min, corresponding to a turnover number (TN) for the biocatalysts of 32400 and an average turnover frequency (TF) of 13.5 s^{-1}. Even more interestingly, at higher flow rates, an apparent TF of up to 38 s^{-1} (RT = 5 min) was observed. This value exceeds significantly the previously determined k_{cat} (*Pe*AAOx) (Figure 1). We attributed this observation to an increased oxygen-transfer rate at high flow rates. In the case of 5 minutes of residence time, this corresponds to an O$_2$-transfer rate of roughly 0.25 mM min^{-1}. Similarly, high values could be obtained previously only under

mechanically demanding reaction conditions or using surfactant-stabilized emulsions.[6] We did not observe a significant effect on the overall rate of the reaction by varying the ratio of gas to liquid (Table 1).

Table 1 Effect of variation of the gas-to-liquid ratio on the rate of the *Pe*AAOx-catalysed aerobic oxidation of *trans*-2-hexen-1-ol.

ratio (liquid:gas)	liquid flow [mL min^{-1}]	gas flow [mL min^{-1}]	residence time [min]	[product] [mM]
1:1	0.20	0.20	15	5.48 (± 0.01)
1:3	0.10	0.30	15	5.18 (± 0.32)
1:5	0.067	0.333	16	4.99 (± 0.49)

Conditions: 3 mL flow reactor, 50 mM KP$_i$ buffer (pH 7, 30 °C), [*trans*-2-hexen-1-ol]$_0$ = 10 mM, [*Pe*AAOx] = 0.25 µM, [catalase] = 600 U mL^{-1}.

Within the experimental error, the conversion in all experiments was identical, indicating that even at a comparably low volumetric ratio (1:1), the O_2 availability was already sufficient not to be overall rate-limited. It is worth mentioning that under batch reaction conditions, similar progression curves were only attainable under very demanding mechanical conditions (i.e., very vigorous stirring and bubbling of O_2 directly into the reaction mixture, Figure 4).
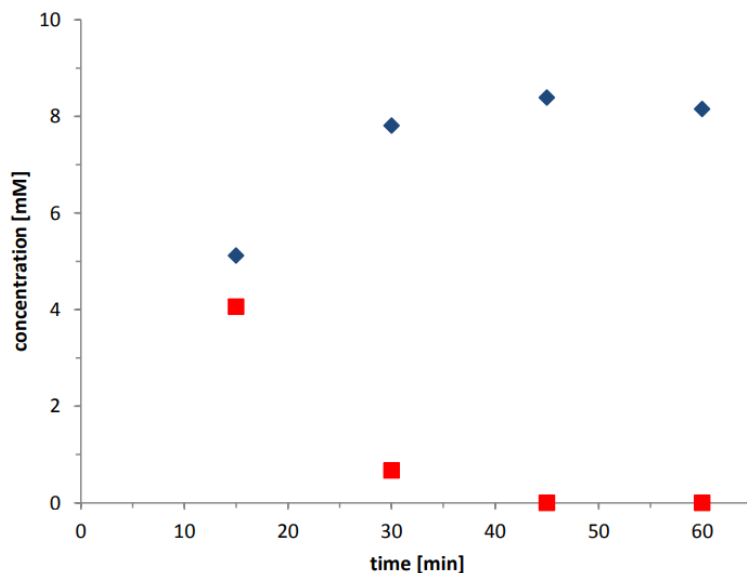
Figure 4 The conversion of *trans*-2-hexen-1-ol (′) to *trans*-2-hexen-1-al (↵) in a batch reactor, with vigorous stirring and oxygen bubbling through the solution. Conditions: 5 mL batch reaction, 50 mM KPi buffer (pH 7, 30 °C), [*trans*-2-hexen-1-ol]0 = 10 mM, [*Pe*AAOx] = 0.25 µM, [catalase] = 600 U ml^{-1} , stirring at 1000 rpm, pure oxygen supplied by a balloon.

These conditions also caused significant evaporation of the substrate at higher substrate concentration (Figure 5), which was much less the case in the flow-reaction setup.
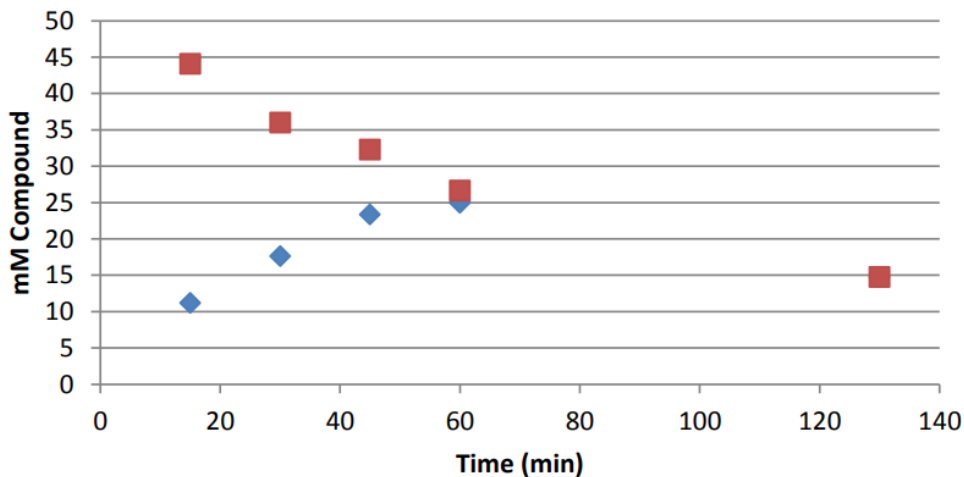
Figure 5 The conversion of 50 mM of *trans*-2-hexen-1-ol to *trans*-2-hexen-1-al (◆) in a batch reactor, with vigorous stirring and oxygen bubbling through the solution. The mass balance over time is also shown (■). Conditions: 5 mL batch reaction, 50 mM KPi buffer (pH 7, 30 °C), [*trans*-2-hexen-1-ol] = 50 mM, [*Pe*AAOx] = 0.25 µM, [catalase] = 600 U ml^{-1} , stirring at 1000 rpm, pure oxygen supplied by a balloon.

From an economic point-of-view, the catalyst performance in terms of turnover number (TN) is of utmost importance as it directly correlates with the cost-contribution of the catalyst to the production costs.[31–33] Therefore, we evaluated the TN attainable for *Pe*AAOx in the flow setup (Figure 6). For the lower *Pe*AAOx concentration as well as significantly increased residence times were applied. The increased residence times were achieved by decreasing the flow rates and using a longer flow reactor (6 mL volume instead of 3 mL).
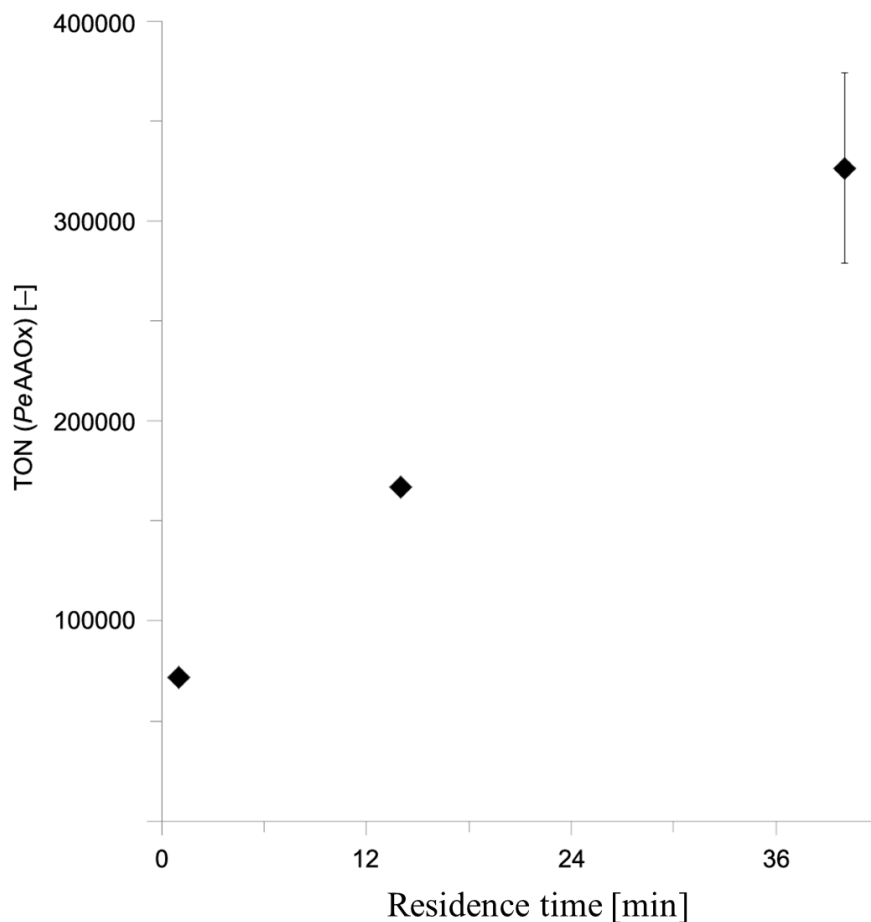
Figure 6 Increasing the PeAAOx turnover numbers (TN) by increasing the residence time. Conditions: 6 mL flow reactor, 50 mM KPi buffer (pH 7, 30 °C), [*trans*-2-hexen-1-ol]0 = 40 mM, [*Pe*AAOx] = 0.02 μM, [catalase] = 600 U mL^{-1}. The TN value was calculated based on the GC yield of every run. The TN was obtained by dividing the product concentration (determined chromatographically) by the biocatalyst concentration.

Pleasingly, we observed a TN higher than 300 000 for the enzyme at long residence times already in the first experiments. This also underlines the robustness of the enzyme under flow conditions. Compared to Figure 3,

somewhat lower TFs for *Pe*AAOx were observed here, which again can be attributed to a lower O_2-transfer rate at lower flow rates. The quasi-linear relationship shown in Figure 6 also suggests that even higher TN may be attainable, however, at the expense of longer reaction times. Therefore, further investigations will focus on identifying conditions satisfying the demand for high TNs and short reaction times. Encouraged by these results, we also tried a semi-preparative scale reaction using 5 g L^{-1} (50 mM) substrate loading in a total of 50 mL with 0.75 µM *Pe*AAOx. As a result, 90% conversion was achieved after 18 h of total reaction time (roughly 80 minutes of residence time in the 6 mL reactor). The product was purified chromatographically, resulting in 200 mg of pure *trans*-2-hexen-1-al (as determined by NMR) in 81% isolated yield, thereby demonstrating the preparative potential of the proposed reaction setup.

Conclusions

Alcohol oxidase-catalyzed oxidation of alcohols to aldehydes bears significant potential for preparative biocatalysis. The reaction does not depend on expensive and unstable nicotinamide cofactors, and the corresponding co-substrates/co-products as well as possible regeneration enzymes, producing only water as a by-product. These advantages, however, are counteracted by the generally low reaction rates caused by the poor O_2 availability. Flow chemistry is a promising technique to provide the aqueous reaction mixture with O_2 needed for the oxidation. It enables high O_2 transfer rates while avoiding enzyme robustness issues frequently observed with 'traditional' aeration methods. Future developments in our laboratories will concentrate on the characterization, extension, and

preparative demonstration of such a powerful combination of oxidase catalysis and flow chemistry.

Experimental section

General information

All reagents and solvents were used as received without further purification unless otherwise stated. Technical solvents were purchased from VWR International and Biosolve and used as received. All capillary tubing and microfluidic fittings were purchased from IDEX Health & Science. The syringes used were BD Discardit II® or NORM-JECT®, purchased from VWR Scientific. Syringe pumps were purchased from Chemix Inc. model Fusion 200 Touch. The mass flow controller (EL-FLOW) was purchased from Bronkhorst.

The product isolation was performed automatically by a Biotage® Isolera Four, with Biotage® SNAP KP-Sil 10 or 25 g flash chromatography cartridges. TLC analysis was performed using silica on aluminum foils TLC plates (F254, Supelco Sigma- S3 Aldrich™), with visualization under ultraviolet light (254 nm and 365 nm) or appropriate TLC staining. ^{1}H (400 MHz) and ^{13}C (100 MHz) NMR spectra were recorded at ambient temperature using a Bruker-Avance 400 or Mercury 400. ^{1}H NMR spectra are reported in parts per million (ppm) downfield relative to CDCl$_3$ (7.26 ppm), and ^{13}C NMR spectra are reported in ppm relative to CDCl3 (77.2 ppm) unless stated otherwise. NMR signals multiplicities are reported using the following abbreviations: s = singlet, d = doublet, t = triplet, q = quartet, p = pentet, h = hextet, hept = heptet, m = multiplet, dd = double doublet, td = triple doublet. NMR data were processed using the MestReNova 9.0.1

software package. Known products were characterized by comparison with the corresponding ^{1}H NMR and ^{13}C NMR reported in the literature. GC analyses were performed on a Shimadzu GC-2014 with an autosampler unit (AOC-20i). The names of all products were generated using the PerkinElmer ChemBioDraw Ultra v.12.0.2 software package.

General

Turnover numbers (TN) and turnover frequencies (TF) reported in this manuscript were calculated based on Equation 1 and Equation 2.

$$\text{TN}\,[-] = \frac{c(\text{product})}{c(\text{PeAAOx})} \qquad (1)$$

$$\text{TF}\,[\text{s}^{-1}] = \frac{\text{TN}}{\text{reaction time}} \qquad (2)$$

Production of PeAAOx

E. coli cultivation

For the production, activation, and purification of *Pe*AAOx, a slightly modified literature protocol was used.[27] Pre-cultures of LB media containing 100 µg mL^{-1} of ampicillin were inoculated with E. coli W3110 containing *p*FLAG1-AAO and incubated overnight at 37 °C and 180 rpm. Overexpression was carried out in 5 L flasks with 1 L of TB medium supplemented with 100 µg mL^{-1} of ampicillin. The medium was inoculated with the pre-culture to an OD of 0.05 and grown at 37 °C and 180 rpm. At an OD$_{600}$ of 0.8, 1 mM isopropyl β-D-thiogalactopyranoside (IPTG) was added, and the cultures were incubated for an additional 4 h at 37 °C and

180 rpm. The bacterial pellets, obtained after harvesting the cells, were resuspended in a total volume of 40 mL 50 mM Tris/HCl buffer, pH 8.0, containing 10 mM EDTA and 5 mM dithiothreitol (DTT).

Refolding

The re-suspended cells were disrupted by incubation with 2 mg mL^{-1} lysozyme for 1 h at 4 °C. Afterward, 0.1 mg mL^{-1} DNase, 1 mM MgCl$_2$, and 0.1 mM PMSF were added followed by sonication. The insoluble fraction was collected by centrifugation (30 min at 15,000 rpm and 4 °C), re-suspended and washed three times with 20 mL 20 mM Tris/HCl buffer, pH 8.0, containing 10 mM EDTA and 5 mM DTT using a potter homogenizing device. The pellets obtained after centrifugation (15 min at 15,000 rpm and 4 °C) were solubilized in a total volume of 30 mL 20 mM Tris/HCl buffer, pH 8.0, containing 2 mM EDTA, 50 mM DTT and 8 M urea. After incubation on ice for 30 min, the solution was cleared by centrifugation (15 min at 15,000 rpm and 4 °C). The obtained supernatant was used as a stock solution for the in vitro refolding. The *Pe*AAOx was solubilized using 150 µg mL^{-1} protein in 20 mM Tris/HCl buffer, pH 9.0, containing 2.5 mM GSSG, 1 mM DTT, 0.02 mM FAD, 34% glycerol and 0.6 M urea at 4 °C for 80 h. After the incubation for *Pe*AAOx activation/refolding, the refolding mixture was concentrated to 100 mL, and the buffer exchanged against 10 mM sodium phosphate buffer, pH 5.5 by diafiltration (DV 20) and, subsequently, concentrated with an Amicon Ultra 15 mL centrifugal filter (MWCO 10 kDa). After centrifugation (overnight at 15,000 rpm and 4 °C), the soluble fraction was further purified using anion exchange chromatography.

Purification

The concentrated *Pe*AAOx solution was purified using a 58 mL Q Sepharose column (GE Healthcare). *Pe*AAOx was eluted with a linear NaCl gradient (0–0.6 M over 6 CV) using 10 mM sodium phosphate buffer, pH 5.5. Fractions containing *Pe*AAOx were pooled, concentrated, and desalted using HiTrap desalting columns (GE Healthcare) and 10 mM sodium phosphate buffer, pH 5.5. The *Pe*AAOx concentration was calculated based on the absorbance using the molar extinction coefficient of ε_{463} 11,050 M^{-1} cm^{-1}.

Activity assay

The activity of *Pe*AAOx was determined by UV–vis spectroscopy, using an Agilent Cary 60 UV–vis spectrophotometer, following the oxidation of ABTS ($\varepsilon_{405} = 36{,}800$ M^{-1} cm^{-1}) by horseradish peroxidase (POD) at the expense of hydrogen peroxide. In general, 0.044 µM *Pe*AAOx was used to convert 3 mM of *trans*-2-hexen-1-ol. The hydrogen peroxide formed in this reaction was subsequently used to convert 2 mM of ABTS to ABTS$\cdot^{+}$ by an excess of POD (500 U mL^{-1}). The reactions were performed at 30 °C in an oxygen-saturated 50 mM KPi buffer at pH 7.0.

Flow reactor experiments

PFA microreactor coils (750 µm ID) with a volume of 3 and 6 mL were constructed. The reaction mixture was introduced via a syringe pump (Fusion 200, Chemyx), while the pure oxygen flow was controlled by a mass flow controller (ELFLOW, Bronkhorst), resulting in a segmented flow (Figure 7).
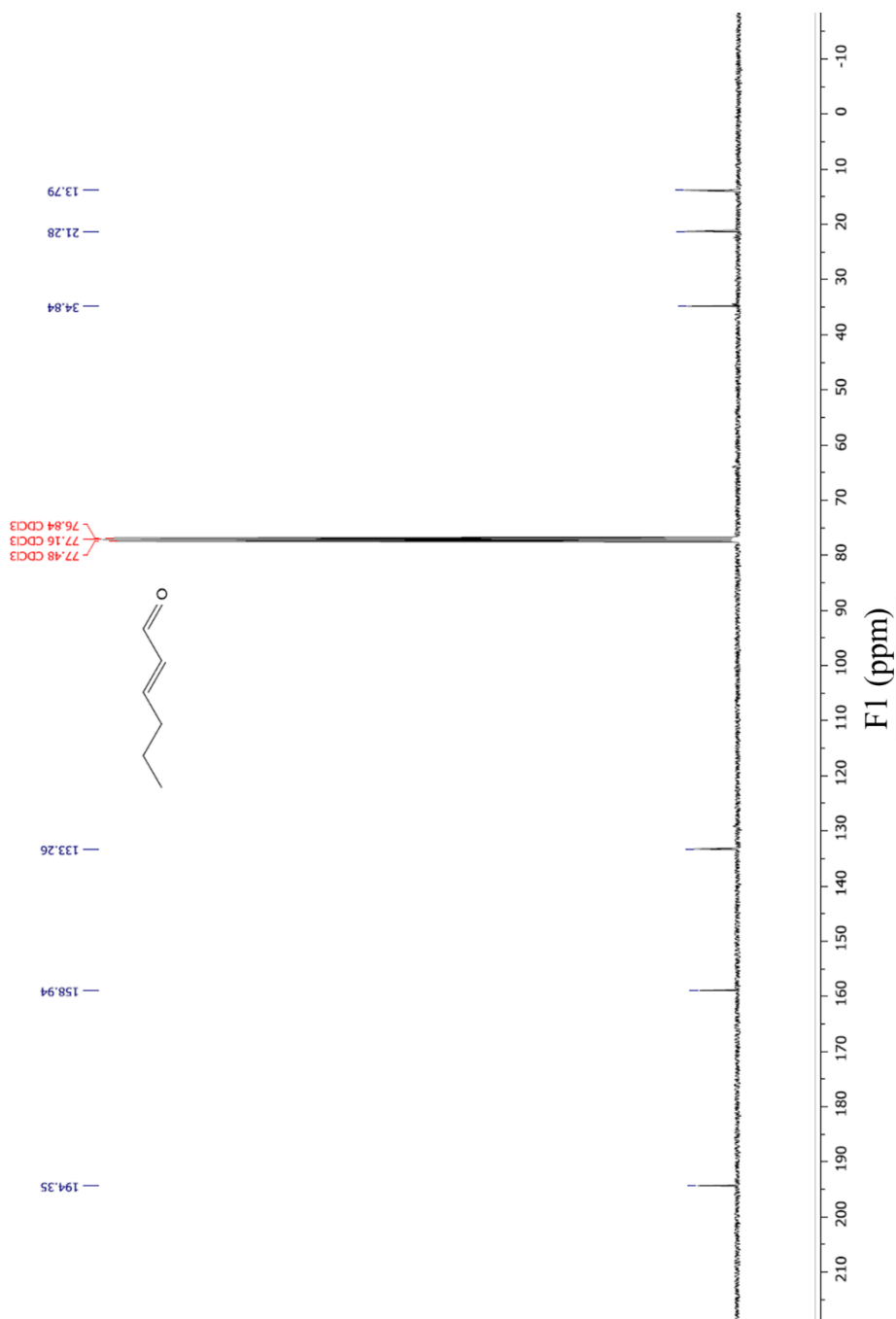
Figure 7 ^{13}C NMR of the product after purification.

We measured the residence times as the time between the inlet and outlet of the solution in the coil, which was varied by altering the flow and keeping the ratio of oxygen to liquid in three to one. Samples were collected on ice, and as soon as enough volume was collected, it was extracted with ethyl acetate and analyzed by GC (vide infra).

GC analysis

The collected reaction mixtures were extracted into an equal volume of ethyl acetate, dried with magnesium sulfate and analyzed on a CP-wax 52 CB GC column (50 m × 0.53 m × 2 µm) (GC method: 60 °C for 3 min; 30 °C.min^{-1} to 105 °C; 105 °C for 7 min; 30 °C .min^{-1} to 250 °C; 250 °C for 1 minute). Dodecane (5 mM) was added as standard.

Work-up semi-preparative scale

The reaction mixture was directly collected in deuterated chloroform at the end of the flow reactor, followed by NMR spectrum to evaluate the conversion (Figure 8 and Figure 9).

Figure 8 ^{1}H NMR spectrum of the reaction mixture prior to purification
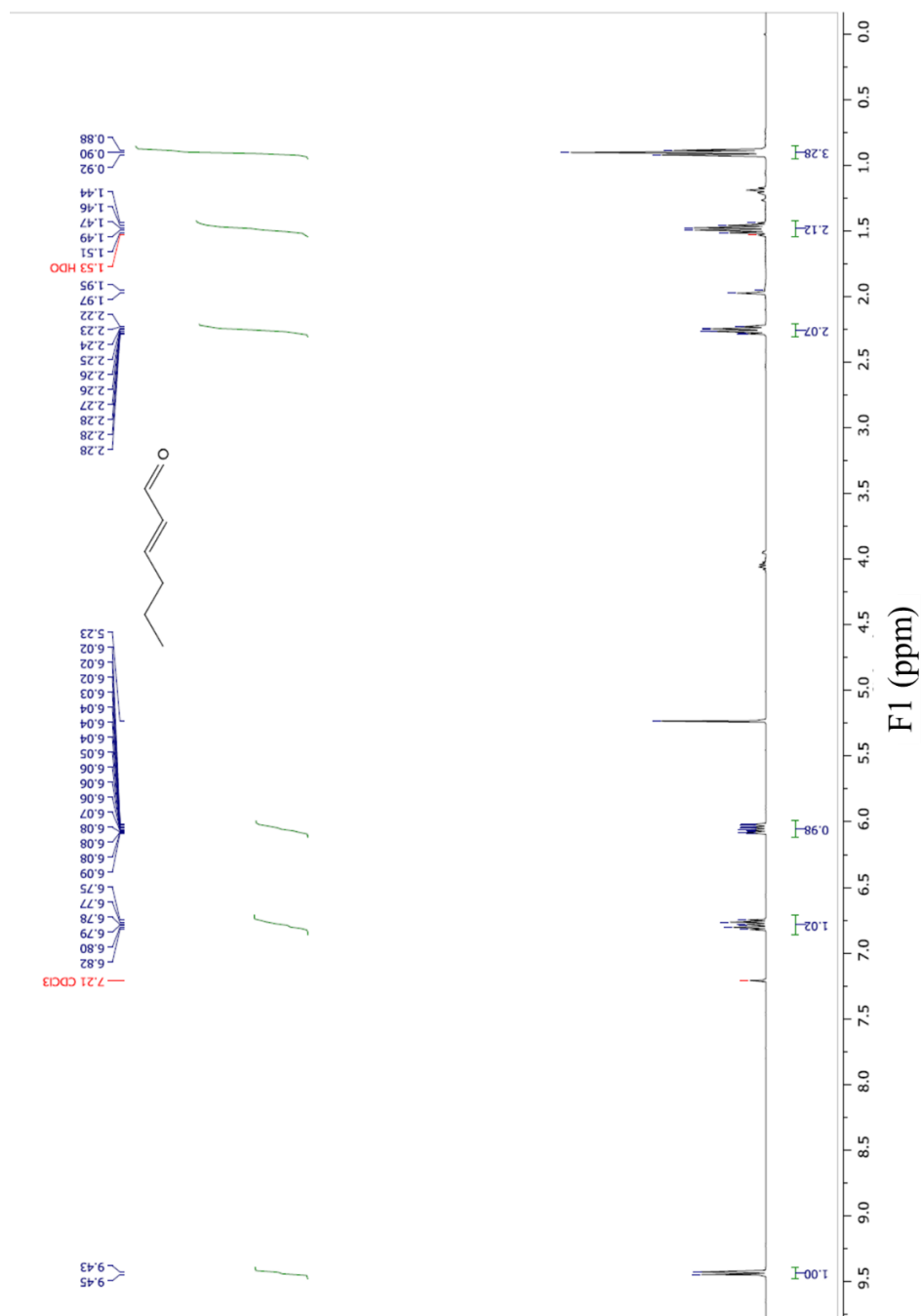
Figure 9 ^{1}H NMR of the product after purification.

The organic mixture was diluted and introduced into a separation funnel and washed with brine. The aqueous phase was backwashed once with DCM. The collected organic phase was dried over $MgSO_4$, filtered, and concentrated under reduced pressure. Purification of the isolated mixture was performed by flash chromatography on silica (pure DCM). The final product was obtained as a colorless oil (200 mg).

(E)-Hex-2-enal

TLC (DCM) R_f 0.9; ^{1}H NMR (399 MHz, CDCl3) δ 9.44 (d, J = 7.7 Hz, 1H), 6.78 (dt, J = 15.6, 6.8 Hz, 1H), 6.05 (ddq, J = 15.5, 7.8, 1.3 Hz, 1H), 2.33–2.18 (m, 2H), 1.48 (h, J = 7.4 Hz, 2H), 0.90 (t, J = 7.4 Hz, 3H); ^{13}C NMR (101 MHz, CDCl3) δ 194.3, 158.9, 133.3, 34.8, 21.3, 13.8.

Photographs of the experimental setup.
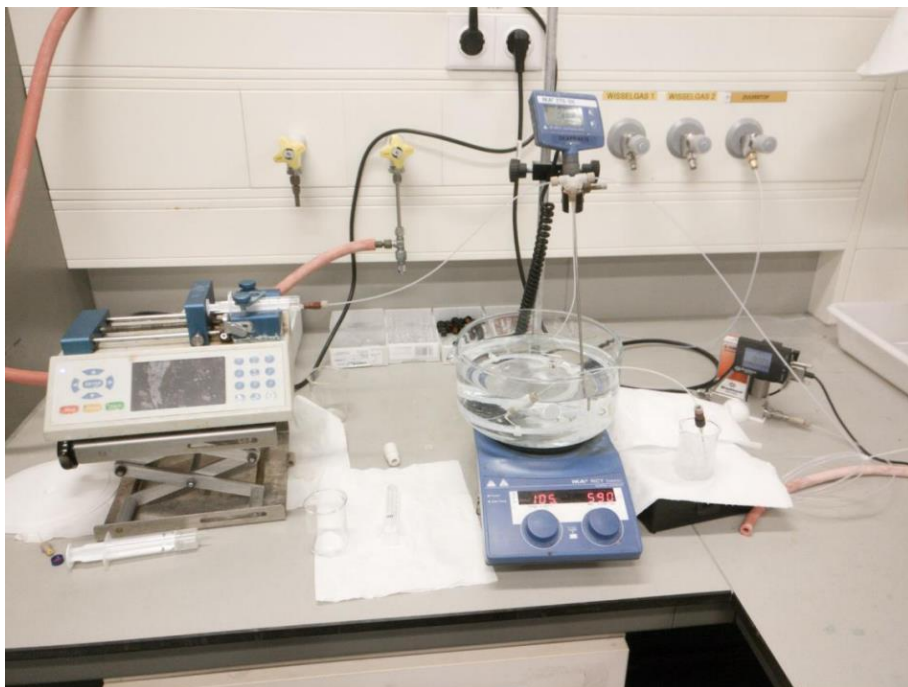
Figure 10 Overview of the flow setup.
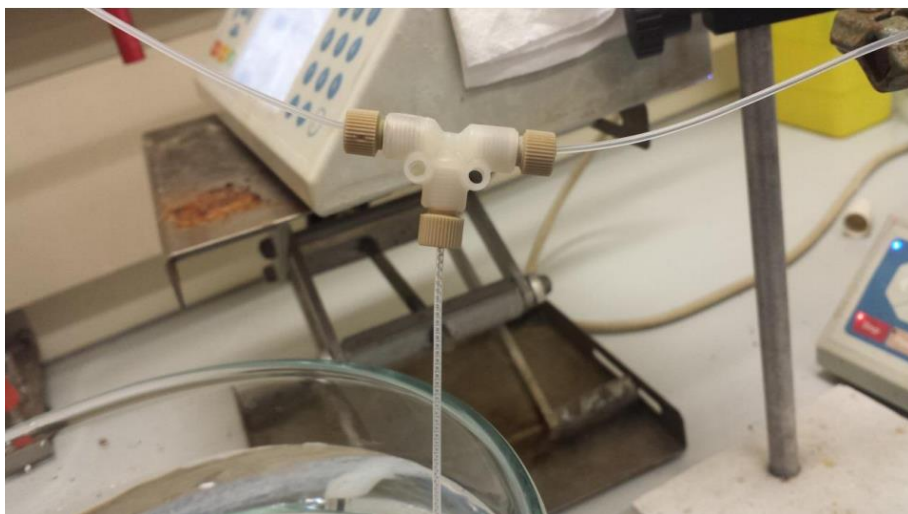
Figure 11 Mixing the two phases.

Figure 12 Image of the segmented flow at an oxygen liquid ratio of three to one at the beginning of the reactor.

Acknowledgments

Contribution to this paper

Almeida T.P. contributed with part of the aryl-alcohol oxidase production and with part of the analyses in a batch reactor.

References

1.   Turner, N. J. Enantioselective Oxidation of C-O and C-N bonds using oxidases. *Chemical Reviews* **111**, 4073–4087 (2011).

2. Hollmann, F., Arends, I. W. C. E., Buehler, K., Schallmey, A. & Bühler, B. Enzyme-mediated oxidations for the chemist. *Green Chem.* **13**, 226–265 (2011).

3. Kroutil, W., Mang, H., Edegger, K. & Faber, K. Recent advances in the biocatalytic reduction of ketones and oxidation of sec-alcohols. *Current Opinion in Chemical Biology* **8**, 120–126 (2004).

4. Pickl, M., Fuchs, M., Glueck, S. M. & Faber, K. The substrate tolerance of alcohol oxidases. *Applied Microbiology and Biotechnology* **99**, 6617–6642 (2015).

5. Ni, Y., Holtmann, D. & Hollmann, F. How green is biocatalysis? to calculate is to know. *ChemCatChem* **6**, 930–943 (2014).

6. Churakova, E., Arends, I. W. C. E. & Hollmann, F. Increasing the Productivity of Peroxidase-Catalyzed Oxyfunctionalization: A Case Study on the Potential of Two-Liquid-Phase Systems. *ChemCatChem* **5**, 565–568 (2013).

7. Bommarius, A. S. & Karau, A. Deactivation of Formate Dehydrogenase (FDH) in solution and at gas-liquid interfaces. *Biotechnol. Prog.* **21**, 1663–1672 (2005).

8. Van Hecke, W. *et al.* Bubble-free oxygenation of a bi-enzymatic system: Effect on biocatalyst stability. *Biotechnol. Bioeng.* **102**, 122–131 (2009).

9. Van, W. *et al.* Kinetic modeling of a bi-enzymatic system for efficient conversion of lactose to lactobionic acid. *Biotechnol. Bioeng.* **102**, 1475–1482 (2009).

10. Illner, S., Hofmann, C., Löb, P. & Kragl, U. A falling-film microreactor for enzymatic oxidation of glucose. *ChemCatChem* **6**, 1748–1754 (2014).

11. Kaufhold, D. *et al.* Generation of Dean vortices and enhancement of oxygen transfer rates in membrane contactors for different hollow fiber geometries. *J. Memb. Sci.* **423**–**424**, 342–347 (2012).

12. Gemoets, H. P. L. *et al.* Liquid phase oxidation chemistry in continuous-flow microreactors. *Chemical Society Reviews* **45**, 83–117 (2016).

13. Plutschack, M. B., Pieber, B., Gilmore, K. & Seeberger, P. H. The Hitchhiker's Guide to Flow Chemistry â¥. *Chemical Reviews* **117**, 11796–11893 (2017).

14. Kockmann, N., Thenée, P., Fleischer-Trebes, C., Laudadio, G. & Noël, T. Safety assessment in development and operation of modular continuous-flow processes. *Reaction Chemistry and Engineering* **2**, 258–280 (2017).

15. Gutmann, B., Cantillo, D. & Kappe, C. O. Continuous-flow technology - A tool for the safe manufacturing of active pharmaceutical ingredients. *Angewandte Chemie - International Edition* **54**, 6688–6728 (2015).

16. Noël, T., Su, Y. & Hessel, V. Beyond organometallic flow chemistry: The principles behind the use of continuous-flow reactors for synthesis. in *Topics in Organometallic Chemistry* **57**, 1–41 (Springer Verlag, 2016).

17. Mallia, C. J. & Baxendale, I. R. The Use of Gases in Flow Synthesis. *Organic Process Research and Development* **20**, 327–360 (2016).

18. Tamborini, L., Fernandes, P., Paradisi, F. & Molinari, F. Flow Bioreactors as Complementary Tools for Biocatalytic Process Intensification. *Trends in Biotechnology* **36**, 73–88 (2018).

19. Peris, E. *et al.* Tuneable 3D printed bioreactors for transaminations under continuous-flow. *Green Chem.* **19**, 5345–5349 (2017).

20. Bolivar, J. M., Wiesbauer, J. & Nidetzky, B. Biotransformations in microstructured reactors: More than flowing with the stream? *Trends in Biotechnology* **29**, 333–342 (2011).

21. Zor, C. *et al.* H2-Driven biocatalytic hydrogenation in continuous flow using enzyme-modified carbon nanotube columns. *Chem. Commun.* **53**, 9839–9841 (2017).

22. Tang, X., Allemann, R. K. & Wirth, T. Optimising Terpene Synthesis with Flow Biocatalysis. *European J. Org. Chem.* **2017**, 414–418 (2017).

23. Tomaszewski, B., Lloyd, R. C., Warr, A. J., Buehler, K. & Schmid, A. Regioselective biocatalytic aromatic hydroxylation in a gas-liquid multiphase tube-in-tube reactor. *ChemCatChem* **6**, 2567–2576 (2014).

24. Jones, E., Mcclean, K., Housden, S., Gasparini, G. & Archer, I. Chemical Engineering Research and Design Biocatalytic oxidase : Batch to continuous. *Chem. Eng. Res. Des.* **90**, 726–731 (2012).

25. Gasparini, G., Archer, I., Jones, E. & Ashe, R. Scaling up biocatalysis reactions in flow reactors. *Org. Process Res. Dev.* **16**, 1013–1016 (2012).

26. Toftgaard Pedersen, A. *et al.* Characterization of a continuous agitated cell reactor for oxygen dependent biocatalysis. *Biotechnol. Bioeng.* **114**, 1222–1230 (2017).

27. Ruiz-Dueñas, F. J., Ferreira, P., Martínez, M. J. & Martínez, A. T. In vitro activation, purification, and characterization of Escherichia coli expressed aryl-alcohol oxidase, a unique H2O2-producing enzyme. *Protein Expr. Purif.* **45**, 191–199 (2006).

28. Ferreira, P. *et al.* Spectral and catalytic properties of aryl-alcohol oxidase, a fungal flavoenzyme acting on polyunsaturated alcohols. *Biochem. J.* **389**, 731–738 (2005).

29. GUILLÉN, F., MARTÍNEZ, A. T. & MARTÍNEZ, M. J. Substrate specificity and properties of the aryl-alcohol oxidase from the ligninolytic fungus Pleurotus eryngii. *Eur. J. Biochem.* **209**, 603–611 (1992).

30. Guillén, F., Martinez, A. T. & Martínez, M. J. Production of hydrogen peroxide by aryl-alcohol oxidase from the ligninolytic fungus Pleurotus eryngii. *Appl. Microbiol. Biotechnol.* **32**, 465–469 (1990).

31. Bormann, S., Gomez Baraibar, A., Ni, Y., Holtmann, D. & Hollmann, F. Specific oxyfunctionalisations catalysed by peroxygenases: Opportunities, challenges and solutions. *Catalysis Science and Technology* **5**, 2038–2052 (2015).

32. Toftgaard Pedersen, A. *et al.* Process Requirements of Galactose Oxidase Catalyzed Oxidation of Alcohols. *Org. Process Res. Dev.* **19**, 1580–1589 (2015).

33.   Tufvesson, P., Lima-Ramos, J., Nordblad, M. & Woodley, J. M. Guidelines and cost analysis for catalyst production in biocatalytic processes. *Org. Process Res. Dev.* **15**, 266–274 (2011).

Toward preparative-scale alcohol oxidase reactions exploiting the two liquid phase approach

4

Introduction

The selective oxidation of functionalized alcohols to the corresponding aldehydes still poses some challenges in synthetic organic chemistry.[1–3] Issues with functional group tolerance, overoxidation, and other undesired side reactions are frequently observed,[4] and traditional chemical routes are sometimes plagued by high energy demand and dependence on environmentally questionable oxidants.[5] Enzymes are generally amongst the first catalysts to be mentioned when selectivity comes to play.[6–8] Nevertheless, only a few synthetic oxidation reactions rely on biocatalysis, with preference usually given to the well-established homogeneous and heterogeneous catalysts. It is partially due to the (perceived) high costs of enzyme production and product titers reported for biocatalytic oxidations that are still at millimolar range (few $g.L^{-1}$), becoming unattractive from a preparative point-of-view.

We choose the oxidation of *trans*-2-hexen-1-ol to the corresponding aldehyde as a model reaction to address these issues. The corresponding aldehyde is widely used in both the flavor and fragrance industries as an afresh flavor ingredient (Green Note).[9,10]

A broad range of enzymes is available for the oxidation of alcohols [8] with alcohol dehydrogenases (ADHs),[7,11] being alcohol oxidases (AOx) the most useful ones.[12] On the one hand, ADHs catalyzes reversibly through Meerwein-Ponndorf-Verley-like oxidation reactions, which generally necessitate high molar surpluses of the sacrificial oxidant (mostly acetone) to drive the equilibrium reaction.

On the other hand, alcohol oxidases use molecular oxygen as the oxidant, yielding H_2O_2 as a stoichiometric by-product in an irreversible fashion. Hazardous hydrogen peroxide can easily be dismutated using catalase. Hence, AOx-catalysed oxidations appear more suitable from an environmentally point-of-view (i. e. yielding fewer waste products) when compared to ADH-catalysed ones. Therefore, we put our attention to the aryl alcohol oxidase from *Pleurotus eryngii* (*Pe*AAOx).[13–17]

Results and discussion

The enzyme was heterologously expressed in *Escherichia coli*, in vitro reactivated and purified. Both substrate and product of the reaction are sparingly soluble in aqueous reaction mixtures (130 and 60mM, respectively, in the reaction buffer used here). Therefore, we evaluated the so-called two-liquid-phase-system approach (2LPS, Scheme 1). Here, a hydrophobic organic phase serves both as substrate reservoir and product sink, enabling overall high reagent loadings as demonstrated previously for various reactions.[18–31]
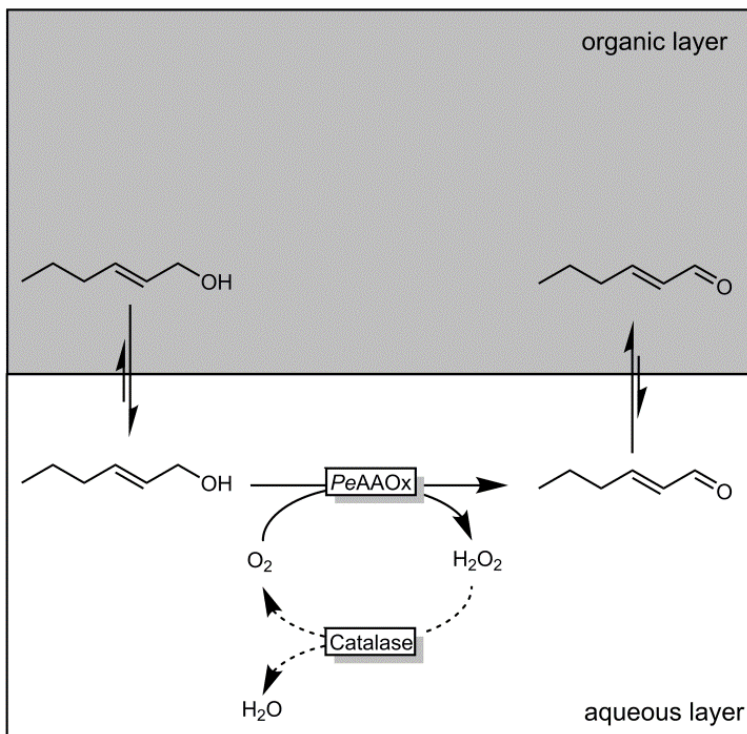
Scheme 1. Biocatalytic oxidation of *trans*-2-hexen-1-ol. To achieve overall high reagent loadings, a hydrophobic organic phase is added to the aqueous reaction buffer. *Pe*AAOx: aryl alcohol oxidase from *Pleurotus eryngii*. Catalase is added to the reaction to alleviate the potentially harmful effect of H2O2.

2LPS also contributes to minimizing enzyme inhibition by the product and undesired side reactions of the aldehyde in the aqueous phase., We further elucidated in the first set of experiments the operational window for *Pe*AAOx in terms of optimal pH, temperature, mechanical and solvent stability. Regarding the optimal pH, *Pe*AAOx is active in a broad pH range, displaying the highest activity in $5 < pH < 8$ range (Figure 1). Based on these results, pH 7 was selected for further experiments due to its compatibility with the activity of catalase, required for the dismutation of H_2O_2.
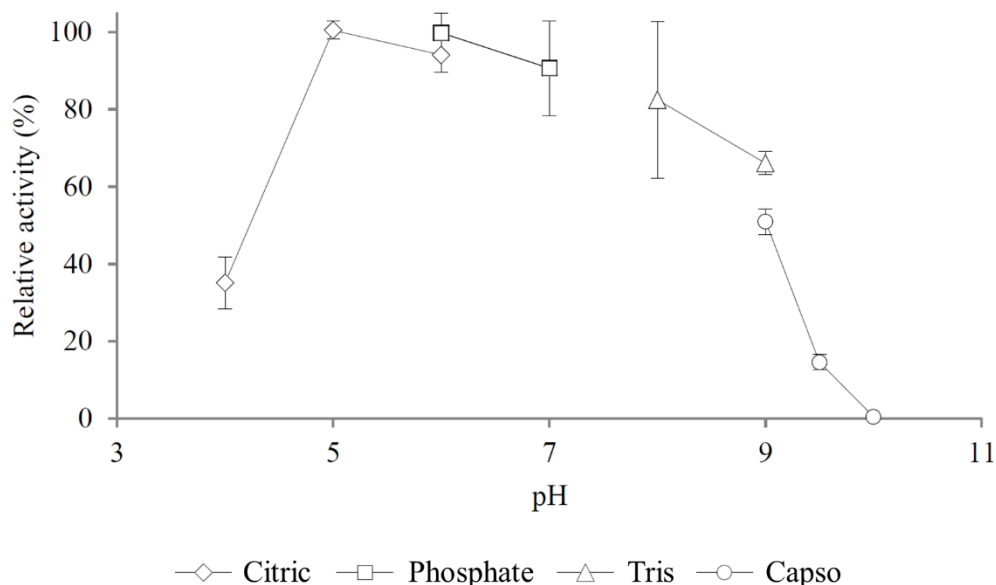
Figure 1. Influence of pH on the activity of *Pe*AAOx. Reactions were performed at 20°C, applying different buffer systems (50 mM) in the 4 < pH < 10 range. The activity assay was performed using 5 nM *Pe*AAOx, 3 mM *trans*-2-hexen-1-ol, 2 mM ABTS and 5 U mL-1 horseradish peroxidase.

*Pe*AAOx exhibits the maximum activity at 30 °C, with a turnover frequency of $25s^{-1}$. The activity dropped dramatically above this temperature, with a 25-fold decrease at 40 °C (TF<$1s^{-1}$, Figure 2). The decrease in activity at elevated temperatures is attributed most likely to the thermal denaturation of the biocatalyst. We, therefore, conducted all further experiments at 20 °C as a compromise between high activity and stability.
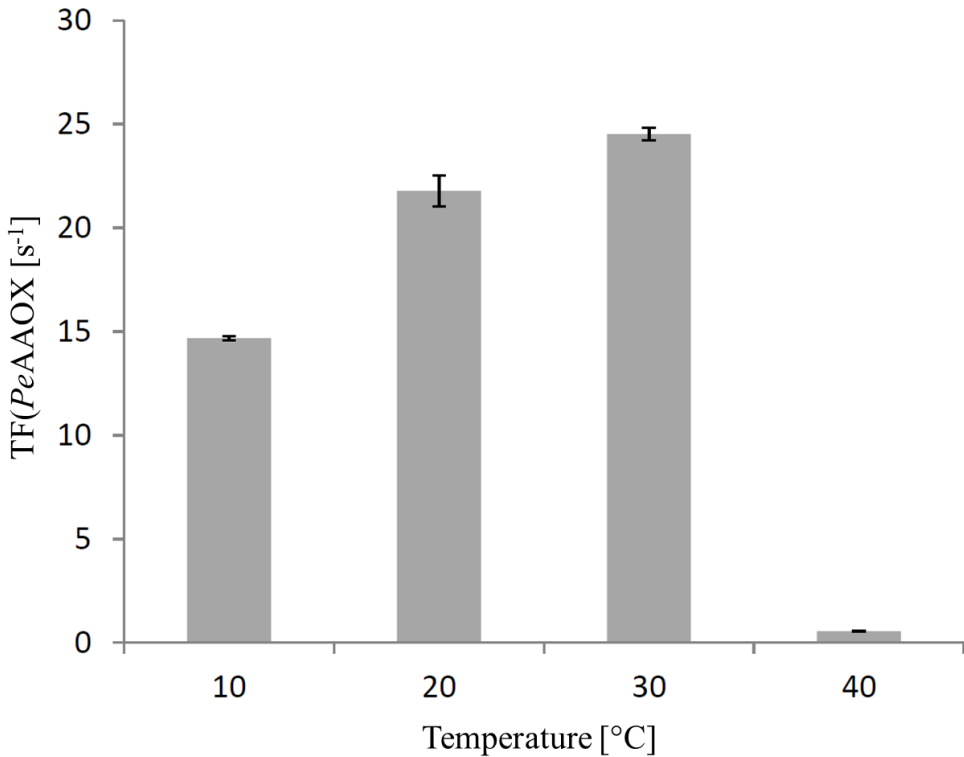
Figure 2 Influence of temperature on the activity of *Pe*AAOx. Reactions performed at 10, 20, 30 or 40°C and 1000 rpm in potassium phosphate buffer (1 mL, 50 mM, pH 7.0) containing 0.05 µM *Pe*AAOx, 720 U mL^{-1} catalase and 50 mM *trans*-2-hexen-1-ol.

2LPSs are frequently plagued by diffusion limitations over the phase border, which can be addressed by e. g. vigorous mixing to increase the surface area. We investigated the robustness of *Pe*AAOx against mechanical stress (Figure 3) and, surprisingly, the enzyme was seemingly not affected by high shaking velocities.
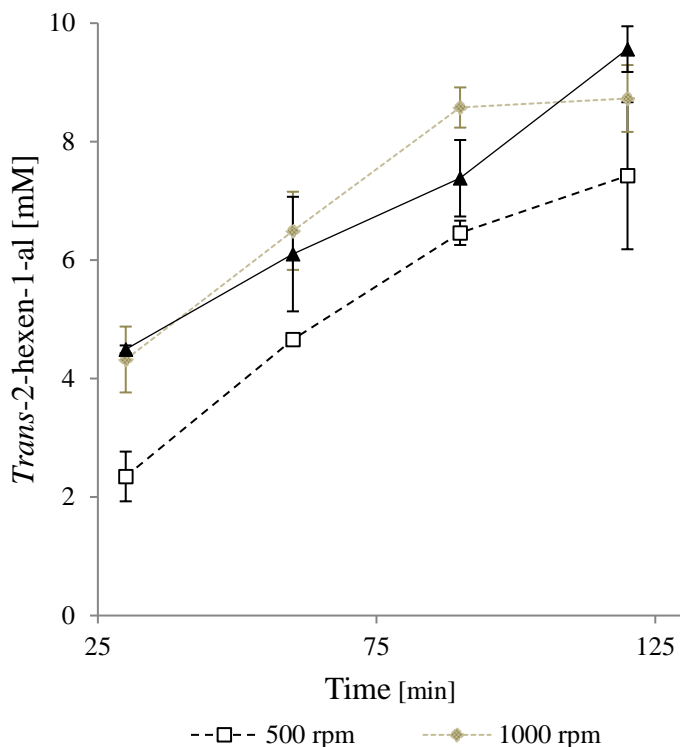
Figure 3. Mechanical resistance of *Pe*AAOx. Reactions were performed at 30°C and 500, 1000 or 1500 rpm in potassium phosphate buffer (1 mL, 50 mM, pH 7.0) containing 0.05 µM *Pe*AAOx, 720 U mL^{-1} catalase and 50 mM *trans*-2-hexen-1-ol.

Finally, the stability of AAOx was also determined in the presence of various organic solvents (Figure 4). Hydrophobic solvents such as isooctane or dodecane were tolerated well by the enzyme, and initial rates up to 13 turnovers per second were achieved. Toluene gave no catalytic conversion at all and, possibly, π-stacking interactions of the aromatic ring with the flavin prosthetic group resulted in a strong competitive inhibition of *Pe*AAOx.[14] Quite surprisingly, ethyl acetate was tolerated by *Pe*AAOx as an organic phase even though reactions ceased rather quickly due to acidification of the aqueous layer caused by autohydrolysis.
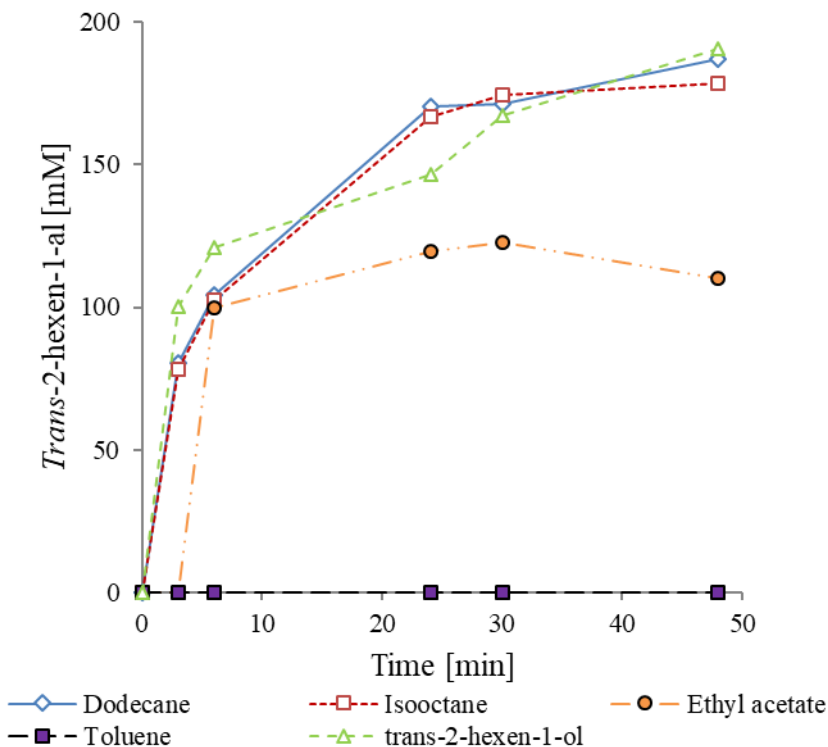
Figure 4. Influence of the organic layer in the oxidation of *trans*-2-hexen-1-ol by *Pe*AAOx. The biphasic reaction systems (1 mL) were composed of an organic solvent layer and an aqueous layer (1:1 phase ratio). The organic layer solvent (dodecane, isooctane, ethyl acetate or toluene) was supplemented with 1M *trans*-2-hexen-1-ol. In addition, *trans*-2-hexen-1-ol was used as an organic layer. The aqueous phase contained 0.2 µM *Pe*AAOx and 720 U mL-1 catalase in potassium phosphate buffer (50 mM, pH 7.0). Reactions were performed at 20°C and 1000 rpm.

From Figure 4, we choose dodecane as the organic phase.

Figure   shows a representative time course of the reaction in the biphasic reaction system. Pleasingly, it was observed full conversion of the starting material into the desired product ($49g.L^{-1}$ organic phase) within 24h. The nominal catalytic performance of *Pe*AAOx in the biphasic system (TF of $14.3s^{-1}$ within the first 5h) was somewhat lower when compared to

the monophasic reaction (TF of $22.8 s^{-1}$, Figure 2). This is most likely attributed to phase transfer limitations of substrates (-hex-2-en-1-ol and O_2).[32] Comparative experiments revealed that O_2 transfer into the aqueous reaction buffer was overall rate-limited (Figure 5).
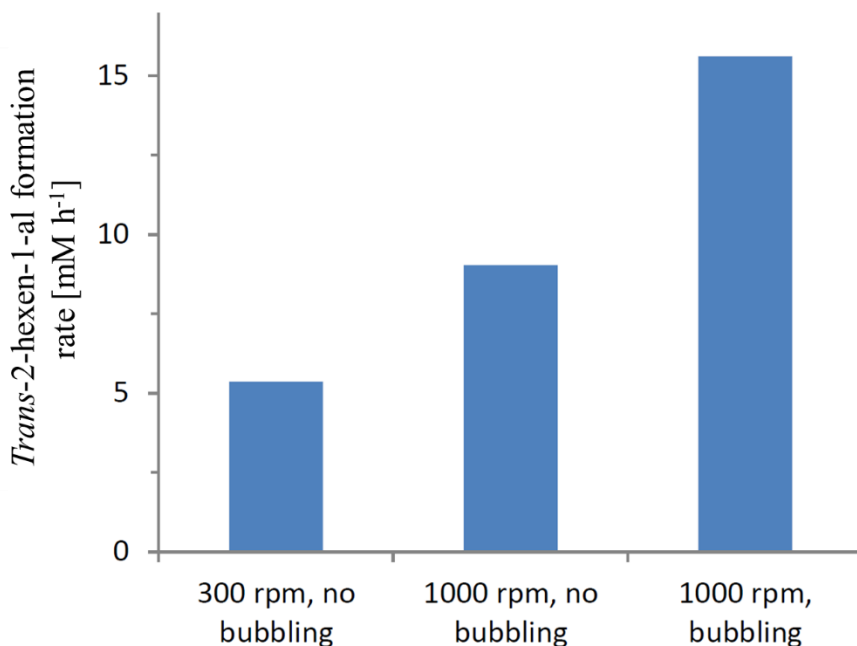
Figure 5 Influence of O_2-supply on the rate of the *Pe*AAOx-catalysed oxidation of *trans*-2-hexen-1-ol. Conditions: potassium phosphate buffer (1 mL, 50 mM, pH 7.0) containing 0.05 µM *Pe*AAOx, 720 U mL^{-1} catalase and 50 mM *trans*-2-hexen-1-ol.

Nevertheless, AAOx performed more than 650.000 catalytic turnovers, corresponding to a catalyst loading of less than 0,0002 mol-% or almost 900 g $_{product}$ g^{-1}$_{PeAAOx}$, respectively. The values for catalase are 0,00002 mol-% and 8166 g $_{product}$ g^{-1}$_{Catalase}$, respectively.

Another advantage of the 2LPS approach lies in the facile downstream processing as simple phase separation is sufficient to separate the dodecane-product mixture (in case of full conversion as e. g. shown in

Figure 6 from the aqueous reaction buffer. Chromatographic and distillation separation of the solvent (dodecane, bp=214 °C) from the product (-2-hexen-1-al, bp=145 °C) or both is straightforward.
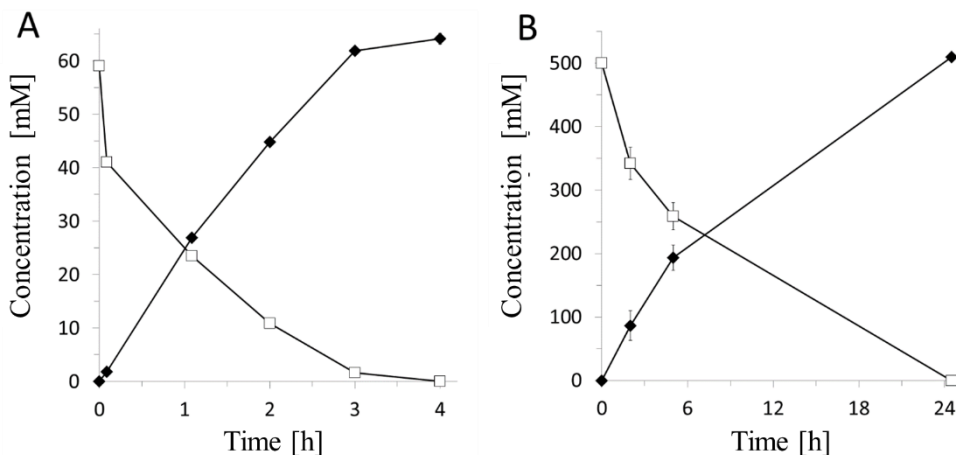
Figure 6. AAOx-catalysed oxidation of -2-hexen-1-ol (□) to -2-hexenal (♦) using a biphasic (2LPS) reaction system. Conditions: T=20 °C, shaking rate=1000 rpm; aqueous phase: 0.5 mL of 50 mM KPi (pH 7), [AAOx]=0.75 μM, [Catalase]=720 U mL^{-1} (0.1 μM); organic phase: 0.5 mL of dodecane, [-2-hexen-1-ol]=500 mM; phase ratio: 1:1 (v/v).

Encouraged by these results, we maximized the catalytic usage of the biocatalyst (i. e., maximizing the turnover number). For this, we also decided to avoid any additional organic solvent and use -2-hexen-1-ol itself as the organic phase (Figure 7). we realized in the first set of experiments that after approximately 48h the rate of the oxidation reaction decreased to some extent. Therefore, fresh AAOx and catalase were added (in total 6 times throughout the entire experiment) to the aqueous layer summing up, respectively, to 300 nM and 600nM of AAOx and catalase. This procedure allowed for at least 14 days the stable accumulation of more than 2.6 M of

the desired product in the -2-hexen-1-ol layer. Overall, a superb turnover number of more than 2.2 Million was calculated for AAOx.
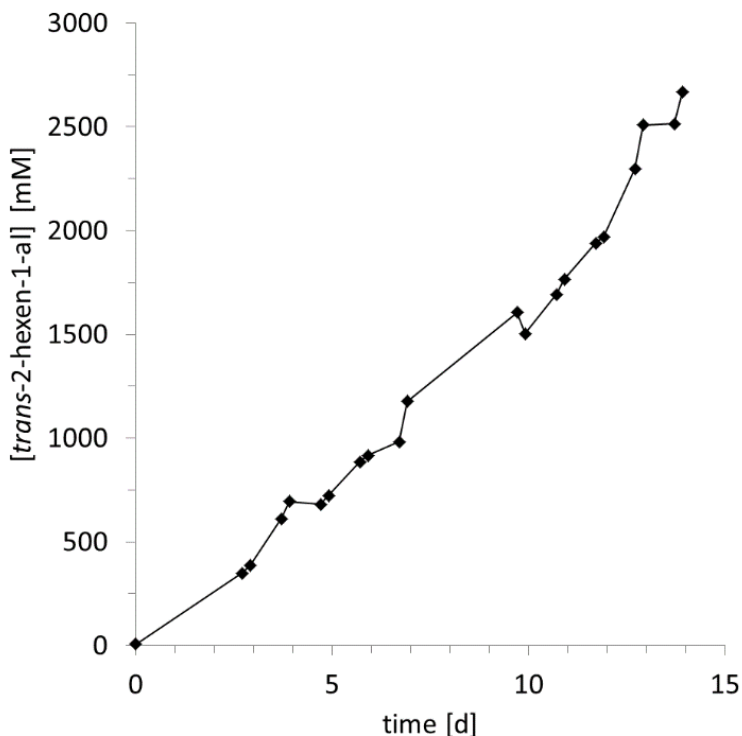
Figure 7. Time course of a long-term oxidation experiment utilising the 2LPS approach. General conditions: T=20 °C, stirring at max speedy = 1000 rpm; aqueous phase: 2.5 mL of 50 mM KPi (pH 7), [AAOx] = 0.3 µM final and [Catalase]=0.6µMfinal (added at 2 d intervals), organic phase: 7.5 mL of [-2-hexen-1-ol]=8.4 M (neat), phase ratio: 1:4 (v/v).

Indeed, 14 days of reaction time is not practical on both lab or industrial scale. Also, the conversion of 31% of the starting material in the case of a next experiment (Figure 7) was not satisfactory as it necessitates the further chromatographic separation of the product from the starting material. Nevertheless, this experiment demonstrated the catalytic potential

of AAOx for the synthesis of -2-hexenal and, possibly, further aldehyde products such as benzaldehydes.[13,15]

According to the cost estimation by Tufvesson and Woodley,[33] these turnover numbers correspond to a *Pe*AAOx cost contribution of less than $0.1 € \, mol^{-1}$ of the product (Figure 8, assuming large-scale enzyme fermentation). Many other factors will play a role en route to the economic feasibility of such a process, but these numbers again underline the potential of this enzyme for preparative application.
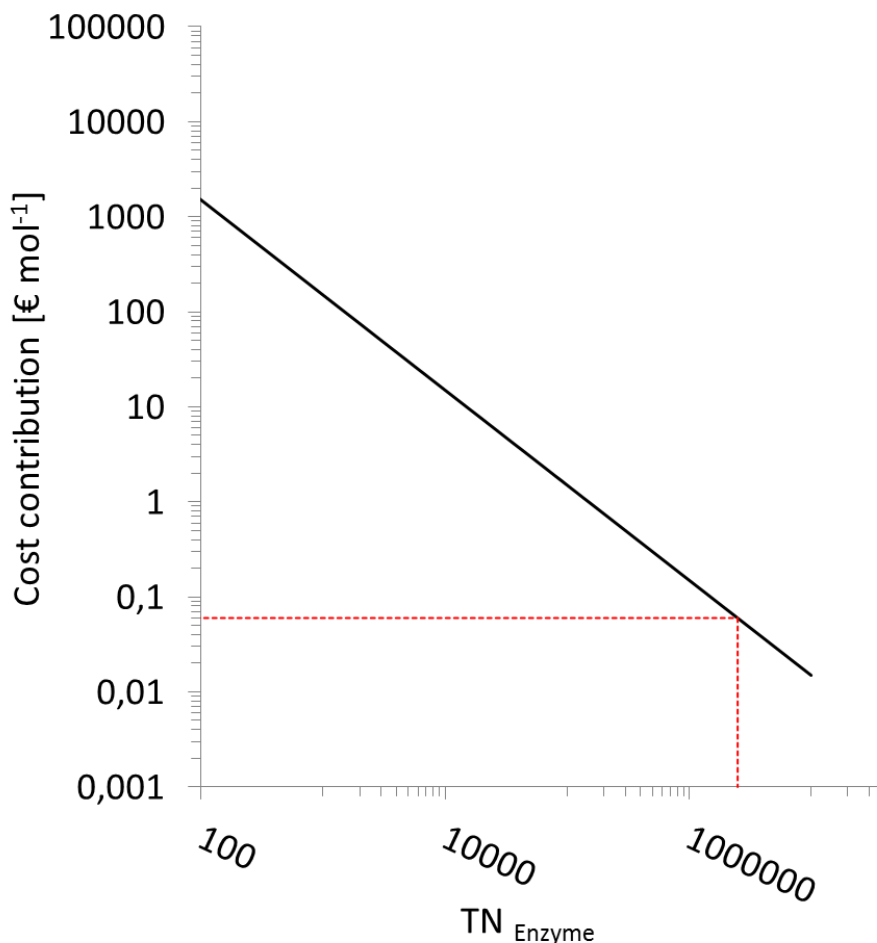
Figure 8. Estimation of the cost contribution of AAOx to the final product.

Conclusion

Overall, this contribution demonstrates that oxidase-catalyzed alcohol oxidation reactions not only represent a selective approach for the production of aldehydes under non-problematic reaction conditions but also represent a promising economic methodology.

Experimental Section

Preparation of the Biocatalyst

*Pe*AAOx was produced by recombinant expression in *Escherichia coli* following a previously established protocol.8a In short: recombinant cells of *E. coli* W3110 pFLAG1-AAO were grown in LB medium at 37 °C. The expression of the enzyme was induced by the addition of IPTG at an OD_{600} of 0.8 followed by an additional incubation for 4h. *Pe*AAOx was obtained in an active form from the insoluble fraction (inclusion bodies) of the cell extract by a refolding and chromatographic purification procedure

Expression of AAOx

The procedure to obtain AAOx was slightly modified from the one described in the literature.[13] A pre-culture in LB media supplemented with ampicillin (100 µg mL^{-1}) was inoculated with *E. coli* W3110 *p*FLAG1-AAO and incubated overnight at 37°C and 180 rpm. AAOx production was performed in TB medium containing ampicillin (100 µg mL^{-1}). The inoculation of the medium was adjusted to OD_{600} 0.05 and grown at 37°C and 180 rpm. At OD_{600} 0.8, the culture was induced adding 1 mM isopropyl-β-D-thiogalactopyranoside (IPTG). After incubation for an additional 4 h at 37°C and 180 rpm, the bacterial cells were harvested.

Refolding of PeAAOx from inclusion bodies

The obtained cells were resuspended in Tris/HCl buffer (50 mM, pH 8.0) containing 10 mM EDTA, 5 mM DTT (dithiothreitol) and 2 mg mL^{-1} lysozyme. After being incubated for 1 h at 4°C, 0.1 mg mL^{-1} DNase, 1 mM $MgCl_2$ and 0.1 mM PMSF were added and the solution homogenized by

sonication. After centrifuge (30 min, 15,000 rpm, 4°C) and removing the supernatant, the obtained pellet of the insoluble fraction was resuspended and washed three times in Tris/HCl buffer (20 mM, pH 8.0) containing 10 mM EDTA and 5 mM DTT using a potter homogenizing device. Afterward, the pellet was resuspended in Tris/HCl buffer (20 mM, pH 8.0) containing 2 mM EDTA, 50 mM DTT and 8 M urea and the mixture incubated on ice for 30 min to solubilize the *Pe*AAOx from inclusion bodies. After another centrifugation, the cleared supernatant was collected and the protein content determined to carry out the *in vitro* refolding with 150 µg mL^{-1} total protein. The *in vitro* refolding was performed in Tris/HCl buffer (20 mM, pH 9.0) containing 2.5 mM GSSG, 1 mM DTT, 0.02 mM FAD, 34% glycerol and 0.6 M urea for 80 h at 4°C. Before the *Pe*AAOx was purified by anion-exchange chromatography, the refolding mixture was subsequently concentrated and the buffer exchanged to sodium phosphate buffer (10 mM, pH 5.5) via ultra-/diafiltration and Amicon ultra centrifugal filters (MWCO 10 kDa). The final purification was performed on a Q Sepharose column using a linear gradient of NaCl (0-0.6 M) in sodium phosphate buffer (10 mM, pH 5.5). *Pe*AAOx containing fractions were collected, concentrated and desalted using a HiTrap column with sodium phosphate buffer (10 mM, pH 5.5). The *Pe*AAOx concentration was calculated based on the molar extinction coefficient (ε_{463}: 11,050 M^{-1} cm^{-1}) at 463 nm.

General Conditions for the Biphasic Reaction System

The biphasic reaction systems (1mL) were composed of an organic solvent layer and an aqueous layer in a (1:1) phase ratio. The organic layer solvent (dodecane, isooctane, ethyl acetate or toluene) was supplemented

with 0.5 M -2-hexen-1-ol. In addition, -2-hexen-1-ol was used as an organic layer. The aqueous phase contained 0.75 µM AAOx and 720 U mL^{-1} (0.1 µM) catalase.

Scale-up and Long-term Experiment in the Biphasic Reaction System

In a scale-up experiment (10 mL), dodecane containing 500 mM -2-hexen-1-ol and potassium phosphate buffer (50 mM, pH 7.0) containing 0.75µM *Pe*AAOx and 720 U.mL^{-1} catalase were used in a (1:1) phase ratio. Long-term experiments were performed in glass flasks under magnetic stirring 1,100 rpm). In a total volume of 10 mL, a phase ratio of (1:4) using pure -2-hexen-1-ol as an organic layer and phosphate buffer (50 mM, pH 7) containing 0.05 µM AAOx and 720 U mL^{-1} as the aqueous layer was applied. Every two days, 0.05µM AAOx and 720 U mL^{-1} was added to the solution in the total amount of 0.3 and 0.6 µM of AAOx and catalase, respectively

Product Characterisation (-2-hexenal)

^{1}H NMR (400 MHz, Chloroform-d) δ9.51 (d, J=7.9 Hz, ^{1}H), 6.85 (dt, J=15.6, 6.8 Hz, ^{1}H), 6.12 (dd, J=15.6, 7.9 Hz, ^{1}H), 2.36–2.28 (m, 2H), 1.58–1.51 (m, 2H), 0.97 (t, J=7.4 Hz, 3H).13C NMR (101 MHz, Chloroform-d) δ194.69, 159.30, 133.56, 35.15, 21.57, 14.10. GC-MS: m/z (99) calc. for $C_6H_{11}O$ [M$^+$H]$^+$

Chemicals

2,2′-Azino-bis(3-ethylbenzothiazoline-6-sulfonic acid) diammonium salt (ABTS), -2-hexen-1-al, dodecane, isooctane, toluene, magnesium sulfate and ethyl acetate were purchased from Sigma Aldrich and were used

without further purification. -2-hexen-1-ol was distilled before use. Columns or column material used during enzyme purification was purchased from GE healthcare. NMR spectra were recorded on a Varian 400 (400 MHz) spectrometer in CDCl$_3$. Chemical shifts are given in ppm concerning tetramethylsilane. Coupling constants are reported as J-values in Hz.

Reaction condition and analytical procedures

The activity of purified *Pe*AAOx was determined indirectly following the oxidation of ABTS (ε_{405}: 36,800 M^{-1} cm^{-1}) by horseradish peroxidase utilizing the hydrogen peroxide formed by *Pe*AAOx. The ABTS-assay was performed at 20°C in oxygen saturated potassium phosphate buffer (50 mM, pH 7.0) containing 44 nM *Pe*AAOx, 3 mM -2-hexen-1-ol, 2 mM ABTS and 500 U mL^{-1} horseradish peroxidase.

The activity of *Pe*AAOx at different pH was measured via ABTS-assay in the presence of 5 U mL^{-1} horseradish peroxidase and 5 nM *Pe*AAOx as described before following incubation of 30 min at 20°C in the corresponding buffer. Citric acid buffer (50 mM, pH 4, 5 or 6), potassium phosphate buffer (50 mM, pH 6 or 7), Tris/HCl buffer (50 mM, pH 7 or 8) or CAPSO buffer (50 mM, pH 9 or 10) were tested.

Additionally, product inhibition was investigated via the ABTS-assay as described before following an incubate of *Pe*AAOx in the presence of different concentrations of -2-hexen-1-al (0.5, 1, 5, 10, 50, 75 mM) for 30 min at 20°C.

Optimization of the aqueous (monophasic) reaction system

All reactions were performed in phosphate buffer (50 mM, pH 7) at 10, 20, 30 or 40°C using a thermos shaker device (500, 1000 or 1500 rpm). Oxygen was supplied to the headspace of the reaction by an oxygen-filled balloon. The reaction mixture (1 mL) contained 0.05 µM *Pe*AAOx, 720 U mL^{-1} catalase and 50 mM -2-hexen-1-ol. The sealing integrity was performed in glass flasks under magnetic stirring (600 or 1,100 rpm) in a total volume of 5 mL in phosphate buffer (50 mM, pH 7) containing 0.5 µM *Pe*AAOx and 720 U mL^{-1} catalase.

Aqueous (monophasic) versus biphasic reaction system

All reactions were performed with phosphate buffer (50 mM, pH 7) at 20°C using a thermos shaker device (1000 rpm). Oxygen was supplied to the headspace of the reaction by an oxygen-filled balloon. In the monophasic, aqueous reaction system the reaction mixture (1 mL) contained 0.25 µM *Pe*AAOx, 720 U mL^{-1} catalase and 60 mM -2-hexen-1-ol.
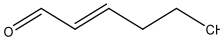
The biphasic reaction systems (1 mL) were composed of an organic solvent layer and an aqueous layer in a (1:1) phase ratio. The organic layer solvent (dodecane, isooctane, ethyl acetate or toluene) was supplemented with 1 M -2-hexen-1-ol. In addition, -2-hexen-1-ol was used as an organic layer. The aqueous phase contained 0.2 µM *Pe*AAOx and 720 U mL^{-1} catalase.

Scale-up and long-term experiment in the biphasic reaction system

In a scale-up experiment (10 mL), dodecane containing 500 mM -2-hexen-1-ol and potassium phosphate buffer (50 mM, pH 7.0) containing 0.75 µM *Pe*AAOx and 720 U mL^{-1} catalase were used in a (1:1) phase ratio.

Long-term experiments were performed in glass flasks under magnetic stirring 1,100 rpm). In a total volume of 10 mL, a phase ratio of (1:4) using pure -2-hexen-1-ol as an organic layer and phosphate buffer (50 mM, pH 7) containing 0.05 µM *Pe*AAOx and 720 U mL^{-1} as the aqueous layer was applied. Every two days, 0.05 µM *Pe*AAOx and 720 U mL^{-1} was added to the solution in the total amount of 0.30 µM of *Pe*AAOx.

-2-hexen-1-al

^{1}H NMR (400 MHz, Chloroform-*d*) δ 9.51 (d, *J* = 7.9 Hz, 1H), 6.85 (dt, *J* = 15.6, 6.8 Hz, 1H), 6.12 (dd, *J* = 15.6, 7.9 Hz, 1H), 2.36-2.28 (m, 2H), 1.58-1.51 (m, 2H), 0.97 (t, *J* = 7.4 Hz, 3H).^{13}C NMR (101 MHz, Chloroform-*d*) δ 194.69, 159.30, 133.56, 35.15, 21.57, 14.10. GC-MS: m/z (99) calc. for $C_6H_{11}O$ [M+H]$^+$

Gas chromatography analysis

Gas chromatography measurements were used to quantify -2-hexen-1-ol and -2-hexen-1-al. In the case of monophasic reactions, 60 µl samples were taken and extracted with 300 µL ethyl acetate containing dodecane as an internal standard. In the case of biphasic reactions, 5 µL of the organic layer was added to 500 µL ethyl acetate (containing internal standard). The organic phase was dried with magnesium sulfate and analyzed by gas chromatography. All concentrations reported, we determined based on calibration curves obtained from authentic standards using 5 mM dodecane or 5 mM 1-octanol as an internal standard. Table 1 summarizes the GC measurements.

Table 1 GC analytics

column	temperature program	retention time
CP-Wax 52 CB (Agilent) (50 m × 0.53 mm × 2 µm)	60°C hold 3 min 30°C min⁻¹ to 105°C hold 7 min 30°C min⁻¹ to 250°C hold 1 min	8.4 min -2-hexen-1-ol 6.5 min -2-hexen-1-al
CP-Wax 52 CB (Agilent) (25 m × 0.25 mm × 1.2 µm)	100°C hold 3 min 20°C min⁻¹ to 140°C hold 1.4 min 20°C min⁻¹ to 160°C hold 1 min 20°C min⁻¹ to 180°C hold 1 min 20°C min⁻¹ to 250°C hold 1 min	7.9 min -2-hexen-1-ol 6.7 min -2-hexen-1-al

GC-MS analysis

Table 2 GC-MS analytics

column	temperature program	retention time
VF-Wax MS column (Varian) (30 m × 0.25 mm × 0.25 µm).	100°C hold 3 min 20°C min⁻¹ to 140°C hold 1.40 min 20°C min⁻¹ to 160°C hold 1 min 20°C min⁻¹ to 180°C hold 1 min 25°C min⁻¹ to 250°C hold 1 min	11.4 min -2-hexen-1-al

Additional results

Influence of the sealing integrity
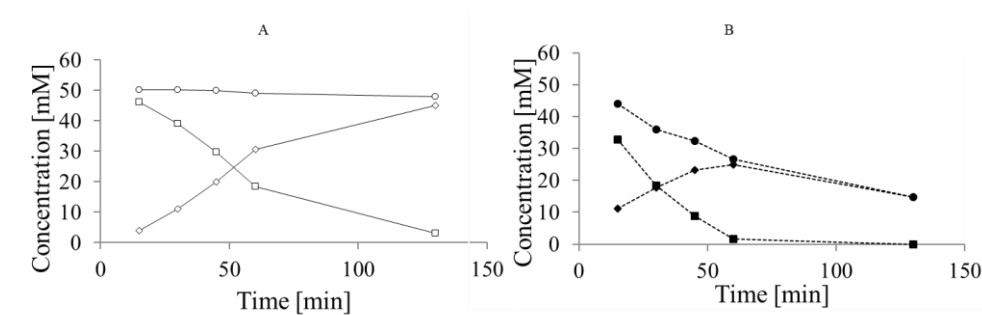
Figure 9. Influence of the sealing integrity on the mass balance under scale-up conditions. (A) (□) -2-hexen-1-ol, (◊) -2-hexen-1-al, (○) mass balance: tightly closed, soft stirring (600 rpm) and (B) (■) -2-hexen-1-ol, (♦) -2-hexen-1-al (●) mass balance: not tightly closed under vigorous stirring (1100 rpm). Reactions were performed in a scale-up experiment (5 mL) under aqueous conditions in potassium phosphate buffer (50 mM, pH 7.0) containing 0.5 µM M *Pe*AAOx, 720 U mL^{-1} catalase and 50 mM -2-hexen-1-ol.

Influence of product inhibition
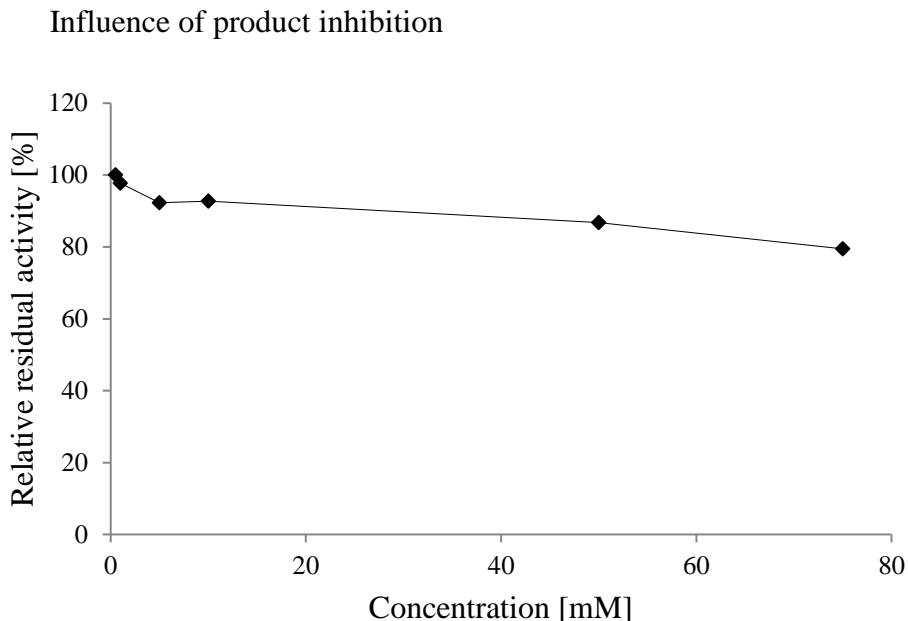
Figure 10. The influence of the product concentration on *Pe*AAOx activity. Product inhibition was investigated via the ABTS-assay following an incubate of *Pe*AAOx in the presence of different concentrations of *trans*-2-hexen-1-al (0.5, 1, 5, 10, 50 or 75 mM) for 30 min at 20°C. The activity assay was performed in potassium phosphate buffer (50 mM, pH 7.0) using 5 nM *Pe*AAOx, 3 mM *trans*-2-hexen-1-ol, 2 mM ABTS and 500 U mL^{-1} horseradish peroxidase. The reaction rate was normalized for the activity in the absence of the product.
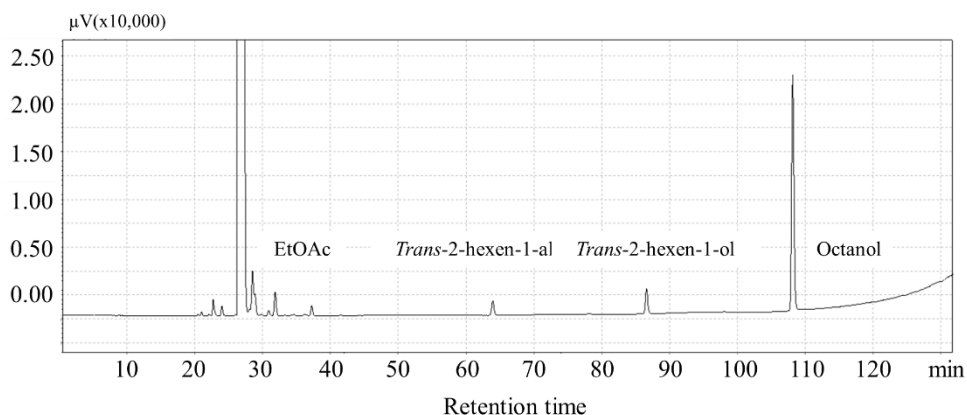
Figure 11 GC of 2-Hexenal
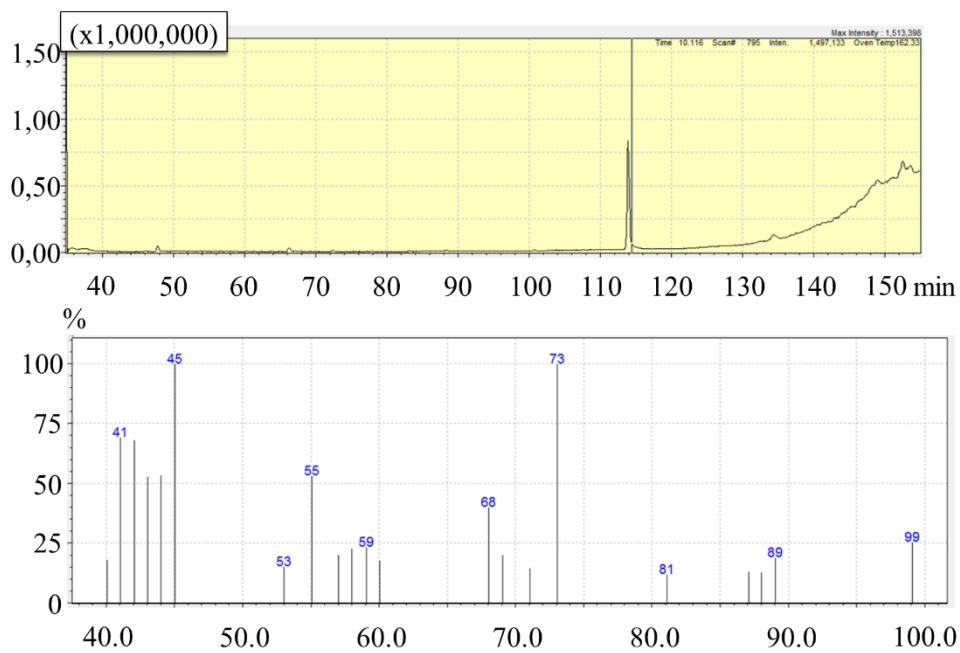
Figure 12 GC-MS of 2-Hexenal
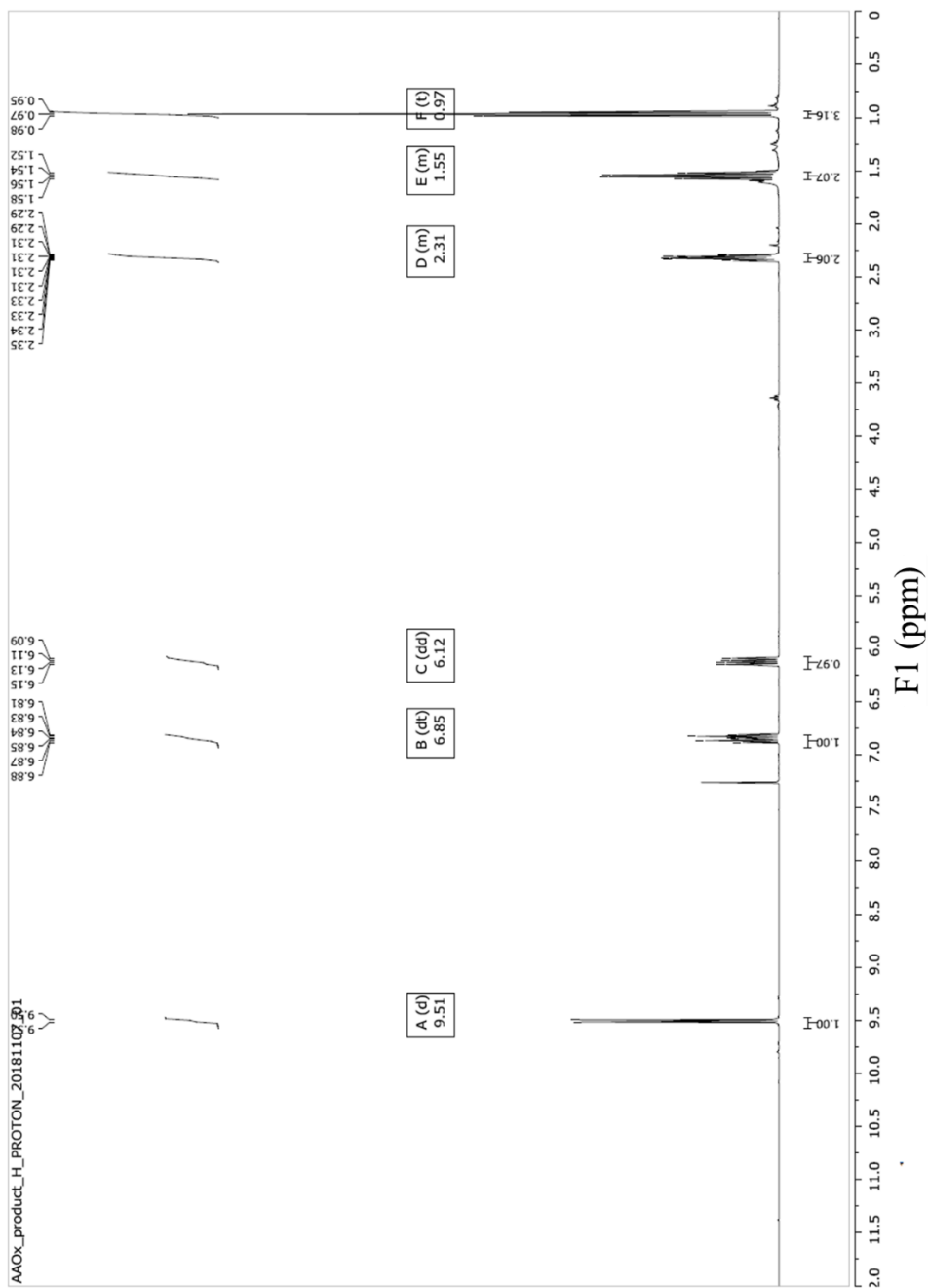
Figure 13. ^{1}H NMR of 2-Hexen-1-al
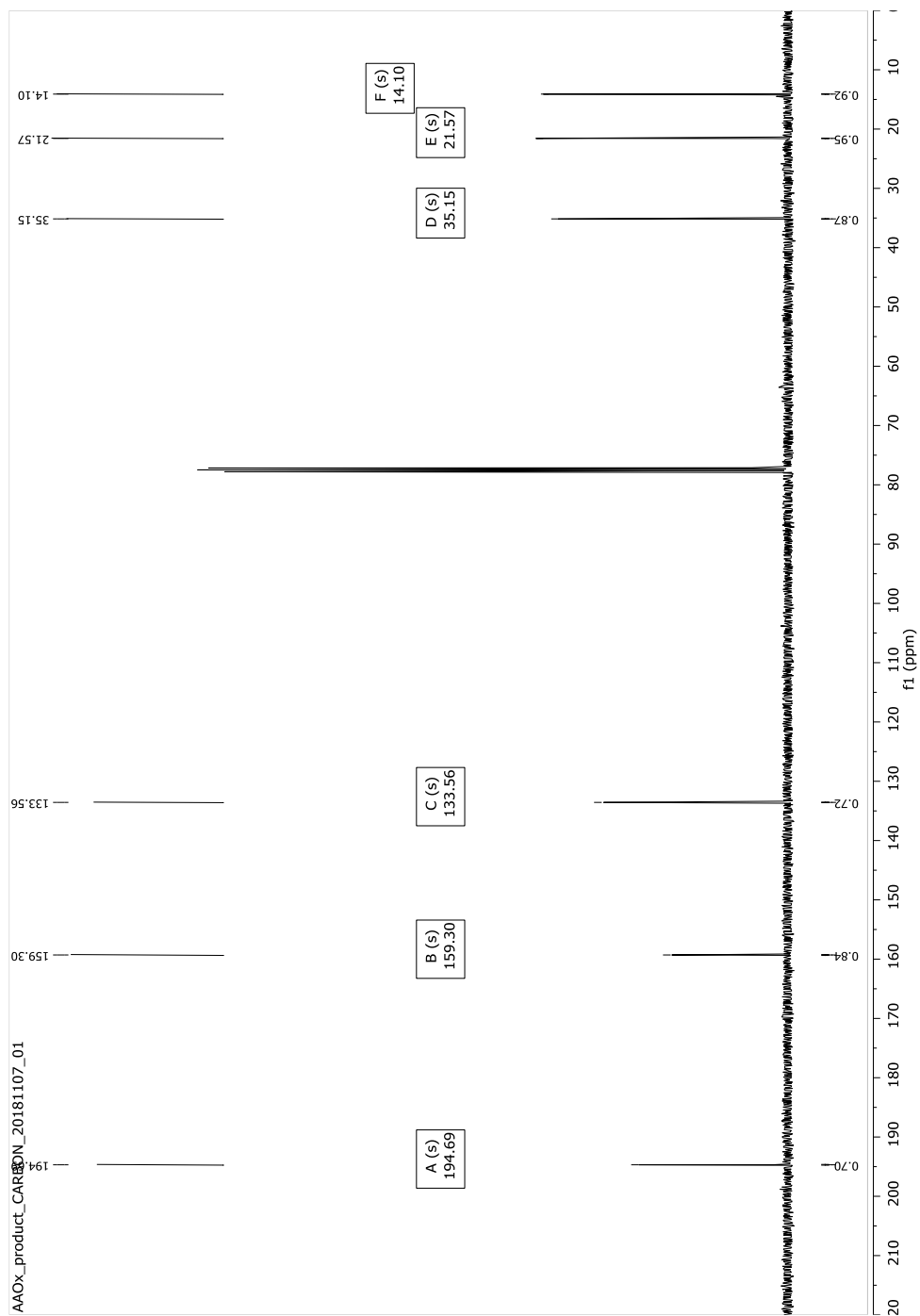
Figure 14 ¹³C NMR of 2-Hexen-1-al.

Acknowledgments

Contribution to this paper

Almeida T.P. contributed with part of the production of alcohol aryl oxidase and, together with Ma A., participated in most of the experiments carried out**.**

References

1.   Sheldon, R. A. & Arenas, I. W. C. E. Organocatalytic oxidations mediated by nitroxyl radicals. *Advanced Synthesis and Catalysis* **346**, 1051–1071 (2004).

2.   Sheldon, R. A., Arends, I. W. C. E., Brink, G. J. Ten & Dijksman, A. Green, catalytic oxidations of alcohols. *Acc. Chem. Res.* **35**, 774–781 (2002).

3.   Ten Brink, G. J., Arends, I. W. C. E. & Sheldon, R. A. Green, catalytic oxidation of alcohols in water. *Science (80-.).* **287**, 1636–1639 (2000).

4.   Alshammari, H., Miedziak, P. J., Morgan, D. J., Knight, D. W. & Hutchings, G. J. Control of the selectivity in multi-functional group molecules using supported gold-palladium nanoparticles. *Green Chem.* **15**, 1244–1254 (2013).

5.   Fleming, G. P. B. T. and I., Pergamon,   undefined, Oxford, undefined & 1991, undefined. Comprehensive Organic Synthesis.

6.   Liu, J., Wu, S. & Li, Z. Recent advances in enzymatic oxidation of alcohols. *Current Opinion in Chemical Biology* **43**, 77–86 (2018).

7.   Kroutil, W., Mang, H., Edegger, K. & Faber, K. Biocatalytic Oxidation of Primary and Secondary Alcohols. *Adv. Synth. Catal.* **346**, 125–142 (2004).

8.   Dong, J. J. *et al.* Biocatalytic Oxidation Reactions: A Chemist's Perspective. *Angewandte Chemie - International Edition* **57**, 9238–9261 (2018).

9.   Panten, J. & Surburg, H. Ullmann's encyclopedia of industrial chemistry flavors and fragrances, 2. Aliphatic compounds, 19, edn. (2015). doi:10.1002/14356007.t14356011_t14356001

10.   Panten, J. & Surburg, H. Ullmann's encyclopedia of industrial chemistry flavors and fragrances, 2. Aliphatic compounds, 19, edn. (2015). doi:10.1002/14356007.t14356011_t14356003

11.   Kroutil, W., Mang, H., Edegger, K. & Faber, K. Recent advances in the biocatalytic reduction of ketones and oxidation of sec-alcohols. *Current Opinion in Chemical Biology* **8**, 120–126 (2004).

12.   Turner, N. J. Enantioselective Oxidation of C-O and C-N bonds using oxidases. *Chemical Reviews* **111**, 4073–4087 (2011).

13.   Ruiz-Dueñas, F. J., Ferreira, P., Martínez, M. J. & Martínez, A. T. In vitro activation, purification, and characterization of Escherichia coli expressed aryl-alcohol oxidase, a unique H2O2-producing enzyme. *Protein Expr. Purif.* **45**, 191–199 (2006).

14. Ferreira, P. *et al.* Spectral and catalytic properties of aryl-alcohol oxidase, a fungal flavoenzyme acting on polyunsaturated alcohols. *Biochem. J.* **389**, 731–738 (2005).

15. GUILLÉN, F., MARTÍNEZ, A. T. & MARTÍNEZ, M. J. Substrate specificity and properties of the aryl-alcohol oxidase from the ligninolytic fungus Pleurotus eryngii. *Eur. J. Biochem.* **209**, 603–611 (1992).

16. Guillén, F., Martinez, A. T. & Martínez, M. J. Production of hydrogen peroxide by aryl-alcohol oxidase from the ligninolytic fungus Pleurotus eryngii. *Appl. Microbiol. Biotechnol.* **32**, 465–469 (1990).

17. Van Schie, M. M. C. H. *et al.* Biocatalytic synthesis of the Green Note trans-2-hexenal in a continuous-flow microreactor. *Beilstein J. Org. Chem.* **14**, 697–703 (2018).

18. Ni, Y., Holtmann, D. & Hollmann, F. How green is biocatalysis? to calculate is to know. *ChemCatChem* **6**, 930–943 (2014).

19. Bühler, B., Bollhalder, I., Hauer, B., Witholt, B. & Schmid, A. Use of the two-liquid phase concept to exploit kinetically controlled multistep biocatalysis. *Biotechnol. Bioeng.* **81**, 683–694 (2003).

20. Bornadel, A., Hatti-Kaul, R., Hollmann, F. & Kara, S. Enhancing the productivity of the bi-enzymatic convergent cascade for ε-caprolactone synthesis through design of experiments and a biphasic system. *Tetrahedron* **72**, 7222–7228 (2016).

21. Kara, S. *et al.* Access to lactone building blocks via horse liver alcohol dehydrogenase-catalyzed oxidative lactonization. *ACS Catal.* **3**, 2436–2439 (2013).

22.   Pennec, A., Hollmann, F., Smit, M. S. & Opperman, D. J. One-pot conversion of cycloalkanes to lactones. *ChemCatChem* **7**, 236–239 (2015).

23.   Pennec, A., Jacobs, C. L., Opperman, D. J. & Smit, M. S. Revisiting cytochrome P450-mediated oxyfunctionalization of linear and cyclic alkanes. *Adv. Synth. Catal.* **357**, 118–130 (2014).

24.   Schmid, A., Vereyken, I., Held, M. & Witholt, B. Preparative regio- and chemoselective functionalization of hydrocarbons catalyzed by cell free preparations of 2-hydroxybiphenyl 3-monooxygenase. in *Journal of Molecular Catalysis - B Enzymatic* **11**, 455–462 (2001).

25.   Schmid, A., Hofstetter, K., Feiten, H.-J., Hollmann, F. & Witholt, B. Integrated Biocatalytic Synthesis on Gram Scale: The Highly Enantioselective Preparation of Chiral Oxiranes with Styrene Monooxygenase. *Adv. Synth. Catal.* **343**, 732–737 (2001).

26.   Wu, X. *et al.* Enantioselective synthesis of ethyl (S)-2-hydroxy-4-phenylbutyrate by recombinant diketoreductase. *Tetrahedron Asymmetry* **20**, 2504–2509 (2009).

27.   Gandolfi, R., Ferrara, N. & Molinari, F. An easy and efficient method for the production of carboxylic acids and aldehydes by microbial oxidation of primary alcohols. *Tetrahedron Lett.* **42**, 513–514 (2001).

28.   Molinari, F., Gandolfi, R., Aragozzini, F., Leon, R. & Prazeres, D. M. F. Biotransformations in two-liquid-phase systems - Production of phenylacetaldehyde by oxidation of 2-phenylethanol with acetic acid bacteria. *Enzyme Microb. Technol.* **25**, 729–735 (1999).

29. Churakova, E. *et al.* Hydrophobic formic acid esters for cofactor regeneration in aqueous/organic two-liquid phase systems. *Top. Catal.* **57**, 385–391 (2014).

30. Ni, Y., Hagedoorn, P. L., Xu, J. H., Arends, I. W. C. E. & Hollmann, F. A biocatalytic hydrogenation of carboxylic acids. *Chem. Commun.* **48**, 12056–12058 (2012).

31. Karande, R., Salamanca, D., Schmid, A. & Buehler, K. Biocatalytic conversion of cycloalkanes to lactones using an in-vivo cascade in Pseudomonas taiwanensis VLB120. *Biotechnol. Bioeng.* **115**, 312–320 (2018).

32. Churakova, E., Arends, I. W. C. E. & Hollmann, F. Increasing the Productivity of Peroxidase-Catalyzed Oxyfunctionalization: A Case Study on the Potential of Two-Liquid-Phase Systems. *ChemCatChem* **5**, 565–568 (2013).

33. Tufvesson, P., Lima-Ramos, J., Nordblad, M. & Woodley, J. M. Guidelines and cost analysis for catalyst production in biocatalytic processes. *Org. Process Res. Dev.* **15**, 266–274 (2011).

Electrochemical in-situ production of H₂O₂ for peroxidase reaction.

5

Introduction

Oxidation reactions are crucial for the formation of chemical groups, and an oxidizing compound is required. To illustrate such compounds, we can mention Cl_2, F_2 and O_2, permanganate, and hydrogen peroxide (H_2O_2). Among them, H_2O_2 is an essential oxidant for biocatalytic reactions, and H_2O_2-driven biocatalysis has the advantage of using an oxidizer that is strong, ecological and has a high solubility in aqueous media, interesting properties when combined with the high selectivity to enzymes.[1] This has motivated several works in the field with different types of reactions, such as hydroxylation, epoxidation or halogenation reactions by using enzymes, and H_2O_2.[1,2] H_2O_2 is the main challenge in peroxygenases as the biocatalyst has a limited resistance in hydrogen peroxide. Above that limit, the enzyme inactivation would occur. Therefore, adequate control of the H_2O_2 concentration is necessary to achieve the highest turnover to minimize inactivation. Enzymatic,[3,4] photochemical[5–7] and electrochemical[8,9] systems are available to make it possible, obtaining higher productivity with oxidant stability.

Another example is the recent electrochemical reduction of O_2 to H_2O_2 using gas-diffusion electrodes (GDEs), an electrode usually applied at fuel cells.[10] Briefly, GDEs work in a three phase system: (i) a solid phase from the support and catalyst; (ii) a liquid part from the solution and (iii) gaseous phase from oxygen. The electrode is made of conductive porous materials where the catalyst is immobilized, with one side of the catalyst staying in contact with the solution. The other part will be in the gaseous phase that diffuses through the porous support reaching the catalyst, which

is activated by the electric charge producing the chemical reaction. Scheme 1 shows the principle of the GDE for the reduction of molecular oxygen to hydrogen peroxide.
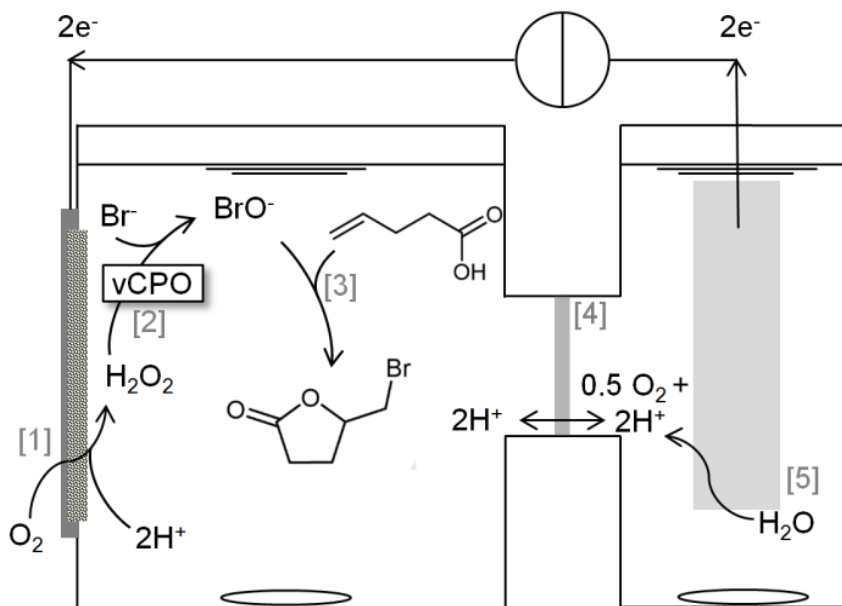
Scheme 1 Schematic view of the electrobiocatalytic 5-(bromomethyl)dihydrofuran-2(3H)-one (bromolactone) synthesis. H_2O_2 is produced at a gas-diffusion electrode (GDE) [1] that consists of oxidized carbon nanotubes (oCNTs) immobilized on carbon paper by drop casting, and oxygen coming from ambient air that diffuses through the GDE. Increased loadings of oCNT reduce the overpotential required for H_2O_2 production. Hypobromite is generated by *Ci*VCPO [2] and reacts with 4-pentenoic acid to form bromolactone [3]. A proton exchange membrane [4] separates anode and cathode chambers, with protons and electrons required for H_2O_2 synthesis being replenished by the water oxidation at the platinum anode [5]. The reference electrode was omitted for clarity.

GDE with enzymes appears successively in the literature with different biocatalysts. For example, we have the unspecific peroxygenase from *Agrocybe aegerita*[11] and a chloroperoxidase from *Caldariomyces*

fumago.[12–14] Usually, in this combination, several parameters are analyzed, such as electrochemical potential, buffer composition, and flow rate. However, the electrocatalyst analysis is an important constraint that has been neglected as most of the applied catalysts have not been investigated or optimized. A significant fall has been reported in the overpotentials required for O2 reduction, even though the application of oCNTs resulted in higher energy-efficient H_2O_2 production, which was attributed to the oxidation of the surface of a carbon catalyst having ether groups inside the structure and carboxylic acidic groups at the edges.[15] These results motivated us to investigate a novel electrocatalyst in combination with an H_2O_2-dependent enzyme. By thermodynamic calculation, the reduction of O_2 in H_2O_2 in aqueous acidic solution requires 0.7V vs standard hydrogen electrode (SHE), or 0.5 V vs. Ag/AgCl$_{satured}$. However, in an electrochemical cell, the overpotentials need to be optimized to save energy.

We have chosen vanadium chloroperoxidase from *Curvularia inaequalis* (*Ci*VCPO) as biocatalyst. This vanadium-dependent chloroperoxidase is able to efficiently produce hypohalides from hydrogen peroxide and a halide. These reactive compounds can participate in various halogenation reactions to keep the stability of the system. It prevents futile H_2O_2 dismutation, preserves enzyme activity, being also preferable to retain the minimal concentration of the peroxide in the reaction solution.[16–18]

Results and discussion

The effect of different concentrations of oCNTs immobilized on the gas-diffusion electrodes was analyzed by a linear sweep experiment (Figure 1). The cell current between the working electrode and the counter

electrode was measured as a function of the applied potential. The analysis demonstrated that the amount of immobilized oCNTs is inversely proportional to overpotential to reduce O_2 to H_2O_2. By adding 1 mg cm^{-2} of oCNTs, the electrode overpotential can be reduced by approximately 0.1 V (calculated from the intersection of the linear range of the current curve and the *y* axis). Thus, promising values in 0.1 M KOH[15] were transferred to an enzyme-compatible electrolyte.
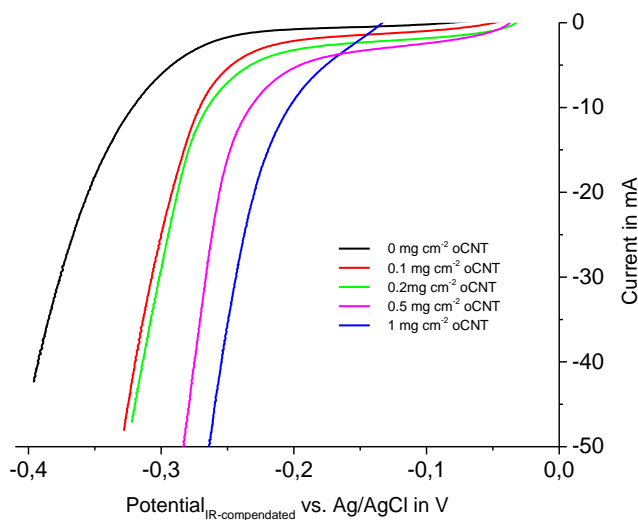
Figure 1   Linear sweep experiments of electrodes modified with different amounts of oCNTs in 100 mM sodium citrate (pH 5) with 100 mM KBr. Potentials are iR-compensated.

The electrodes were compared in an electrochemical set-up to evaluate the H_2O_2 production rates using different amounts of oCNTs. Different potentials were applied, with the resulting H_2O_2 production rates measured (Figure 2). The addition of oCNTs not only has a positive influence on the overpotential in the electrochemical measurements (Figure 1) but also leads to improved H_2O_2 production. Briefly, the addition

of 0.1 mg cm^{-2} oCNTs leads to a 2.3-fold higher production rate of H_2O_2 at a potential of -0.35 vs. Ag/AgCl. An increase in the oCNTs loading to 1 mg cm^{-2} leads to a 4.6-fold increase in the production rate at the chosen potential. The application of oCNTs thus leads to an improved H_2O_2 production rate at different potentials, therefore, it improves the use of electric energy.
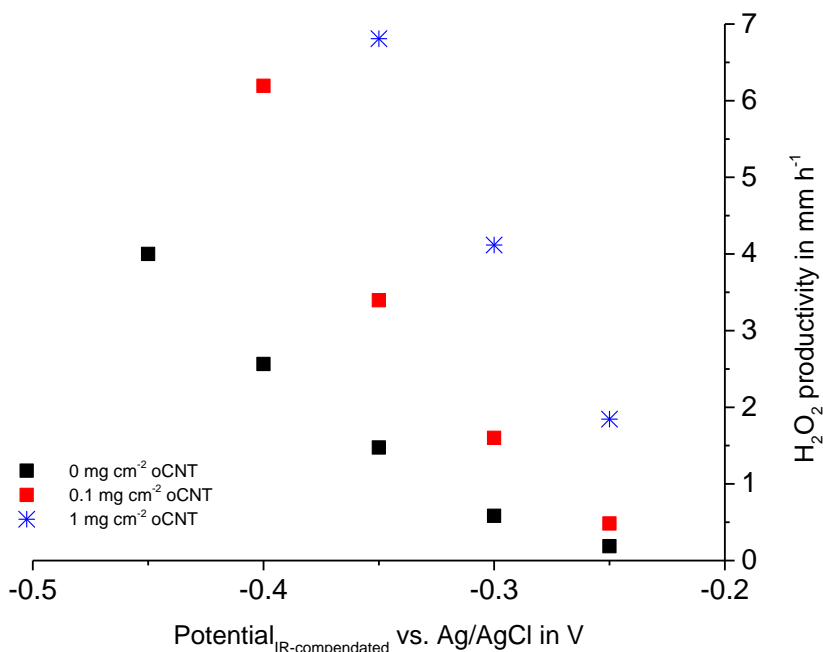
Figure 2   Hydrogen peroxide production at oCNT-modified electrodes at different potentials. Production rates were determined by linear regression. The regression coefficient was at least R2 > 0.99. Potentials are iR-compensated.

In the next step of the investigation, the electrochemical production of H_2O_2 was combined with enzymatic conversion of 4-pentenoic acid to bromolactone (Scheme 1). Figure 3 compares the product formation at an unmodified electrode and that at an electrode with 1 mg of oCNTs cm^{-2} at -250 and -350 mV vs. Ag/AgCl. The highest production rate can be

measured at the modified electrode at the more negative potential. Bromolactone was produced at approximately 4.5 mM h^{-1}. The productivity at the modified electrode was more than 8 times higher than in the unmodified electrode. This is mainly due to improved H_2O_2 production (see Figure 2), an improvement in the product formation rate that can also be observed at -250 mV vs. Ag/AgCl. The modified electrode produces roughly 4 times more product in the first 5 h than the unmodified electrode. A brief comparison of the H_2O_2 generation (Figure 2) with the actual product accumulation rates reveals that about 50 % of the electrochemically generated H_2O_2 is used productively. This rather poor efficiency can most likely be attributed to the undesired, spontaneous reaction between H_2O_2 and hypobromite.[19] In all experiments, the current efficiencies were around 80 %.
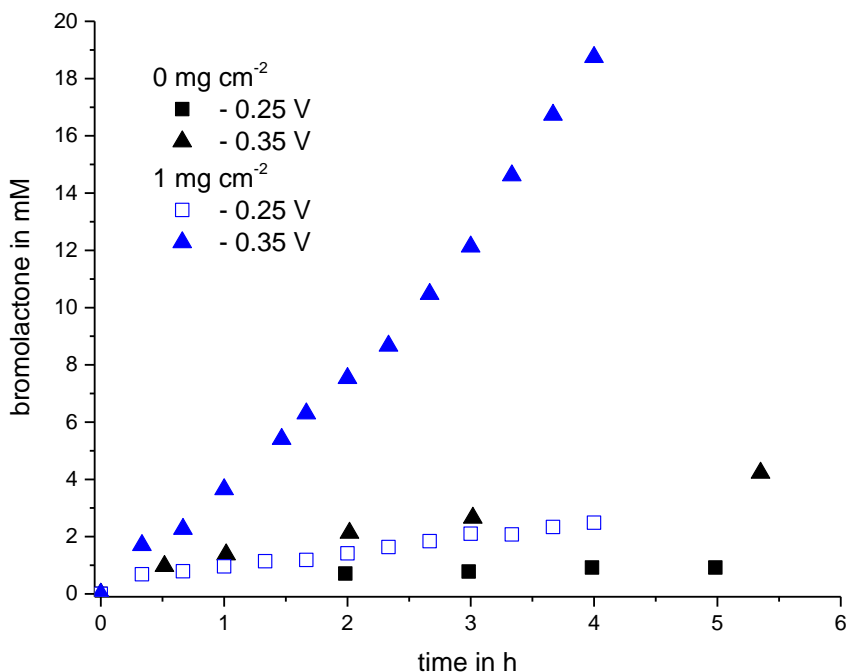
Figure 3   Electroenzymatic product formation at an unmodified electrode and an oCNT-coated electrode at -0.25 and -0.35 V vs. Ag/AgCl.

Further adjustments of the reaction parameters (particularly of the concentrations of *Ci*VCPO and Br⁻) will reduce this futile reaction. As shown in Figure 3, the modified electrode at -250 mV performs roughly as the untreated electrode at -350 mV. Usually, noble metals are used to decrease the overpotential of different electrode reactions, but here we have made it using abundant carbon-based materials that also have ecological and economic appeal.

As these results demonstrate, doping of the catalyst allows reduction of the overpotential that has to be applied to this system by about 100 mV while essentially maintaining the same productivity - thus directly increasing the energy efficiency of this electroenzymatic catalysis.

Conclusion

The results show the importance of the optimization studies of the catalyst used in the GDEs, where the electrode functionalized with carbon-based material considerably reduces its overpotential, making it a potential candidate for use with peroxygenase enzymes.

Experimental Section

All chemicals were purchased for Sigma--Aldrich at the highest purity available. The oxidized carbon nanotubes (*o*-CNT) were a gift from the group of Yi Cui (Stanford University, Stanford, CA, USA). The Sigracet GDL 38 BC carbon paper was a gift from SGL Carbon (Germany).

Synthesis of 5-(bromomethyl)dihydrofuran-2(3H)-one (bromolactone)

The synthesis of the bromolactone as an authentic standard was performed at room temperature for 24 h with stirring. A 100 mM citrate buffer (pH 5, the final volume of 50 mL) contained 160 mM KBr, 10 mmol 4-pentenoic acid, 100 nM *Ci*VCPO and 100 mM of H_2O_2. At the end of the reaction, the mixture was extracted by dichloromethane ($3\times$, 100 mL) and dried over anhydrous Na_2SO_4. The combined organic layers were concentrated under reduced pressure. The bromolactone compound was isolated by using flash column chromatography on silica gel (EtOAc/hexanes, 1:2) and analyzed by ^{1}H NMR spectroscopy to give 1.4 g of isolated product (80 % yield).

Enzyme preparation

100 mL pre-cultures of LB (in g L^{-1}: tryptone 10, yeast extract 5, NaCl 10) medium containing 50 µg mL^{-1} ampicillin were inoculated with *E. coli* TOP10 pBADgIIIB VCPO and incubated overnight at 37 °C and 180 rpm. Overexpression was carried out in 5 L flasks with 1 L of TB (in g L^{-1}: tryptone 12, yeast extract 24, glycerol 5, in 89 mM KPi buffer pH 7.5) medium supplemented with 50 µg mL^{-1} of ampicillin and grown at 37 °C and 180 rpm. At an OD_{600} of 0.9 A.U., 0.02 wt. % of L-arabinose was added. After induction, cultures were incubated for an additional 24 h at 25 °C and 180 rpm. The bacterial pellets obtained after centrifugation were re-suspended in 50 mM Tris/H_2SO_4 buffer (pH 8.1). 0.1 mM phenylmethylsulfonyl fluoride (100 mM stock in isopropanol) was added to the re-suspended cells, which were ruptured by sonication on ice (output 4, cycle 40 %). The samples were then centrifuged (10 000 rpm for 20 minutes) and the supernatant was incubated at 70 °C for 1.5 h. After centrifugation (10 000 rpm for 10 minutes), the absence of catalase activity was determined by adding the enzyme to a solution of 0.1 % Triton and 3 % H_2O_2 in a KPi buffer (50 mM, pH 7.0). [20] The clarified protein solution was further purified with a Q Sepharose FF column. After washing with 2 column volumes of 50 mM Tris/H_2SO_4, pH 8.1 and 2 column volumes of 0.1 M NaCl in 50 mM Tris/H_2SO_4, pH 8.1, the enzyme was loaded at 7.5 mL min^{-1} and after that eluted with 0.6 M NaCl in 50 mM Tris/H_2SO_4, pH 8.1. Fractions containing *Ci*VCPO (determined by the MCD activity assay) were pooled, concentrated (Amicon 10 kDa cut-off membrane), and desalted by using HiTrap desalting or PD10 columns (GE Healthcare) and 50 mM Tris/H_2SO_4, pH 8.1 containing 100 µM orthovanadate.

*Ci*VCPO activity was quantified by the monochlorodimedone (MCD) assay. The enzyme solution was added to a reaction mixture containing MCD (50 μM), KBr (5 mM), and orthovanadate (100 μM) in a 100 mM citrate buffer at pH 5.0. After the addition of H_2O_2 (5 mM), the enzyme activity could be determined by following the decrease in absorbance at 290 nm. After purification, the *Ci*VCPO solution used in this study had a purity of 64 %, as determined by gel densitometry, with a specific MCD-activity of 65.5±6.1 U mg^{-1}.

Electrode preparation

A solution of oxidized carbon nanotubes (*o*-CNTs; 2 mg mL^{-1} or 5 mg mL^{-1}) was suspended in ethanol containing 1 % w/v Nafion 117 (Sigma--Aldrich, Germany) and sonicated for 60 min. This suspension was evenly pipetted onto 5 cm×5 cm sheets of Sigracet GDL 38 BC. Electrodes were left out to dry overnight and used without further conditioning.

(Bio)electrochemical setup

Experiments were carried out in a H-cell [21] divided by a proton exchange membrane (Nafion 117, Sigma--Aldrich, St. Louis, USA). The anode consisted of a 4 cm×2 cm platinum sheet contacted by a glass-coated platinum wire. The anode chamber was filled with 100 mL of a 100 mM Na-Citrate buffer of pH 5. The cathode was prepared as described above and used as a gas-diffusion electrode (GDE) by mounting it to the circular opening at the side of the H-cell (2.4 cm diameter). The coated side of the paper was in contact with the aqueous phase. A Ni-mesh was added to the air side of the GDE to ensure proper contact. The cathode chamber was filled with 100 mL 100 mM Na-Citrate buffer pH 5 containing 100 mM

KBr. An Ag/AgCl electrode in a Luggin capillary filled with 0.5 M Na$_2$SO$_4$ was used as a reference electrode. The tip of the Luggin capillary was placed at a distance of about 4 mm from the cathode. All experiments were carried out by using a GAMRY Reference 600 potentiostat/galvanostat. Prior to all experiments, the internal resistance was determined by impedance spectroscopy (about 17 Ω) by using the manufacturer provided program "Get Ru". Linear sweep/cyclic voltammetry measurements were carried out without *iR* correction and were *iR* corrected after the experiments. Chronoamperometric experiments were carried out by using positive-feedback *iR* compensation by applying 90 % of the internal resistance that had been determined before starting the experiments. Bioelectrochemical experiments were carried out in the same setup. For these experiments, 50 mM 4-pentenoic acid and either 25 nM *Ci*VCPO for experiments carried out at -250 mV vs. Ag/AgCl or 100 nM *Ci*VCPO for experiments carried out at 350 mV vs. Ag/AgCl, were added to the cathode chamber containing 100 mM sodium citrate buffer (100 mL, pH 5) with 100 mM KBr. Experiments were started by applying a constant voltage using positive feedback iR compensation as described above.

Electrochemical H₂O₂ measurement

Hydrogen peroxide concentrations were determined electrochemically by using a Select 2700 Biochemistry Analyzer (Yellow Springs Instruments, OH, USA) equipped with blank membranes. The calibration solution consisted of 30 mg L^{-1} H$_2$O$_2$ in a 20 mM Na-citrate buffer. The sample size taken was 25 μL and the measurement time was 30 s. A typical calibration sample yielded a 10 nA signal with a baseline current below 2 nA.

Gas chromatography

Aqueous samples (500 μL) were acidified by the addition of 6 M HCl (50 μL) and extracted with ethyl acetate (500 μL) containing 10 mM acetophenone as an internal standard. Concentrations of 4-pentenoic acid and the bromolactone were determined by gas chromatography coupled with flame ionization detection (FID; GC-17A, Shimadzu, Japan). The compounds were separated on a DB-WAXetr column (30 m×0.25 mM×0.25 μM; Agilent, CA, USA) with a split ratio of 1:20, at a linear velocity of 31.5 cm s^{-1} with helium as a carrier gas by using the following temperature profile: 130 °C to 190 °C at 7 °C min^{-1}; to 230 °C at 15 °C min^{-1}; hold 3 min. The resulting retention times were 4.0 min for acetophenone, 5.1 min for 4-pentenoic acid, and 10.4 min for bromolactone.

Contribution to this paper

Almeida T.P. contributed here determining starting parameters such as the potential applied on to electrode vs. H_2O_2 production.

Reference

1. Burek, B. O., Bormann, S., Hollmann, F., Bloh, J. Z. & Holtmann, D. Hydrogen peroxide driven biocatalysis. *Green Chemistry* **21**, 3232–3249 (2019).

2. Bormann, S., Gomez Baraibar, A., Ni, Y., Holtmann, D. & Hollmann, F. Specific oxyfunctionalisations catalysed by peroxygenases: Opportunities, challenges and solutions. *Catalysis Science and Technology* **5**, 2038–2052 (2015).

3. Ni, Y. *et al.* Peroxygenase-Catalyzed Oxyfunctionalization Reactions Promoted by the Complete Oxidation of Methanol. *Angew. Chemie Int. Ed.* **55**, 798–801 (2016).

4. Jung, D., Streb, C. & Hartmann, M. Covalent Anchoring of Chloroperoxidase and Glucose Oxidase on the Mesoporous Molecular Sieve SBA-15. *Int. J. Mol. Sci.* **11**, 762–778 (2010).

5. Willot, S. J.-P. *et al.* Expanding the Spectrum of Light-Driven Peroxygenase Reactions. *ACS Catal.* **9**, 890–894 (2019).

6. Perez, D. I., Grau, M. M., Arends, I. W. C. E. & Hollmann, F. Visible light-driven and chloroperoxidase-catalyzed oxygenation reactions. *Chem. Commun.* 6848–6850 (2009). doi:10.1039/b915078a

7. Zhang, W. *et al.* Selective Activation of C−H Bonds in a Cascade Process Combining Photochemistry and Biocatalysis. *Angew. Chemie Int. Ed.* **56**, 15451–15455 (2017).

8. Lütz, S., Vuorilehto, K. & Liese, A. Process development for the electroenzymatic synthesis of (*R*)-methylphenylsulfoxide by use of a 3-dimensional electrode. *Biotechnol. Bioeng.* **98**, 525–534 (2007).

9. La Rotta Hernández, C. E., Werberich, D. S., Mattos, M. C. S. de & D'Elia, E. Electrogeneration of hydrogen peroxide applied to the peroxide-mediated oxidation of (R)-limonene in organic media. *Electron. J. Biotechnol.* **10**, 521–535 (2007).

10. Horst, A. E. W., Mangold, K.-M. & Holtmann, D. Application of gas diffusion electrodes in bioelectrochemical syntheses and energy conversion. *Biotechnol. Bioeng.* **113**, 260–267 (2016).

11. Horst, A. E. W. *et al.* Electro-enzymatic hydroxylation of ethylbenzene by the evolved unspecific peroxygenase of Agrocybe aegerita. *J. Mol. Catal. B Enzym.* **133**, S137–S142 (2016).

12. Holtmann, D., Krieg, T., Getrey, L. & Schrader, J. Electroenzymatic process to overcome enzyme instabilities. *Catal. Commun.* **51**, 82–85 (2014).

13. Krieg, T., Hüttmann, S., Mangold, K. M., Schrader, J. & Holtmann, D. Gas diffusion electrode as novel reaction system for an electro-enzymatic process with chloroperoxidase. *Green Chem.* **13**, 2686–2689 (2011).

14. Getrey, L., Krieg, T., Hollmann, F., Schrader, J. & Holtmann, D. Enzymatic halogenation of the phenolic monoterpenes thymol and carvacrol with chloroperoxidase. *Green Chem.* **16**, 1104–1108 (2014).

15. Lu, Z. *et al.* High-efficiency oxygen reduction to hydrogen peroxide catalysed by oxidized carbon materials. *Nat. Catal.* **1**, 156–162 (2018).

16. Dong, J. J. *et al.* Halofunctionalization of alkenes by vanadium chloroperoxidase from Curvularia inaequalis. *Chem. Commun.* **53**, 6207–6210 (2017).

17. Fernández-Fueyo, E. *et al.* Chemoenzymatic Halogenation of Phenols by using the Haloperoxidase from *Curvularia inaequalis*. *ChemCatChem* **7**, 4035–4038 (2015).

18. Fernández-Fueyo, E. *et al.* A Biocatalytic Aza-Achmatowicz Reaction. *ACS Catal.* **6**, 5904–5907 (2016).

19. Renirie, R. *et al.* Vanadium Chloroperoxidase as a Catalyst for Hydrogen Peroxide Disproportionation to Singlet Oxygen in Mildly Acidic Aqueous Environment. *Adv. Synth. Catal.* **345**, 849–858 (2003).

20. Iwase, T. *et al.* A simple assay for measuring catalase activity: A visual approach. *Sci. Rep.* **3**, (2013).

21. Stöckl, M., Teubner, N. C., Holtmann, D., Mangold, K.-M. & Sand, W. Extracellular Polymeric Substances from *Geobacter sulfurreducens* Biofilms in Microbial Fuel Cells. *ACS Appl. Mater. Interfaces* **11**, 8961–8968 (2019).

| Ultra-Thin Films of Reduced Graphene Oxide (rGO) Nanoplatelets Functionalized with Different Organic Materials | **6** |

Introduction

Here, we present electrochemical studies of graphene nanoplates (GNPs) that were nanostructured in multilayers with glucose oxidase. The literature is abundant in applications using graphene derivatives, such as catalysis,[1] supercapacitors[2], and even bactericidal uses.[3] They are exciting materials to tailor some properties, such as the reported significant increase in charge carrier mobility just changing the size of the nanoplatelets in multilayered GNPs.[4]

Graphene oxide (GO) used here was produced by the Hummers method[5,6], and briefly, GO is an atomically thin sheet of graphite covalently linked to oxygenated functional groups on the basal plane and at the edges, containing a mixture of sp^2 and sp^3 carbon atoms.[7] The reduced form of graphene oxide (rGO) studied here has low oxygenated functional group content and exhibits electric and mechanical properties similar to pristine graphene.[8] Despite being a milestone in 2D materials,[9] there are still some drawbacks of using pristine graphene to cover large areas and that has paved the way in using GNPs as alternative materials resembling graphene properties. Here, we employed the Layer-by-Layer (LbL) technique to build up a laminated interlocked structure of rGO nanoplatelets with Glucose Oxidase (GOx). The LbL method allows a simple, fast, versatile and reproducible way to modify large areas with excellent control over the thickness and morphology of the film. It has been successfully applied to form ultrathin films of graphene and carbon nanotubes,[10–13] enabling the immobilization of enzymes in highly-ordered nanostructures.[14,15] The presence of graphene nanoplatelets dispersed in multilayered LbL architectures might bridge a favorable charge transfer path from

immobilized enzymes to the electrode, paving the way for future applications in biofuel cells and biosensing. Within this context, the multilayered film reported here is a straightforward approach to sequestrate electrons at the electrode interface. Here, rGO nanoplatelets were functionalized with poly (styrenesulfonic acid) (GPSS) and chitosan (G-chitosan) to produce stable water suspensions, enabling the film grown by the LbL deposition. The materials were characterized by UV-vis and Fourier transform infrared (FTIR) spectroscopies, indicating an effective reduction process from GO to rGO nanoplatelets. LbL films were easily assembled using GPSS and G-chitosan with GOx, further characterized by cyclic voltammetry, which pointed out an increase in the current intensities due to the presence of graphene nanoplatelets in the film nanostructure.

Results and discussion

The UV-vis absorbance spectra for GO, chitosan and G-chitosan are illustrated in Figure 1a, while those for PSS and GPSS solutions are shown in Figure 1b, confirming the successful synthesis and functionalization processes. All spectra were normalized to remove concentration effects over the samples analyzed, focusing mainly on the peak positions. It is possible to observe two characteristics GO bands, one at 232 nm characteristic of $\pi\rightarrow\pi^*$ transition in aromatic C-C bonds, and other at 302 nm assigned to $n\rightarrow\pi^*$ transition in C=O.[16] It is possible to note a redshift in the $\pi\rightarrow\pi^*$ transition band with PSS or chitosan functionalization. The GO band at 232 nm shifts to 271 nm in GPSS and 263 nm in G-chitosan, clearly indicating the electronic conjugation reestablishment after the reduction process.[17,18] It is also remarkable the presence of a band at 225 nm in the GPSS spectrum, corresponding to the absorption of the PSS benzene group,[19] readily

comparable to the pristine PSS spectra. It was also observed a band at 197 nm in the chitosan spectrum, from N-acetyl-glucosamine (GlcNAc) and glucosamine (GlcN) chromophoric groups.[19]
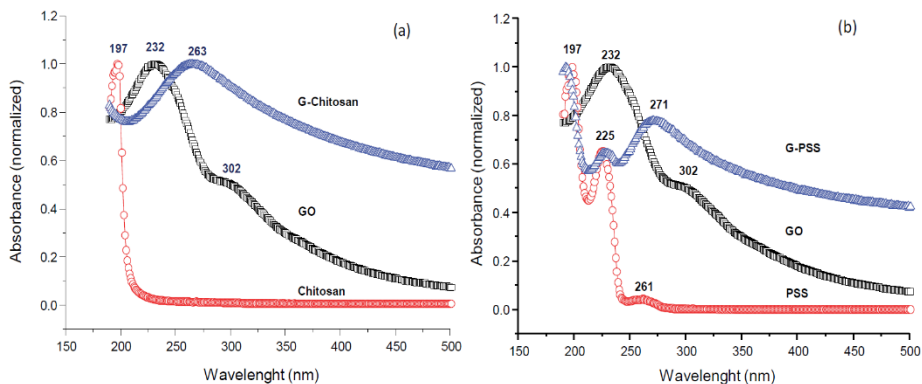
Figure 1: UV-Vis absorbance spectra of solutions prepared in ultrapure water.

From the solutions of G-chitosan and GPSS, LbL films were grown using GOx as a counter-solution required for the electrostatic interactions governing the film fabrication. The adsorption kinetics of the LbL films is illustrated in Figure 2. In short, the LbL film formation was monitored at each deposition step, fixing the GOx deposition time at 180 s, with a varying immersion time deposition for G-chitosan (Figure 2a). A plot of the cumulative G-chitosan time (Figure 2b) indicates a plateau after 900 s, indicative that no effective material adsorption occurs after that. The same procedure was repeated fixing the G-chitosan deposition time at 900 s, now varying the GOx immersion time (results not shown). Similarly, the best deposition time for G-chitosan was obtained at ~ 900 s (results not show). A linear dependence was observed (Figure 2c) in the LbL film growth using

the optimized deposition times, revealing that a similar amount of material was transferred at each deposition step in the nanostructured films.[20]
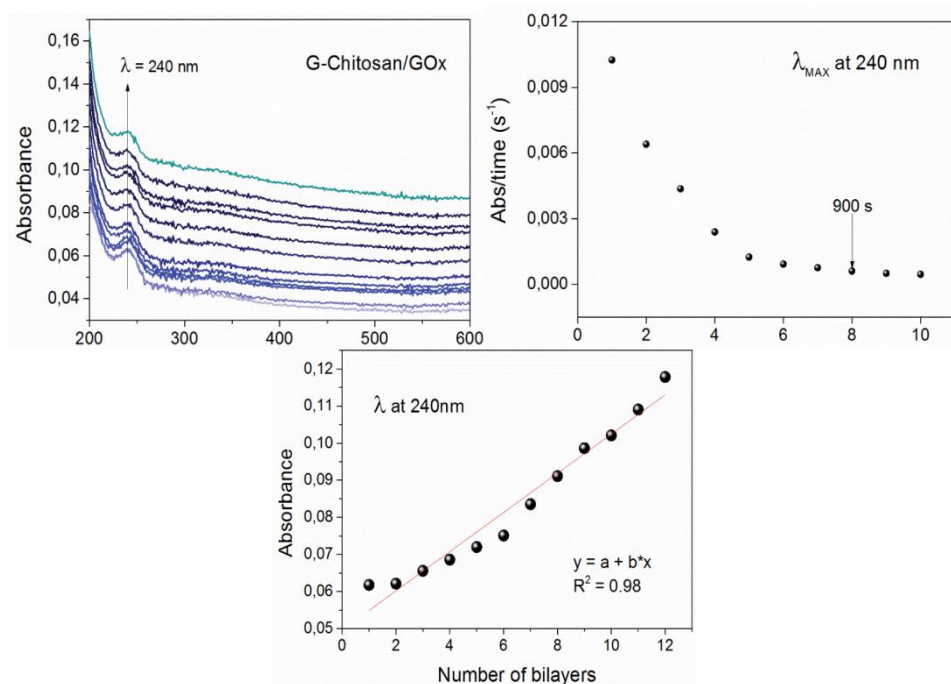
Figure 2 (a) UV absorbance for the LbL assembly. Black arrow indicates increasing absorbance at 240 nm with the number of deposited layers; (b) kinetic growth plot used to choose the best deposition time; (c) linear dependence of absorbance (λmax=225 nm) at each deposition step for the (G-chitosan/GPSS/ GOx) LbL film. No significant changes in absorbance are observed after 900 s.

Likewise, the best deposition time for GPSS was achieved at 300 s (results not shown), but we decided to use 900 s to keep the same deposition parameters in the LbL film fabrication. FTIR spectra for GO, chitosan, G-chitosan, PSS and GPSS (presented in Figures 3a and 3b) were acquired to investigate the intermolecular interactions governing the rGO functionalization, to confirm both the interactions between materials and the

effectiveness of the reduction process adopted. However, the nature of those interactions is different for both G-Chitosan and GPSS. The FTIR spectrum of GO nanoplatelets shows characteristic peaks at 1735 cm^{-1} (C=O carbonyl stretching), 1602 cm^{-1} (sp^2 -hybridized C=C in plane vibrations), 1423 cm^{-1} (OH deformation of the C-OH groups), 1219 cm^{-1} (C-OH stretching vibration) and 1045 cm^{-1} (C-O stretching vibrations).[21,22] In Figure 3a, two characteristic peaks were slightly shifted in the G-chitosan spectrum when compared to pristine chitosan and GO. The main observed changes were from 1735 to 1717 cm^{-1} (C=O carbonyl stretching vibrations assigned to GO), and from 1089 to 1100 cm^{-1}(C-O stretching glucoside ring in chitosan)[23,24]. A third peak could also be a shift from 1508 cm^{-1} (chitosan) or 1427 cm^{-1} (GO) to 1451 cm^{-1} (G-Chitosan), and that might probably be an interaction between chitosan and the formed rGO nanoplatelets.[23,24] However, the uncertainty about this broad peak hampers its assignment, but it does not compromise the conclusions about a chemical interaction between the GO and chitosan. On the other hand, physical interaction (van der Waals) was noticed between PSS and rGO nanoplatelets since there hasn't been observed new bands or shifts in the GPSS spectrum when compared with the pristine materials spectra; the GPSS spectrum can be called a sum of the bands observed in the PSS and rGO spectra. Very small shifts were observed, for instance from 1128 to 1132 cm^{-1} possibly due to hydrophobic interactions between the sp^2 network in the nanoplatelets with the benzene ring in PSS.[25]

Conclusions cannot be drawn in this region since it is within the equipment error (4 cm^{-1}), reinforcing physical interactions between these materials. It is important to mention the analysis in the 2800 up to 3700 cm^{-}

[1]region, normally assigned to C-H, N-H and O-H stretchings. No relevant results were obtained due to the low signal-to-noise ratio (results not shown).
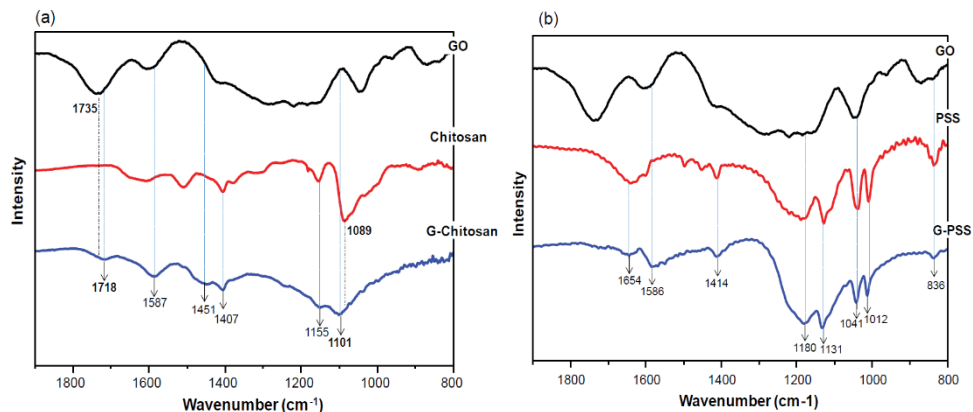
Figure 3 FTIR spectra in transmission mode for (a) GO, chitosan and G-chitosan; (b) GO, PSS and GPSS.

These findings are in good agreement with the sp^2 conjugation re-establishment displayed in Figure 2, followed by an active functionalization of the rGO nanoplatelets with chitosan (G-chitosan) and PSS (GPSS) during the synthesis. The primary FTIR peak assignments for GO, chitosan and PSS are displayed in Table 1.

Table 1 FTIR peaks positions and assignments [21–24,26] for GO, chitosan and PSS films. In the table, the vibrations of the molecules are abbreviated using v: stretching; vas: asymmetric stretching; vs: symmetric stretching; δ: bending.

GO		Chitosan		PSS	
Wavenumber (cm^{-1})	Assignment	Wavenumber (cm^{-1})	Assignment	Wavenumber (cm^{-1})	Assignment
1733	v C=O	~1655	v C=O	1633	v C=C
1610	v$_{as}$ COO$^-$	1510	δ −NH$_3^+$	1598	C=C
1427	v$_s$ COO$^-$	1409	δ O−H/C−H	1498	v C=C
1222	v C=O	1155	C−O−C	1452	C=C
1045	v C−O	1089	v CO	1180	v$_{as}$ S=O
				1128	ring
				1041	v$_s$ S=O
				1006	δ ring

Figure 4 indicates a linear electrochemical response, thus indicating the presence of a diffusive process controlled by the surface of the LbL modified electrodes.
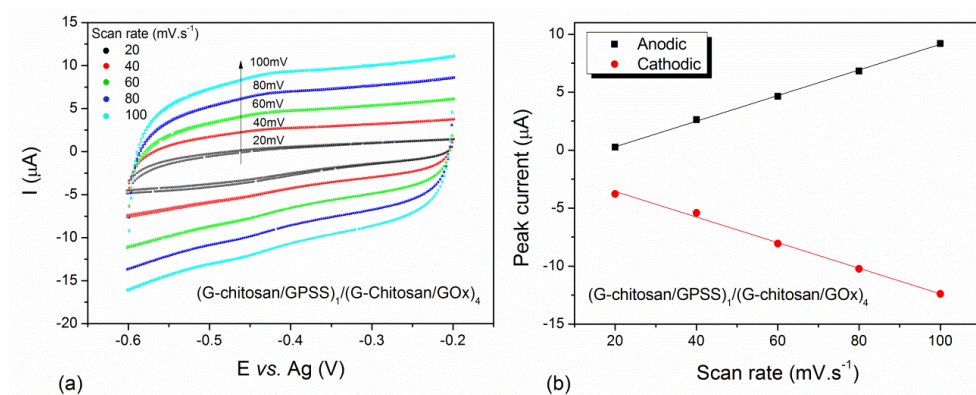
Figure 4 (a) Cyclic voltammetry at different scan rates; (b) Peak current vs. scan rate for (G-chitosan/GPSS)1/(G-chitosan/GOx)4 LbL film immersed in 0.1 M PBS and pH 6.2.

The absence of redox peaks in the CV experiments pointed to a possible strong electrochemical double-layer effect ruling the system.[26,27] In addition, the analysis of the currents as a function of the scanning rate in the 20 - 100 mV.s^{-1} window indicated higher currents for the LbL films, when compared with bare SPE electrodes, Each curve displayed in Figure 4 presented good stabilization after 3 scan cycles, a significant capacitive behavior due to the presence of graphene nanoplatelets. The flat oxidative performance in the voltammograms implies in lower resistance of the system to release storage charges due to the presence of the rGO nanoplatelets, which also promotes a better electron transfer between the LbL modified electrode and buffer solution.

The anodic peak current exhibited a linear relationship with the number of deposited bilayers (Figure 5), displaying once again excellent capacitance contribution from the rGO nanoplatelets. The linearity observed in Figure 5B points to equal changes in the measured current as the film thickness increases, due to the same amount of material transferred at each LbL step deposition, corroborating results presented in Figure 2. Here, identical changes in current can be attributed to effective interlocked conductive pathways formed in the LbL film structure by the rGO nanoplatelets with the electrode surface, without noticeable effects from the wrapping materials (chitosan or PSS).
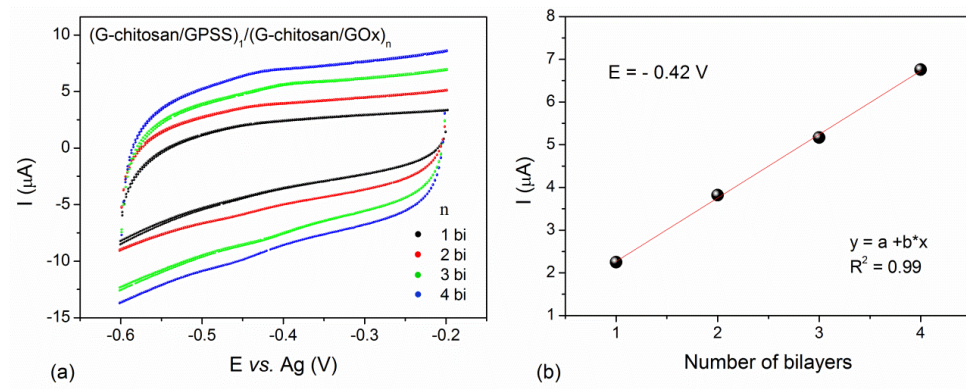
Figure 5 (a) Cyclic voltammograms conducted at 80 mV.s^{-1} scan rate for 1, 2, 3 and 4 bilayers and (b) plot of the anodic peak vs. the number of bilayers for (G-chitosan/ GPSS)1/(G-chitosan/GOx)4 immersed in aqueous 0.1M PBS pH 6.2.

Conclusions

The reduction process was efficient in creating rGO nanoplatelets wrapped with chitosan or PSS. The spectroscopic characterization indicated an excellent conversion from GO to rGO, pointing to a chemical interaction between chitosan and the rGO nanoplatelets, and physical interaction between PSS and the rGO nanoplatelets. A linear transfer of the materials was observed in the LbL film formation, indicative that similar amounts of material were transferred at each deposition step. The electrochemical characterization displayed a possible double-layer effect ruling the system, with higher current intensities (excellent capacitance contribution) observed in the presence of the LbL films due to conductive pathways formed by the rGO nanoplatelets in the multi-layered LbL film structure, without noticeable effects from the wrapping materials (chitosan or PSS). The results presented here are a promising step for future studies were the rGO can be easily explored in electron transfer mechanisms between enzymes and electrodes.

Materials and methods

Graphite powder (98%) from Synth, potassium permanganate ($KMnO_4$, 99%), sulfuric acid (H_2SO_4, 97%) and potassium thiosulfate ($K_2S_2O_3$, 99%) from Ecibra, hydrogen peroxide (H_2O_2, 30%), hydrazine sulfate ($H_6N_2O_4S$) and phosphorus pentoxide (P_2O_5) from Vetec, glucose oxidase (from Aspergillus niger) (GOx) (type VII, lyophilized powder, $\geq$ 100,000 units.g^{-1} solid, without added oxygen) and poly(sodium 4-styrenesulfonate) (PSS) (Mw 70,000) from Sigma-Aldrich were all used as received. Chitosan was obtained from shrimp shells using the method described by Bought et al. resulting in a material with molecular weight Mw=9.104 g.mol^{-1} with acetylation degree.[28]

Procedures

Initially, graphene oxide (GO) was obtained from the Hummers' method,[6,29] 0.1 g of GO was solubilized in water (50 mL) and sonicated for 600 s. 250 mg of chitosan was solubilized in 50 mL of HCl 0.05 mol.L^{-1} and similarly sonicated for 600 s. After that, both solutions were mixed with 0.1302 g of $H_6N_2O_4S$ (hydrazine) to start the reduction and functionalization processes, stirred at 70 °C and kept under closed reflux for 20 hours. The final product consists of rGO nanoplatelets functionalized with chitosan (G-chitosan). A similar process was applied to obtain reduced graphene oxide functionalized with PSS (GPSS). To this end, 0.5 g of GO were sonicated in 50 mL of water for 600 s. Then, 0.5 g of PSS and 0.0651 g of hydrazine were added, with the final solution stirred at 90 °C for 12 hours under reflux.

LbL films fabrication

Instead of using the traditional dipping method [12], we applied small drops of the polyelectrolytes to cover the surface of the carbon Screen-Printed Electrode (SPE), as described below. Briefly, a drop of G-chitosan was kept 15 min onto the SPE, followed by a washing step to remove molecules loosely bound to the electrode surface. Then a drop of GPSS (oppositely charged material) was sequentially spread on the same area and kept 15 min onto the SPE/G-chitosan interface, thus forming a (G-chitosan/GPSS)$_1$ bilayer. The process is repeated until the formation of five bilayers (G-chitosan/GPSS)$_5$ onto the SPE, with a final top GOx layer deposited onto it. GPSS, GOx and G-chitosan solutions were all at 1.0 mg.mL^{-1} suspended in 0.1 mol.L^{-1} phosphate buffer salt (PBS) solution (pH 6.2).

Casting films fabrication

For the FTIR analysis casting films were formed onto silicon substrates from concentrated solutions of the polyelectrolytes.

Instrumentation

All solutions were prepared with ultrapure water acquired from a Sartorius system, model Arium Comfort. The solutions were also briefly sonicated using a probe from QSonica Sonicators, model Q700. UV-Vis (Biochrom Libra S60 spectrophotometer) and FTIR (Thermo Nicolet spectrometer, model Nexus 470 in transmission) spectroscopies were used to confirm the effectiveness of the rGO synthesis and functionalization. The performance of the LbL films composed of GOx, G-chitosan and GPSS was evaluated using cyclic voltammetry (Autolab Potentiostat/Galvanostat,

model PGSTAT302N). All LbL films were deposited onto carbon screen-printed electrodes (SPE DropSens 110, commercially obtained from Methron) as described previously, with electrochemical measurements taken at a scan rate potential of 80 mV.s^{-1}.

Acknowledgments

Contribution to this paper

Almeida T.P. contributed to the synthesis of the rGOs and participated in all parts of these experiments**.**

References

1. Huang, H., Chen, H., Sun, D. & Wang, X. Graphene nanoplate-Pt composite as a high performance electrocatalyst for direct methanol fuel cells. *J. Power Sources* **204**, 46–52 (2012).

2. Huang, H. & Wang, X. Graphene nanoplate-MnO2 composites for supercapacitors: A controllable oxidation approach. *Nanoscale* **3**, 3185–3191 (2011).

3. Mahmoudi, E., Ng, L. Y., Ba-Abbad, M. M. & Mohammad, A. W. Novel nanohybrid polysulfone membrane embedded with silver nanoparticles on graphene oxide nanoplates. *Chem. Eng. J.* **277**, 1–10 (2015).

4. Jimenez, M. J. M. *et al.* Charge carrier transport in defective reduced graphene oxide as quantum dots and nanoplatelets in multilayer films. *Nanotechnology* **28**, (2017).

5. Soldano, C., Mahmood, A. & Dujardin, E. Production, properties and potential of graphene. *Carbon* **48**, 2127–2150 (2010).

6. Hummers, W. S. & Offeman, R. E. Preparation of Graphitic Oxide. *J. Am. Chem. Soc.* **80**, 1339 (1958).

7. Zhang, S. *et al.* Polyelectrolyte-Induced Reduction of Exfoliated Graphite Oxide: A Facile Route to Synthesis of Soluble Graphene Nanosheets. *ACS Nano* **5**, 1785–1791 (2011).

8. Loh, K. P., Bao, Q., Eda, G. & Chhowalla, M. Graphene oxide as a chemically tunable platform for optical applications. *Nat. Chem.* **2**, 1015–1024 (2010).

9. Ruoff, Y. Z. S. M. W. C. X. L. J. W. S. J. R. P. R. S. *et al.* Graphene and Graphene and Oxide: Sy and Applications. *Adv. Mater.* **22**, 3906 (2010).

10. Silva, J. S., De Barros, A., Constantino, C. J. L., Simões, F. R. & Ferreira, M. Layer-by-layer films based on carbon nanotubes and polyaniline for detecting 2-chlorophenol. *J. Nanosci. Nanotechnol.* **14**, 6586–92 (2014).

11. Tian, M. *et al.* Versatile and ductile cotton fabric achieved via layer-by-layer self-assembly by consecutive adsorption of graphene doped PEDOT: PSS and chitosan. *Carbon N. Y.* **96**, 1166–1174 (2016).

12. Decher, G. Fuzzy nanoassemblies: toward layered polymeric multicomposites. *Science (80-.).* (1997).

13.   Richardson, J. J., Björnmalm, M. & Caruso, F. Multilayer assembly. Technology-driven layer-by-layer assembly of nanofilms. *Science* **348**, aaa2491 (2015).

14.   Lutkenhaus, J. L. & Hammond, P. T. Electrochemically enabled polyelectrolyte multilayer devices: From fuel cells to sensors. *Soft Matter* **3**, 804–816 (2007).

15.   Graça, J. S., de Oliveira, R. F., de Moraes, M. L. & Ferreira, M. Amperometric glucose biosensor based on layer-by-layer films of microperoxidase-11 and liposome-encapsulated glucose oxidase. *Bioelectrochemistry* **96**, 37–42 (2014).

16.   Kumirska, J. *et al.* Application of Spectroscopic Methods for Structural Analysis of Chitin and Chitosan. *Mar. Drugs* **8**, 1567–1636 (2010).

17.   Khanra, P. *et al.* Simultaneous bio-functionalization and reduction of graphene oxide by baker's yeast. *Chem. Eng. J.* **183**, 526–533 (2012).

18.   Villar-Rodil, S. *et al.* Preparation of graphene dispersions and graphene-polymer composites in organic media. *J. Mater. Chem.* **19**, 3591 (2009).

19.   Jiang, G., Baba, A. & Advincula, R. Nanopatterning and fabrication of memory devices from layer-by-layer poly(3,4-ethylenedioxythiophene)-poly(styrene sulfonate) ultrathin films. *Langmuir* **23**, 817–25 (2007).

20.   Volpati, D. *et al.* Physical vapor deposited thin films of lignins extracted from sugar cane bagasse: Morphology, electrical properties, and sensing applications. *Biomacromolecules* **12**, 3223–3231 (2011).

21. Wu, N., She, X., Yang, D., Wu, X. & Su, F. Synthesis of network reduced graphene oxide in polystyrene matrix by a two-step reduction method for superior conductivity of the composite. *J. Mater.* (2012).

22. Stankovich, S. *et al.* Stable aqueous dispersions of graphitic nanoplatelets via the reduction of exfoliated graphite oxide in the presence of poly(sodium 4-styrenesulfonate). *J. Mater. Chem.* **16**, 155–158 (2006).

23. Espinosa-Andrews, H. & Sandoval-Castilla, O. Determination of the gum Arabic–chitosan interactions by Fourier Transform Infrared Spectroscopy and characterization of the microstructure and rheological features. *Carbohydrate* (2010).

24. Fernandes, L., Resende, C., Tavares, D. & Soares, G. Cytocompatibility of chitosan and collagen-chitosan scaffolds for tissue engineering. *Polimeros* (2011).

25. Lu, J., Do, I., Fukushima, H., Lee, I. & Drzal, L. T. Stable aqueous suspension and self-assembly of graphite nanoplatelets coated with various polyelectrolytes. *J. Nanomater.* **2010**, (2010).

26. CARDENAS, G. & MIRANDA, S. P. FTIR AND TGA STUDIES OF CHITOSAN COMPOSITE FILMS. *J. Chil. Chem. Soc.* **49**, 291–295 (2004).

27. Pullini, D. *et al.* Enhancing the capacitance and active surface utilization of supercapacitor electrode by graphene nanoplatelets. *Compos. Sci. Technol.* **112**, 16–21 (2015).

28.   Bough, W. A., Salter, W. L., Wu, A. C. M. & Perkins, B. E. Influence of manufacturing variables on the characteristics and effectiveness of chitosan products. I. Chemical composition, viscosity, and molecular-weight distribution of chitosan products. *Biotechnol. Bioeng.* **20**, 1931–1943 (1978).

29.   Kovtyukhova, N. I. *et al.* Layer-by-Layer Assembly of Ultrathin Composite Films from Micron-Sized Graphite Oxide Sheets and Polycations. *Chem. Mater.* **11**, 771–778 (1999).

LIST OF PUBLICATIONS

Publications

1.   Bormann, S. et al. H2O2 Production at Low Overpotentials for Electroenzymatic Halogenation Reactions. ChemSusChem 12, 4759–4763 (2019).

2.   de Almeida, T. P. et al. Efficient Aerobic Oxidation of trans -2-Hexen-1-ol using the Aryl Alcohol Oxidase from Pleurotus eryngii. Adv. Synth. Catal. 361, 2668–2672 (2019).

3.   Van Schie, M. M. C. H. et al. Biocatalytic synthesis of the Green Note *trans*-2-hexenal in a continuous-flow microreactor. Beilstein J. Org. Chem. 14, 697–703 (2018).

4.   Jimenez, M. J. M. et al. Charge carrier transport in defective reduced graphene oxide as quantum dots and nanoplatelets in multilayer films. Nanotechnology 28, (2017).

5.   Gaal, G. et al. Simplified fabrication of integrated microfluidic devices using fused deposition modeling 3D printing. Sensors Actuators, B Chem. 242, 35–40 (2017).

6.   Schmidt, S., Pedroso de Almeida, T., Rother, D. & Hollmann, F. Towards environmentally acceptable synthesis of chiral α-hydroxy ketones via oxidase-lyase cascades. Green Chem. 19, 1226–1229 (2017).

7.   Almeida, T. P., Miyazaki, C. M., Volpati, D., Silva, T. A. & Braunger, M. L. Ultra-Thin Films of Reduced Graphene Oxide

(RGO) Nanoplatelets Functionalized with Different Organic Materials. J Bioprocess Biotech 6, 272 (2016).

8.   Almeida, T. P. et al. PEDOT: PSS self-assembled films to methanol crossover reduction in Nafion ® membranes. In Applied Surface Science 323, 7–12 (Elsevier B.V., 2014).

Submitted

1-Water enabled self-healing polymeric coating with reduced graphene oxide-reinforcement, K Ly, M Martínez, S Cucatti, D Volpati, MA Pereira-da-Silva, F Shimizu, TP Almeida, V Rodrigues, JF Silva, F Alvarez, A Riul Jr,

Posters

1. <u>ALMEIDA, T. P.</u>; HOLLMAN, F.; MIYAZAKI, CELINA M.; RIUL, ANTONIO. Influence of graphene-chitosan nanoplatelets in the direct electron transfer process of enzymes. 2015, MRS Boston, USA.

2. ALMEIDA, T. P.; SCHMIDT, S.; RIUL, A.; HOLLMANN, F., Characterization of the alcohol oxidase from Pichia pastoris for the application in cascade reactions, NCCC 2017, Noordwijkerhout, The Netherlands.

3. ALMEIDA, T. P.; YOUNES S.; FUEYO E. F.; SCHIMIDT, S.; ARENDS, I. RIUL JR., A.; HOLLMAN, F. Setup and characterization of a cascade transforming aryl alcohols into b-nitro-aryl alcohols, Biotrans 2017 - Budapest, Hungary

4. ALMEIDA, T. P.; VAN SCHIE; M, MA, A.; TIEVES, F.; FERNANDEZ-FUEYO, E.; ARENDS, I.; HOLLMANN, F., Aryl alcohol oxidase from *Pleurotus eryngii*; a promising candidate for industrial scale application, NCCC 2018, Noordwijkerhout, The Netherlands.

Acknowledgments

Antonio Riul Jr thank you for the day in your office when you accepted me, a biologist, to work with you in my master's degree in materials science. You started as a tutor and quickly became a friend. I am very grateful when a year of my master's degree, you invited me to start a PhD project in the new bioenergy program.

Frank Hollmann, thanks a lot for hosting me as his student in Delft. I have learned a lot from you Frank, not only in science but also as a person. I saw your concern for all the people around you and also the environment

I am also so grateful to the committee that agreed to help me in my work.Ernest, Patricia, Luuk, Kawieta, Mieke, Anka, Andreas, Camila, J Johinislan, Guilherme, thank you so much for all support with the bureaucracies at the university and also in the payments.

Isabel Arends showed me how good is the feeling to treat everyone equally, regardless of their superior position.

To all friends in the lab, Mawin for several conversations and many ideas, Maria Luisa for her aid and excellent musical taste, Varlei, Rafael, Ane, Murilo, Tatiana, Gabriel thanks for all help and good environment at UNICAMP.

To my office's friends Sébastien for all the good time and to bring me back to the gym, Georg thanks for the good moments and also correcting my manuscript in English, Marine thanks for the excellent time and pleasant conversation. Morten, you are the fastest worker that I have seen and always available to help, Gaurav thanks for all the good talks, Wuyan thank you for

all the new ideas about projects and personal tips. Sandy, Florian, Mieke, Sabry, and Elena, working with you guys, taught me a lot.

Thanks, Renco, Marc, Laura, Linda and Lloyd, for all the help.

To the BOC group for this great experience.

To all the dual degree students, Rafael, Bianca, Wesley, Andreia, Ana, Renato, Meissa, Carla, Elisa, Felipe, Lucas.

To my masters Farzin and Floris, and also my training colleagues who helped me deal with stress

To Jeniken and Max, for being much more than just great neighbors

To my friends/family who, regardless of the time we have known each other or the geographical distance that separates us, are always close, providing great stories and wonderful company.

To my father who at my early age always give me toys to stimulate my curiosity and my mother who unconditionally believed me when the school said the I could not follow the other students because I was slow. She put me to study hard every day and help me to manage this.

To Tais, Fabiene who always supporting and encouraging me.

To my little Beatriz and , who made my time shorter but made my life better.

Delft, 24-2-2020

Curriculum Vitae

Tiago Pedroso de Almeida was born on July 15, 1987, in Sorocaba-SP, Brazil. He was in 2007 admitted to Universidade Federal de São Carlos (Brazil). After four years of studying biology, he received his Bachelor's degree in March 2011. Afterward, he continued his Master's research at the same university under the supervision of Dr. Antonio Riul Jr. He obtained his Master's degree in April 2013, with the thesis entitled "*Application study of PAH / PEDOT automated films: PSS in Nafion® membranes*". In March 2014, he started his PhD in bioenergy at UNICAMP and in 2015 enrolled in the dual degree, part in Brazil under the supervision of Dr. Antonio Riul Jr. at UNICAMP and part in the Netherlands under the supervision of Dr. Frank Hollmann in the group of Biocatalysis at Delft University of Technology. The project has been focusing on the study of the use of oxidases for organic synthesis and biofuel cells. After graduation, he starts teaching in high school and got a position as an assistant professor on a private faculty in Brazil.